WETTING OF COMPLEX LIQUIDS

Dissertation

zur Erlangung des Grades
„Doktor der Naturwissenschaften“
im Promotionsfach Chemie

am Fachbereich Chemie, Pharmazie und Geowissenschaften
der Johannes Gutenberg-Universität Mainz

Dorota Linke
(Geburstname: Truszkowska)

geb. in Katowice

Mainz, 2017

Dekan:

1. Berichterstatter:
2. Berichterstatter:

Tag der mündlichen Prüfung: 29.08.2017

Die vorliegende Arbeit wurde von März 2014 bis Juli 2017 unter der Betreuung von Dr. G.K. Auernhammer und Prof. H.-J. Butt am Max Planck Institut für Polymerforschung in Mainz angefertig.

Zusammenfassung

In früheren Arbeiten wurde gezeigt, dass sich der dynamische Kontaktwinkel von Wasser ändert, wenn man kleine Mengen von Tensiden, in Konzentrationen unterhalb der kritischen Mizellen Konzentration (CMC), hinzufügt [1-4]. Diese Arbeiten haben sich mit Tensiden mit einem molekulare Gewicht von 100 - 400 g/mol beschäftigt. Weniger Aufmerksamkeit ist bisher auf Tenside gelegt worden welche 10 bis 50 mal schwerer sind. Daher gibt es immer noch unbeantwortete Fragen zum Einfluss des molekularen Gewichtes von Tensiden auf das Benetzungsverhalten von Flüssigkeiten. In dieser Arbeit beschäftige ich mich mit dem dynamischen Entnetzungsverhalten von großen Triblock Polymer Tensiden, Pluronic, und vergleiche es mit dem von Tensiden mit geringerem molekularen Gewicht. Pluronic ist aktiver ander Oberfläche und ändert die Oberflächenspannung schon bei nanomolaren Konzentrationen im Vergleich zu kleingewichtigen Tensiden.Der dynamische Kontaktwinkel wurde mit einer eigens gebauten rotierenden Walze gemessen. Ähnlich wie bei klein gewichtigen Tensiden führt die Zugabe von Pluronic zu einer Verkleinerung des dynamischen Kontaktwinkels. Schon bei Konzentrationen unter 0.5% CMC und geringeren Geschwindigkeiten ergeben sich signifikante Änderung im dynamischen Kontaktwinkel. In Kombination mit den Entnetzungs-Experimenten, Oberflächen-Rheologie Untersuchungen und Messungen der Oberflächen-Aggregat-Konzentrationen konnte ich zeigen das die relevante Vergleichsgröße nicht der CMC ist, sondern die Konzentration der kompletten Oberflächen Bedeckung (CFSC). Für klein gewichtige Tenside stimmt CMC und CFSC überein. Für Pluronic hingegen unterscheiden sich die beiden Konzentrationsskalen. Dies konnte ich für Entnetzungsgeschwindigkeiten bis 200 mm/s experimentell überprüfen

Dynamische Benetzung findet auch statt bei viel größeren Geschwindigkeiten und Temperaturen unter 0 ^{o}C, zum Beispiel beim Aufschlag von Tropfen auf Flugzeugen bei Geschwindigkeiten über 100 m/s. Es gab schon unterschiedliche Bemühungen zur Untersuchung von Tropfenaufschlag in unterschiedlichen Bedingungen[5-13] denoch ist wenig bekannt zum Aufschlag von Tropfen bei Geschwindigkeiten über 50 m/s und Temperaturen unter 0^{o}C. Im zweiten Teil meiner Arbeit untersuche ich den Aufschlag von Tropfen auf

unterschiedlich hydrophoben und weichen Oberflächen bei Geschwindigkeiten von 50 und 90 m/s, und Temperaturen zwischen 0^{o}C und 15^{o}C. Dafür habe ich einen speziellen experimentellen Aufbau entwickelt zur Beobachtung vom Tropfenaufschlag in einem Windtunnel. Dieses Projekt wurde zusammen mit Dr. E. Banaccurso von der Surface Technology Advanced Material Gruppe der Airbus Group Innovations in München Deutschland durchgeführt. Ich konnte durch die Experimente zeigen dass das Benetzungsverhalten von unterkühlten Tropfen bei Geschwindigkeiten über 50 m/s und Temperaturen unter 0°C von unterschiedlichen Parametern, unter anderem der Hydrophobizität und Weichheit der Oberfläche, der Temperatur und Aufschlagsgeschwindigkeit abhängt.

Abstract

Previous worked showed that adding surfactants to water, even at concentration below the critical micelle concentration (CMC) results in changes in the dynamic contact angles[1-4]. These previous works were focused on surfactants with a molecular weight between 100 - 400 g/mol. Less focus has been given to surfactants with molecular weight 10 to 50 times higher. In this range of molecular weights there are still many unanswered question regarding the influence of the molecular weight of the surfactants on the wetting behavior. In this thesis, I look into the dynamic dewetting behavior of large triblock polymeric surfactants, Pluronic, and compare it with small molecular weight surfactants. In comparison to them, the larger Pluronic changes the surface tension already at nanomolar concentration. The dynamic contact angles were measured using a home built rotating-drum set-up. Just like small molecular weight surfactants, addition of Pluronic leads to a decrease in the dynamic contact angles. Different is the much lower surfactant concentration needed. Already at concentrations below 0.5% CMC there is a significant difference in the dynamic contact angle. The combination of dewetting experiments, surface rheology and bulk measurements of aggregates concentration shows that the relevant concentration scale is the concentration of full surface coverage (CFSC). For small molecular weight surfactants the CMC and CFSC are equal. For Pluronic those two concentrations differ. The dynamic contact angles of Pluronic solutions were measured for velocities up to 200 mm/s at room temperature.

Dynamic wetting can also happen at much higher velocities and temperatures below 0^oC, e.g. when suporcooled rain drops impact an airplane flying with speed over 100 m/s .Even though there were some efforts in the last years to study drop impact at different conditions of speed and temperature[5-13]. Little is known about impacts at speeds higher than 50m/s and temperatures below 0^oC. Second part of the thesis concerns drop impact on different surfaces with speed of the impacting droplets was 50 and 90 m/s and the temperature varied between -15^oC and 0^oC. A special experimental set-up was developed to observe the drop impact at those conditions. This side project was done in collaboration with Dr. E. Bonaccurso from the Surface Technology & Advanced Materials Airbus Group Innovations, Munich, Germany. I show that the impact, wetting and freezing of supercooled drops at velocities above 50 m/s and temperatures below 0^oC, depends on different parameters, such as hydrophobicity and softness of the surface, surrounding air temperature and impact speed.

Table of Contents

1.Motivation

Wetting is the process of liquids covering a surface. Depending if the liquid is in movement or not two types of wetting are distinguished. When the liquid is not in movement it called static wetting. While when the liquid moves, it is dynamic wetting. For example, the distribution of liquids on different surfaces is described by dynamic wetting. For one component liquids the dynamic wetting was studied previously[14-23] . Also the static wetting of more complex liquids, such as surfactant solution, is rather well understood[17,20,21,24-26]. But the dynamic wetting of two component liquids, such as surfactant solutions of polymer dispersions, is less well understood. We know that in two component liquids the wetting process is heavily influenced by the concentration of surfactants[1-3]. Already at concentration well below the critical micelle concentration (CMC), the dynamic contact angle is significantly reduced in comparison to water. This happens because the surfactants change the flow close to the three-phase contact line of surface, liquid and air. It is not well understood how the surfactants change this flow and if the diffusivity of the surfactants influences their transport to the three-phase contact line. However, previous studies only focused on surfactants with molecular weight between around 100 to 400 g/mol[1-4], such as cetyl trimethyl ammonium bromide (CTAB). So far only a little bit of focus was given to surfactants that are 10 to 50 times larger. The questions addressed in this thesis include: What is the influence of the molecular weight? Does the number of hydrophobic groups affect the dynamic wetting? The dynamic contact angles of surfactant solutions[1-4] were measured for velocity up to 200 mm/s and at room temperature. However, dynamic wetting can also happen at more extreme conditions, such as temperatures below 0^oC and high speeds. For example, the impact of super cooled droplets with on airplane flying at a speed of over 100 m/s. When they impact with a surface they freeze, creating a layer of ice. This ice formation can cause problems in many different situation, for example in-flight icing on aircrafts[5,8,27] or ice formation on wind turbines[7,28]. In recent years there has been some effort to gain a better understanding of the process of the drop impact of super cooled droplet at different speeds, temperatures and surfaces[5-13,29]. But there is still not much known about drop impact at high speeds, more than 50 m/s. Furthermore, it is not known how the drop impact at this velocity and temperatures below 0^oC.

1.1 Structure of the thesis

This work was part of Marie Curie initial training network (ITN) called "CoWet". The focus of this ITN was wetting of complex liquids. "CoWet" consisted of different partners from both Academia and Industry all over Europe. Giving a chance to cooperate and study different aspects of wetting. This thesis consists of two separate projects concerning the dynamic wetting of complex liquids.

The first part is about the dewetting of high molecular weight surfactants. In this case we compare the wetting behavior of large surfactants (Pluronic) with smaller previously studied surfactants[1-4]. In this study I use different methods, such as measuring the dynamic contact angle, surface tension and dilatational rheology, to understand Pluronic solution. I use a variety of different Pluronic, which have different molecular weight and ratio of hydrophobic (polypropylene oxide PPO) and hydrophilic (Polyethylene oxide PEO).

The second topic was done on cooperation with Dr. E. Bonaccurso from Airbus Group, which was one of the partners in "CoWet". The focus is on the drop impact of super cooled droplets at high velocities (between 50 and 90 m/s) and at low temperatures (between 0 and -15^{o}C). In this work, we develop a way to measure the drop impact at high speeds and low temperatures simultaneously from two different view (bottom and side view). With this I could observe the impact and the freezing of super cooled droplets with a volume between 40 - 400 μl.

2.Fundamentals

2.1 Dewetting of high molecular weight surfactants

2.1.1 Surfactant

Surfactant are amphiphilic molecules, which means they have hydrophobic (tail) and hydrophilic (head) part (Figure 2.1). They are widely used in various industries, such as in food production (emulsifiers) or in cosmetic industry (soap, detergents, etc.). Since surfactant are amphiphilic, when they are put into water the hydrophobic part will adsorb into the air-water interface (Figure 2.3). At the same time the hydrophilic part stays in the water solution. In case of water-oil systems the hydrophilic part will like to stay in the water phase while the hydrophobic part will prefer to be in oil phase. Due to this, surfactants can support mixing of two immiscible liquids, such as oil and water.

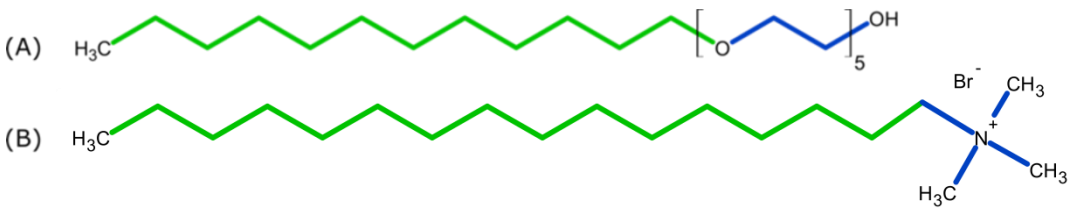

Figure 2.1. Chemical structure of ethylene glycol monododecyl ether (C12E5) (A) and cetyl trimethyl ammonium bromide (CTAB) (B). Surfactants are amphiphilic, which means that they have hydrophobic (green) and hydrophobic (blue) part. Depending on the charge, surfactant can be divided into either nonionic (A) or ionic (B).

Depending on the charge surfactants can be separated into ionic, nonionic or amphoteric. Ionic surfactants can be further divided into either cationic or anionic, depending on the charge the surfactants have after the dissociation. In case of cationic the charge is positive charge in case of anionic the charge is negative. In comparison to ionic surfactants the nonionic ones have no charge. For the amphoteric group, the surfactants can have both negative and positive charges depending on the pH.

Surfactants are a large group of chemical. They differ from each other not only depending on the charge. They can also have different molecular weight, varying between few hundreds to few thousands g/mol. In this work the depending on the molecular weight they can be divided into two groups:

- low molecular weight surfactants- with molecular weight smaller than 1500 g/mol
- high molecular weight surfactants- with molecular weight larger than 1500 g/mol

An example of low molecular weight surfactants is ethylene glycol monododecyl ether (C12E5) (Figure 2.1. A) or cetyl trimethyl ammonium bromide (CTAB) (Figure 2.1. B). Their molecular weight is 406 and 364 g/mol respectively (Table 2.1.). Even though they have similar molecular weight their critical micelle concentration differs. A big difference between them is the charge. Since C12E5 is nonionic and CTAB is cationic. The wetting behavior of low molecular weight surfactants was studied before[1-4] and is discussed in further chapter 3.

Name	Short name	Ionic/nonionic	Molecular weight (g/mol)	Critical micelle concentration (μmol/l)
ethylene glycol monododecyl ether	C12E5	nonionic	406	7
cetyltrimethyl ammonium bromide	CTAB	Ionic (cationic)	364	1000

Table 2.1. Name, charge, molecular weight and charge of C12E5 and CTAB. Both are an example of low molecular weight surfactants.

As high molecular weight surfactants Pluronic was used (Fig 2.2). Just like small molecular weight surfactants they are amphiphilic. They are made of hydrophilic polypropylene oxide (PPO) and hydrophobic polyethylene oxide (PEO) blocks. Pluronic are non-ionic triblock copolymers. There are various types of Pluronic with different molecular weight as well as different ratio of PEO to PPO. They can be found in various applications, for example in cosmetics, agrochemicals, food and others.

Recently there was an increased interested in them[30-39]. It was especially seen in pharmaceutical studies, where Pluronic where used to develop new drugs[36,37,39,40].

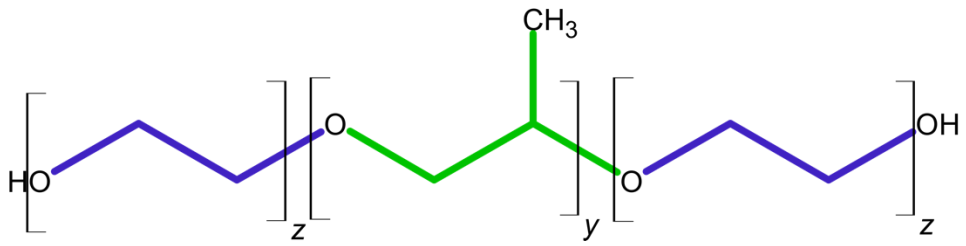

Figure 2.2. Chemical sketch of Pluronic. Like small molecular weight surfactants, they have hydrophobic (green) and hydrophilic (blue) part. The hydrophobic polyethylene oxide (PEO) blocks are in middle and the hydrophilic polypropylene oxide are on the outside.

The industrial name of Pluronic starts with L, P or F and is followed by two or three digits. The letter in front indicates what is the physical form of the Pluronic at room temperature, L-liquid, P- paste and F- flakes. The digits afterwards indicate the approximate molecular weight and the length of the PEO block. The molecular weight can be calculated by multiplying the first digit (or two first digit) by 300 and the amount of PEO can be calculated by multiplying the last digit by 10.

2.1.2. Surfactants at interface.

Independent from the molecular weight when surfactants are added to water, the surfactant will adsorb into the air-water interface. The hydrophilic part will stay in water, while the hydrophobic part will be in air. In water and oil mixtures, the surfactants will adsorb to the water-oil interface. The hydrophilic part of the surfactant will stay in the water phase and the hydrophobic part will be in oil phase. When surfactants adsorb into the interface, this results in a decrease in the surface tension. Independent if we look at water-air or water-oil systems a part of the surfactants will stay in a bulk, forming micelles or will be in a form of a free surfactant (Figure 2.3). Depending on a type of surfactant, hydration and environment (e.g. temperature or ionic strength) the shape of the micelles will differ (e.g. cylindrical, spherical).

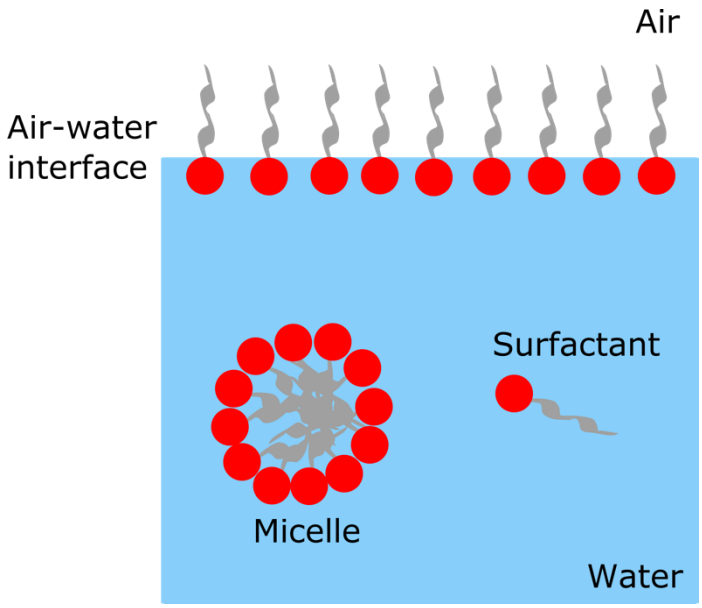

Figure 2.3 Different behaviour of surfactants in air-water system. Close to the air-water interface surfactants absorbs into the interface. In the bulk surfactants can either swim freely or create micelles.

The behaviour of Pluronic at interfaces, either water-oil[31,41-43]or water-air interface[44,45], was studied and it slightly differ from the one of small surfactants. It was reported that at higher concentration there is a change in the molecular conformation of Pluronic at the interface[42,46,47] (Figure 2.4.).

When Pluronic is added to water, the Pluronic molecules adsorbs into the water-air interface. At lower concentration Pluronic molecules adsorbs with both the hydrophobic PPO blocks and hydrophilic PEO blocks to the surface. Pluronic continues to adsorb in this way until the whole surface is fully taken by the surfactants. However, at higher concentration the hydrophilic PEO is displaced from the surface and is replaced by the hydrophobic PPO. This will continue until the surface is fully covered with the PPO blocks and only afterwards there will be aggregates in the bulk.

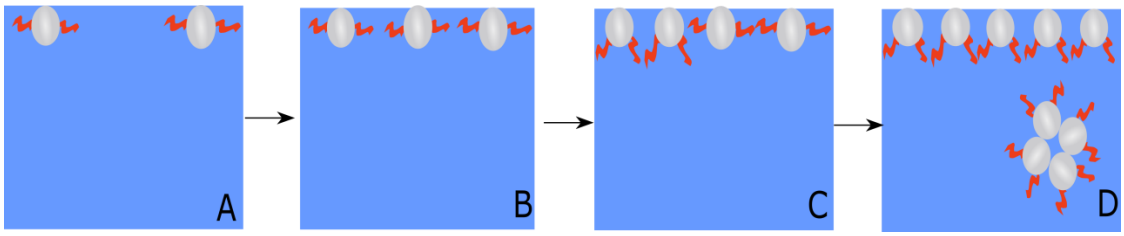

Figure 2.4. The adsorption of Pluronic at water-air interface[34,44]*.At lower concentration, the Pluronic adsorbs flatly to the air-water interface (A and B). With increasing concentration the conformation of Pluronic molecules changes and at higher concentration, the outside PEO blocks are replaces by the PPO blocks at the interface (C and D)*[34,44].

Pluronic just like small molecular weight surfactants can form micelles. Apart from this Pluronic can also have other forms in the bulk (Figure 2.5). At concentration below the CMC most of the Pluronic will adsorb to the surface but there still will be some present in the bulk in the form of free surfactant. Apart from this Pluronic can be in a form of self-micelles, in this work named as unimer, in which the hydrophilic PEO blocks create a shell around the middle hydrophobic PPO blocks[34,35,38,48,49]. When, this unimer form is only in case of Pluronic, which have long PEO blocks. Since when the PEO block is much shorter than the middle PPO block it is unable to create shell around the middle blocks. Lastly, with increasing concentration, but below the CMC, it possible for Pluronic to form aggregates. Those aggregates are made from two or more Pluronic molecules. The higher the concentration the bigger will those aggregates be.

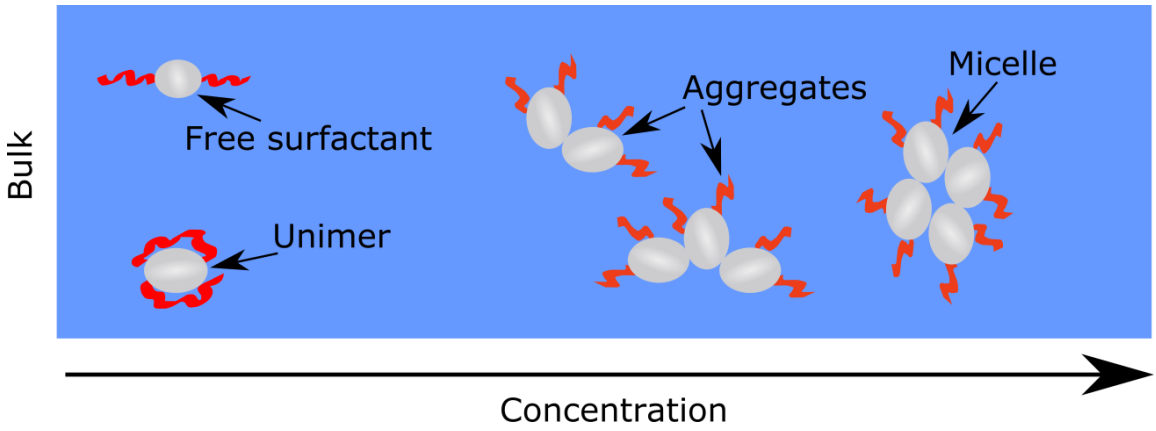

Figure 2.5 Different forms of Pluronic can exist in the bulk depending on concentration. At low concentrations Pluronic can either be in the form of a free surfactant or a unimer, in which the PEO blocks create a shell around the middle PPO blocks [35,48]*. With increasing concentrations, still below the CMC, Pluronics can form aggregates made from two or more molecules. Finally, at concentration over the CMC they create micelles.*

2.1.3. Critical micelle concentration (CMC)

Surfactant are soluble at low concentrations. Above certain concentrations surfactants can form micelles, whose shape will depend on the type of surfactant, hydration and environment factors (temperature or ionic strength). This concentration is known as critical micelle concentration (CMC). However, this does not mean that micelles are only present at concentration above the CMC. At concentration below the CMC most of the surfactant is dissolved as individual molecules but there is also a small number of micelles present.

One way of measuring the CMC is observing the number of micelles present in the bulk. With increasing concentration, the number of micelles in the bulk increases. In this case the CMC is considered the concentration at which 50% of molecules are inside of micelles[50].

Another way of determining the CMC is through the changes in surface tension (Figure 2.6.). Since, when added to a solution, surfactants will adsorb into the surface thus resulting in a decrease in the surface tension. With increasing concentration, the surface tension continues to decrease further. This will continue until the whole surface will be full of the surfactant molecules at this point the surface tension reaches a minimum. Afterwards, even with increasing concentration the surface tension remains

stable. However, in many situations after the CMC the surface tension slightly increases. The reason for it might be contaminations in the solutions. The contamination will first adsorb in the surface, thus reducing the surface tension. After the CMC is reached the contaminations are replaced by the surfactant. This results in an increase in the surface tension. Contaminations in this case can come from various sources. For example, from dissociation of the surfactant (Sodium dodecyl sulfate) or come from the environment (not entirely cleaned glass equipment).

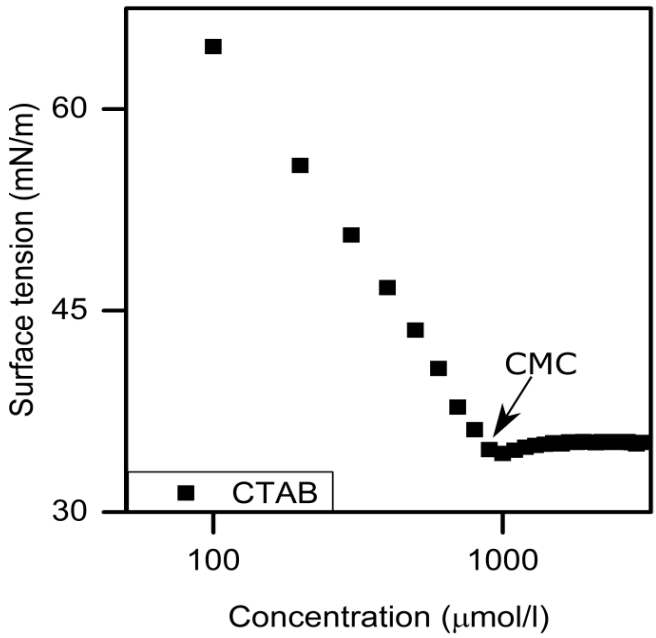

Figure 2.6. Surface tension curve of surfactant solution, in this case CTAB. The surface tension decreases with increasing concentration of surfactant. This continues until the whole surface is covered by surfactants and micelle are present in the bulk. This concentration is the known as the critical micelle concentration (CMC). Afterwards the surface tension reaches a plateau.

2.1.4 Ways of measuring surface tension

2.1.4.1 Wilhelmy Plate and du Noüy ring

There are few ways of measuring the surface tension, such as the Wilhelmy plate, the du Noüy ring and pendant drops. In case of the Wilhelmy plate method (Figure 2.7 A) a platinum plate is immersed into a liquid. There are few reasons why platinum is used. One being that platinum is chemically stable. Additionally, the platinum plate is easily wetted by the different liquids and the contact angle of a liquid on platinum plate

$\theta = 0^{o}$. The contact angle is explained in detail in chapter 2.1.6. Lastly, platinum surface can be easily cleaned. Most of the contamination on the surface of the platinum plate can be cleaned by heating up the plate. During measurements, the force acting into the plate as the result of wetting is measured by a microbalance. The force acting on the plate is given by the following equation:

$$F_{\gamma\theta} = 2l\gamma \cos\theta \qquad (2.1)$$

where l is the length of the plate, θ is the contact angle and γ is the surface tension or interfacial tension. From this equation, it is possible to calculate the surface tension. A similar method is the du Noüy ring (Figure 2.7 B). In this case, a platinum ring is immersed into the liquid and then the ring is slowly pulled out and pushed into the liquid. The force needed to raise the ring from the liquid is measured and it is given by equation 2.2:

$$F = 2\pi * (r_i + r_a) * \gamma \qquad (2.2)$$

The r_i is the radius of the inner ring of the liquid, while r_a is the radius of the outer ring of liquid.

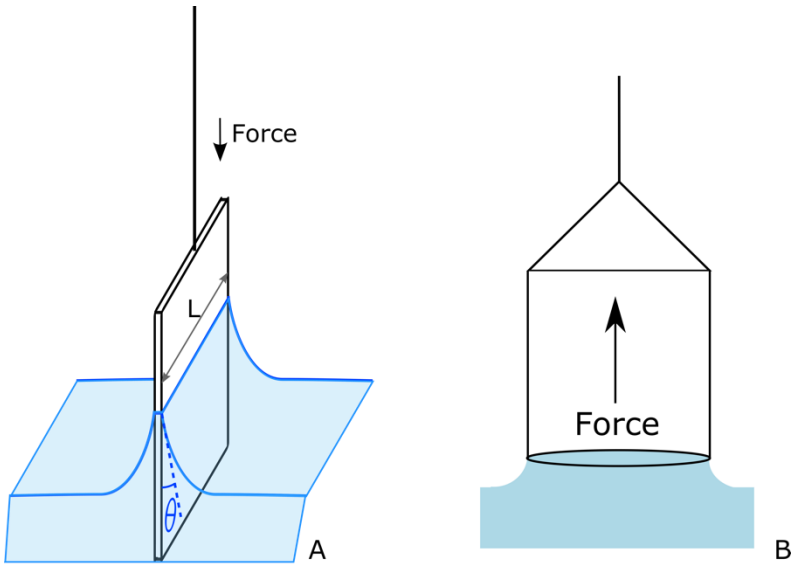

Figure 2.7. Wilhelmy Plate (A) and du Noüy ring (B) method of measuring surface tension.

The main difference between these two methods is the way the surface tension is measured. In case of the du Noüy ring method the ring is in constant movement during

the measurements and the liquid is in non-equilibrium. This makes it impossible to measure the surface tension variation over time using this method. The Wilhelmy Plate method is static. This means that the plate is not in motion during the measurement, thus the surface is in equilibrium.

2.1.4.2 Profile analysis tensiometry (PAT)

Another method used to determinate the surface tension uses a pendant drop. In this case, a drop is suspended from a needle. The shape of the droplet is determined by the interplay between the interfacial tension and gravity. Surface tension favours a spherical shape of the drop, while gravity forces result in a vertical elongation of the drop. Using drop profile analysis tensiometry (PAT)[21]of the drop profile (Figure 2.8.), it is possible to calculate the surface tension, using the Young-Laplace equation:

$$\Delta P = \gamma \left(\frac{1}{R_1} + \frac{1}{R_2}\right) \quad (2.3)$$

where ΔP is the difference in pressure over the interface. R_1 and R_2 are the principal radii of the surface, R_1 is the meridional curvature and R_2 is the azimuthal curvature. They can then further be expressed as:

$$\frac{1}{R_1} = \frac{d\varphi}{dS} \quad (2.4)$$

and

$$\frac{1}{R_2} = \frac{\sin\varphi}{X} \quad (2.5)$$

where φ is the contact angle of the profile and *S* is the arc length along the profile of the drop. X is one of the coordinates in the coordinate system, that can be found in Figure 2.8. φ is not the same as the dynamic contact angle mentioned earlier. Figure 2.8. shows how each of the values can be derived from the pendant drop. In case of gravitational field the weight of the liquid column is added:

$$\Delta P = \frac{2\gamma}{b} + \Delta\rho g Z \quad (2.6)$$

Where b is the radius if the curvature of the drop apex, $\Delta\rho$ is the density difference between the drop and the air surrounding it. The equations 2.3 and 2.6 can be

reformulated into a set of a first- order differential equations. Representing the arc length s, the contact angle φ and the z-axis

$$\frac{d\varphi}{ds} = \mp\frac{B_z}{b^2} + \frac{2}{b} - \frac{\sin\theta}{x} \quad (2.7)$$

$$\frac{dx}{ds} = \cos(\varphi) \quad (2.8)$$

$$\frac{dz}{ds} = \sin(\varphi) \quad (2.9)$$

where *s*, *x* and *z* are the length, horizontal and vertical coordinates:

$$s = \frac{S}{b} \quad (2.10)$$

$$x = \frac{X}{b} \quad (2.11)$$

$$z = \frac{Z}{b} \quad (2.12)$$

and Bo is the shape factor.

$$Bo = \frac{\Delta\rho g c^2}{\gamma} \quad (2.13)$$

$\Delta\rho$ is the density between drop and the surrounding it air, g is the gravitational acceleration. c is a scaling factor, in this case it is curvature of the drop apex. From the numerical integration of the Laplace equation (equations 2.7 – 2.9) and the fit of the acquired profile coordinates from a bubble or a drop by nonlinear regression it is possible to get the values for apex radius and shape factor. Then as a result it is possible to get the value of the surface tension.

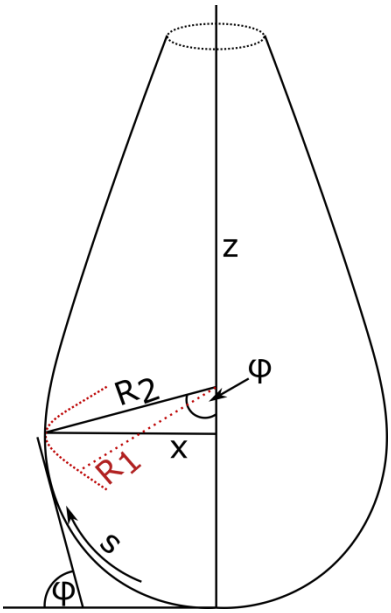

Figure 2.8. Sketch of a pending drop. Showing he principal radii of the drop, R_1 and R_2 and the contact angle φ. Additionally, the sketch also shows the length (s), horizontal (x) and vertical (z).

The PAT method has many advantages. The main one is that only a small amount of liquid is needed to measure the surface tension. Additionally, this method is usable for a range of different materials, such as organic solvents, surfactant solutions or molten materials[21]. There are also some limitations regarding this method. For this method to work the droplet needs to be symmetrical and have an oblong shape. Otherwise, the measured surface tension is inaccurate.

2.1.5 Dilational interfacial rheology

Using dilational interfacial rheology it is possible to measure the viscoelasticity of solutions. The viscoelasticity depends on the type of studied liquids. When surfactants are added to water, they will adsorb to the air-water interface and change the viscoelasticity. The amount how much the viscoelasticity is changed depends on the number of surfactants at the air-liquid interface. At low concentration, the viscoelasticity is low. When the concentration of surfactant is increased, a larger number of molecules is at the air-water interface, the viscoelasticity increases. It reaches its peak at the CMC, where the whole surface is fully occupied by the surfactants molecules. After the CMC with increasing concentration more and more surfactants are close to air-water interface. This results in a decrease in the viscoelasticity of the studied

liquid. It means that measuring the viscoelasticity of the surfactant solution can give information about the processes happening at the air-water interface.

In case of dilational interfacial rheology, surface of the droplet is constantly compressing and expanding (Figure 2.9.). The response of the surface tension to the dilation stress is known as the dilation viscoelasticity, E[21,51,52] . It describes by the ratio of changes of the surface tension and the interfacial area, *A*,:

$$E = \frac{\Delta\gamma}{\Delta lnA} = E_r + iE_i \qquad (2.14)$$

in which E_r is the real part, also known as the storus modulus or dilational elasticity, E_i is then the imaginary part and it represents the dilational viscosity.

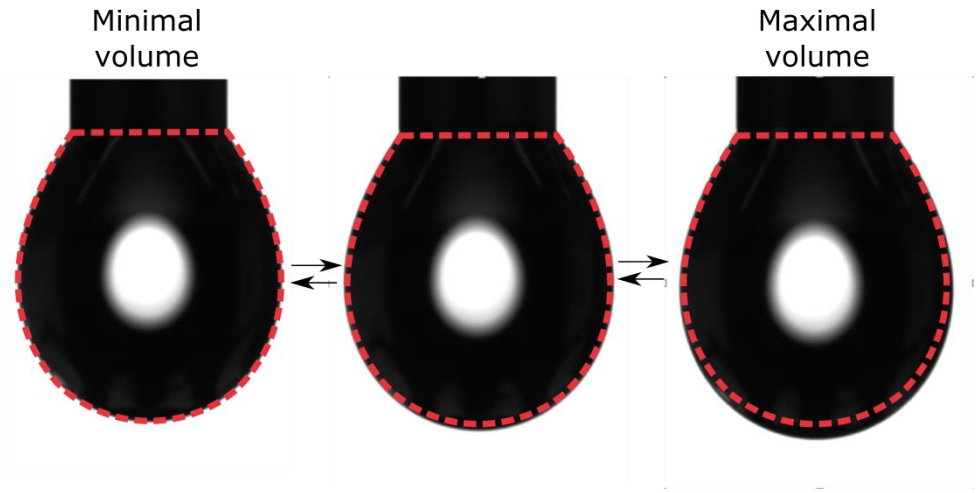

Figure 2.9. Dilational interfacial rheology measurement of a droplet. The drop is constantly changing its volume by compressing and expanding. The compressing and expanding is made at a chosen frequency. The red line represents the shape of the drop before the oscillations started.

There are few methods that make it possible to measure dilational viscoelasticity. In this work, the main focus is based on methods in which a drop or bubble is compressing and expanding. Those methods are known as oscillating bubble or drop method [21,41,51,52].

They can be divided into two groups depending on the way of measurements the interfacial tension. The first one is based on measuring the capillary pressure inside a drop or a bubble, while the other one is based on the analysis of the drop profile. Both ways make it possible to measure at liquid-liquid or liquid-gas interface in a large range of frequencies. In most cases, the used frequencies are between 10^{-5}-10^{-1} Hz.

The capillary pressure tensiometry is based on measuring the capillary pressure of a spherical or nearly-spherical droplet. The Laplace pressure is determined by the Young-Laplace equation (equation 2.3). For spherical shapes, for example bubble or drops, the difference in Laplace pressure is described as

$$\Delta P = \frac{\gamma 2}{R} \qquad (2.15)$$

Where γ is the surface tension and R is the drop radius. In this method, drops or bubbles are used and they are situated at the tip of capillary. Then harmonic perturbations are applied to the interface area of the droplet. This compression and expansion of the drop results in change in the capillary pressure.

In the case of the drop profile analysis, the used drops or bubbles are rather large, with diameters above 1 mm. This size is due to the limitation of PAT. For too small droplets the surface tension cannot be measured accurately. The droplet is then suspended at the tip of a needle or capillary. The measurements can be then performed either in liquid-gas or liquid-liquid environment. Under gravity the shape of the droplet will want to be in a state where the total energy of the system is minimal. This is the result of combination of surface tension and gravity forces. Then the drop is oscillated with specific frequency. Depending on the environment, liquid-liquid or air-liquid, the range of frequencies varies between 10^{-5}– 10^{-1} Hz.

In this method, the oscillation of the drop or bubble result in a harmonic expansion and compression of the surface area. This then results in periodic changes in the interfacial tension (Figure 2.10.). Those changes always happen with the same frequency and it has some delay to the change of the surface area. For measurements with small amplitude oscillations, it is possible to calculate the dilational viscoelasticity, using equation 2.14 by observing the changes in the interfacial tension of the oscillating drop.

It is possible to measure the oscillating drop through either volume or shape oscillation. In the first option, the oscillation is a periodic change in the volume of the droplet. In shape oscillations, the volume of the droplet remains constant. In this case, the oscillation of the droplet is a result of periodic movement of the needle or capillary to which the drop is attached. In this work, I used measured the volume oscillations, the details of the experimental set-up is in chapter 3.3.3.

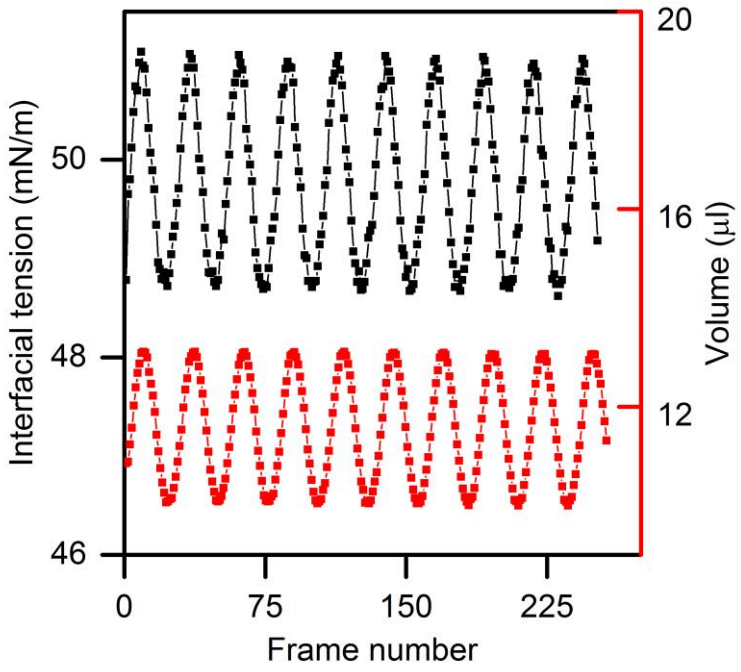

Figure 2.10. Changes of interfacial tension and volume of the drop during volume oscillations using ODG connected with goniometer OCA 35, both from DataPhysic, Germany. This data is for Pluronic P136PG26 at concentration of 0.1 µmol/l at 0.02 Hz. Changes in the interfacial tension always happen with the same frequency and there is some delay to the change of the surface area.

2.1.6 Contact angle

When liquid is deposited on a substrate, it has a characteristic contact angle between the air-liquid and solid liquid interface, known as contact angle θ (Fig. 2.11.). At the edge of the droplets all three phases (air, liquid and substrate) meet and the line between them is called three-phase contact line.

There will be interfacial tension between liquid-vapour γ_{LV}, liquid-solid γ_{SL} and solid-vapour γ_{SV}. Using those interfacial tensions Young could describe the equilibrium contact angle θ_{eq}. In this case those tensions are acting on the three-phase contact line. Thus, balancing the contact angle. This relation is known as Young equation (equation 2.16). It is only accurate in situation where all forces are balanced[14]

$$\gamma_{LV} \cos \theta_{eq} = \gamma_{SV} - \gamma_{SL} \qquad (2.16)$$

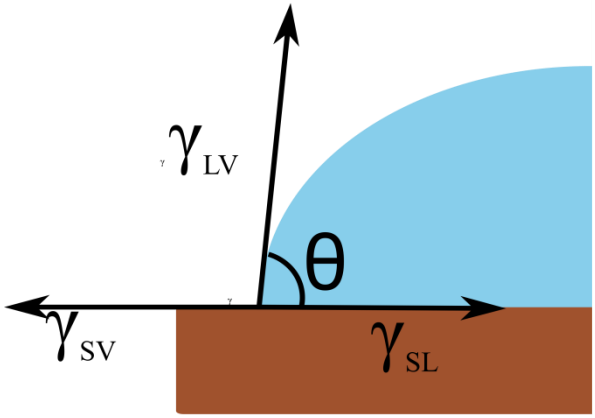

Figure 2.11. Drop sitting on substrate will have a specific contact angle θ. In this situation there are interfacial tension between liquid, liquid-solid and solid.

Additionally, the contact angle will differ depending if the drop is in movement or not. When the drop is not in movement, static contact angles are measured (Figure 2.12). When droplet is moving dynamic contact angles are observed (Figure 2.14).

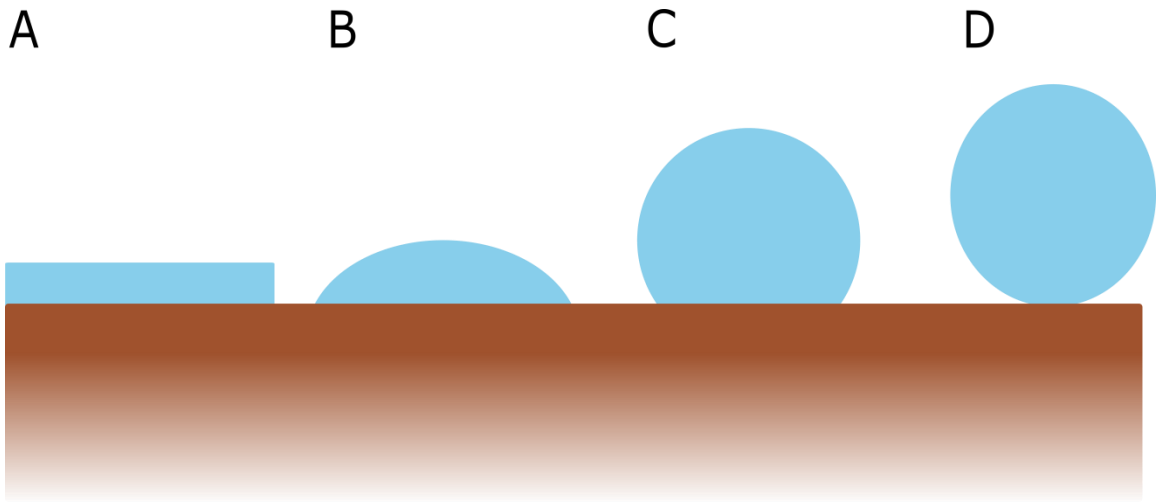

Figure 2.12. The static contact angle differs depending on the wettability. In case of full wettability, the contact angle is 0° (A), while for high wettability it varies between 0° and 90° (B). If the contact angle is even higher (C), between 90° and 180°, the wettability is low. In the last situation where contact angle is 180° (D) and it is a case of non-wetting Depending on the contact angle it is possible to see if a surface is more hydrophobic or hydrophilic. For hydrophilic surfaces the contact angle will be low (A, B), while for hydrophobic surfaces the contact angle will be high (C, D).

Depending on the surface tensions of the substrate as well as the liquid, the contact angle will differ. In case of complete wettability, the liquid will completely wet the surface (θ = 0°). With decreasing wettability, the contact angle will increase. The contact angle θ between 0° and 90° means high wettability, while an even higher (θ between 90° and 180°) contact angle means that wettability is low. There is also a situation in which a droplet forms a sphere at the surface (θ = 180°) in which case there is non-wetting. The most common way of measuring static contact angle is just by looking at the shape of the droplet.

For both the static (Figure 2.13.) and the dynamic case (Figure 2.14) it is possible to distinguish the advancing and receding contact angle. Those two dynamic contact angles differ from each other and the difference between them is known as hysteresis. Depending on the velocity there is static and dynamic hysteresis. When the velocity of the droplet U is zero then the difference between the advancing and dynamic contact angle is known as static hysteresis. When the droplet is moving with velocity U >0 then the difference between the advancing and receding dynamic contact angle is called dynamic hysteresis (Fig. 2.15).

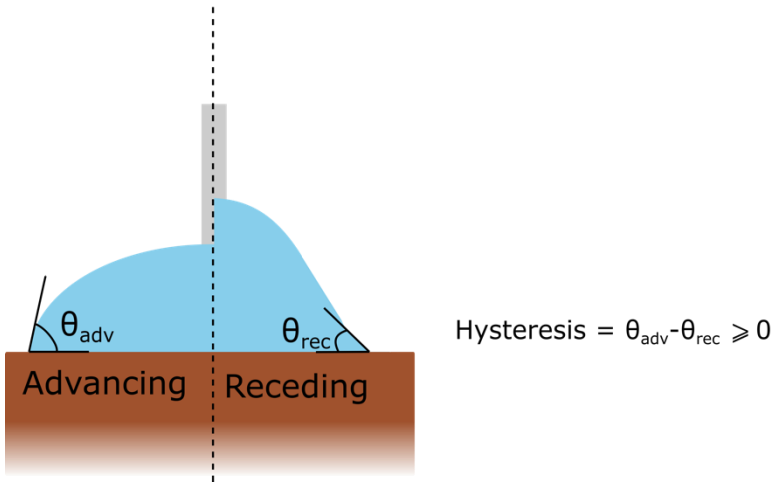

Figure 2.13. The advancing, θ_{adv}, and receding , θ_{rec} , static contact angle. When the velocity, U=0, the difference between the advancing and dynamic contact angle is known as static hysteresis. In this method, the volume of the droplet changes during the measurements. Then contact angle is advancing the volume increases, while when the contact angle is decreasing the volume decreases.

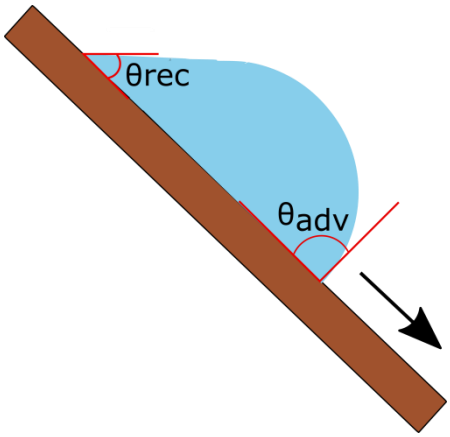

Figure 2.14. In case of moving droplets there are two different contact angles, the advancing θ_{adv} and the receding dynamic contact angle θ_{rec}.

The dynamic contact angles depend on the velocity. With increasing velocity, the advancing dynamic contact angle θ_{adv} increases and the receding dynamic contact θ_{rec} decreases.

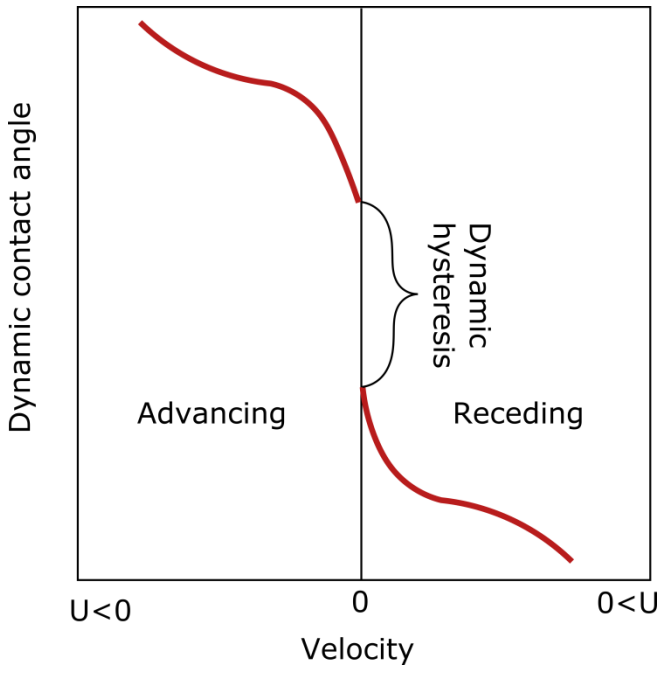

Figure 2.15. Sketch of change in the dynamic contact angle depending on the velocity. The advancing contact angle (θ_{adv}) increases with increasing speed, while the receding contact angle (θ_{rec}) decreases. When velocity of moving droplet U non-zero then the difference between the advancing contact angle (θ_{adv}) and the receding contact angle (θ_{rec}) is known as dynamic hysteresis.

2.1.7 Forced and spontaneous wetting

Depending on the situation there are two types of dynamic wetting, forced and spontaneous. In the first case, external forces are applied on the liquid or substrate to achieve wetting of the substrate. This plays an important role in various situation in industry, such as printing or coating. While in case of spontaneous wetting, also known as spreading, the droplet spreads spontaneously and without external forces until equilibrium is reached.

The dynamic contact angles will depend on many factors, such as the velocity U, viscosity η and surface tension γ of the liquid. However, all those parameters can be combined to one parameter called Capillary number[53]:

$$Ca = \frac{U\eta}{\gamma} \tag{2.17}$$

2.1.8 Theories of dynamic wetting

Both the advancing and receding dynamic contact angle depends in the velocity of the moving three-phase line. This indicates that this process must be thermodynamically irreversible. Thus it must be dissipative[54]. Several theories[22,55-62] have been developed to explain this phenomena. Not one model was fully able to describe the multi-scale aspects of dynamic wetting. Two main theories concerning the dynamic wetting are the molecular kinetic theory and the hydrodynamic theory. An important difference between those two theories is the source of the energy dissipation close to three-phase contact line. This will be further discussed in folloairfoil chapters describing both models.

2.1.8.1 Molecular kinetic theory

In the molecular kinetic theory, the movement of the three-phase contact line is based on the detachment and attachment of the fluid molecules to or from the solid surface (Figure 2.16)[54,55]. In this model the velocity dependence of the dynamic contact angle is the result of the disturbance in the adsorption equilibria. Consequently, the surface tension changes and the three-phase contact line moves through the surface. The direction it moves depends if the liquid replaces the air molecules on the solid surface or if the air molecules replace the liquid ones. In the first case, the contact line advances while the second situation is for a receding contact line. Furthermore, the

experimentally measured contact angle, θ_{app}, is the same as the velocity dependent microscopic contact angle. This model assumes, there are two length scales:

- molecular- at which the detachment and attachment of fluid molecules to or from solid surface occurs.
- macroscopic- where the effects of the molecular dissipation are visible

As mentioned before the velocity dependent movement of the contact line is a result of disturbance in the adsorption equilibrium and thus the local change in the surface tension. In this model, the driving force behind the movement of the three-phase contact line is equal to the surface tension force when the equilibrium is disturbed:

$$F_w = \gamma\left(cos\ \theta_{eq} - \cos\theta_{app}\right) \tag{2.18}$$

For the wetting-line velocity is then:

$$V = \frac{\gamma\left(\cos\theta_{eq} - \cos\theta_{ap}\right)}{\zeta} \tag{2.19}$$

where ζ is the friction parameter:

$$\zeta = \frac{k_b T}{\kappa^o \lambda^3} \tag{2.20}$$

Where $\kappa^o$is the equilibrium frequency, of a random displacement of molecules at the three-phase contact line, and λ is the average distance of the displacement, which is usually in the nanometer range.

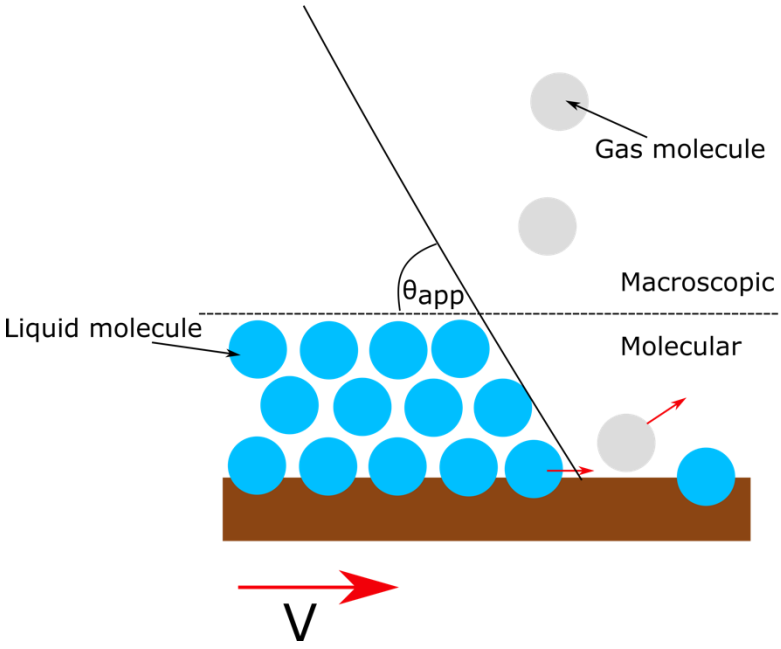

Figure 2.16. Close to the 3-phase contact line liquid molecules replace air molecules at the solid surface. This results in a local change in the surface tension, which leads to movement of the 3-phase contact line.

2.1.8.2 Hydrodynamic theory

In the hydrodynamic theory describes the movement close to the 3-phase contact line in which the energy dissipation due to viscous flow of the liquid at the wedge close to the contact line[22,54,55,58,60,62,63] (Figure 2.17).

This theory assumes three separate scales. The first one is macroscopic. It is in the millimeter scale. Here the apparent contact angle, θ_{app}, is observed. Usually the θ_{app} is measured during contact angle measurements. The second regime is called mesoscopic. It is in micrometer range. In this region, the viscous bending of air-liquid interface is observed. The last region is closest to the 3-phase contact line. It is called microscopic. It is in nanometer scale. In this regime the microscopic contact angle, θ_m , is observed.

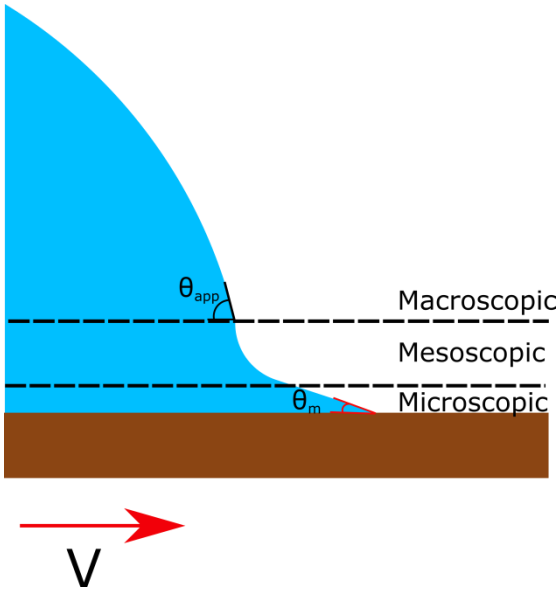

Figure 2.17. Sketch of the behaviour close to the 3-phase contact line in the hydrodynamic model. This area can be divided into 3 ranges, macroscopic, mesoscopic and microscopic.

The relation between the apparent dynamic contact angle θ_{app} and the viscous bending of the interface, close to the microscopic contact angle, is given by the Vox-Coinov relation:

$$\theta_{app}^3 - \theta_m^3 = 9Ca\ ln\left(\frac{L}{L_m}\right) \qquad (2.21)$$

the L and L_m are the macroscopic and microscopic length scale. The macroscopic length scale is usually in the range of 1 μm while the microscopic one is in the range of 1 nm.

2.1.9 Marangoni effect

If there are local surface tension gradients, there will be a force along the free surface acting from a region with lower surface tension to one with higher surface tension. This force is known as the Marangoni effect. This gradient in surface tension can be the result of a change in the solute or surfactant concentration. Also, temperature changes happening at the interface change the surface tension.

2.1.10 Ways of measuring contact angle

2.1.10.1 Static

There are various ways of measuring dynamic contact angle on solid surfaces[53]. For measuring the static contact angle the most popular method is observing a sessile drop through microscope or telescope (Figure 2.18). The contact angle then is determinate with a goniometer or the shape of the droplet is fitted with the Young equation (Equation 2.16). As mentioned in chapter 2.1.6 there can be advancing and receding static contact angle.

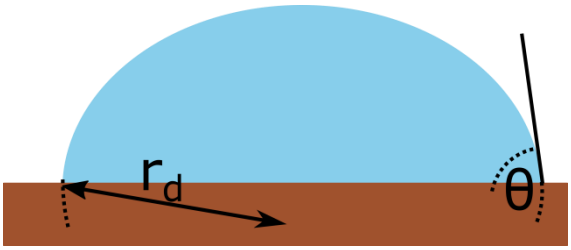

Figure. 2.18. In the sessile drop method, a droplet is situated on a substrate and the static contact angle θ is measured by fitting the contour by the radius r_d of the drop.

2.1.10.2 Dynamic

One way of measuring the dynamic contact angles is by immersing a plate/tape/fiber into a liquid. This is principle is used in the plunging tape method[56] or Wilhelmy plate method, which was explained in detail in 2.1.4.1. Another way is to measure the dynamic contact angle using a rotating drum set-up[1-4,64,65].

Using our home built rotating drum set-up[1,2,4] it is possible to measure the change in the dynamic contact angles (Figure 2.19). The rotating drum set-up consist of a water bath and a cylindrical stainless steel drum. In this work two water baths have been used:

- older one made from polyvinyl chloride PVC (Fig. 2.19 A)[1-3]. It had three windows, one in the front and two on the side. This made it possible to observe the motion of the 3-phase contact line (front window) or the dynamic contact angle (the side

windows). The disadvantage of it is the limited type of solvent that can be used for cleaning PVC.

- new set-up made from stainless steel (Fig. 2.19 B) [4,65]. The advantage of this system is that stainless steel is resistant to much more solvents than PVC used in the previous bath. That makes the cleaning procedure easier. This version also has a larger number of windows through with which it is possible to observe either the 3-phase contact line (front and back windows) or the dynamic contact angle (side windows). Unlike the previous water bath, it is possible to observe the receding and advancing side at the same time.

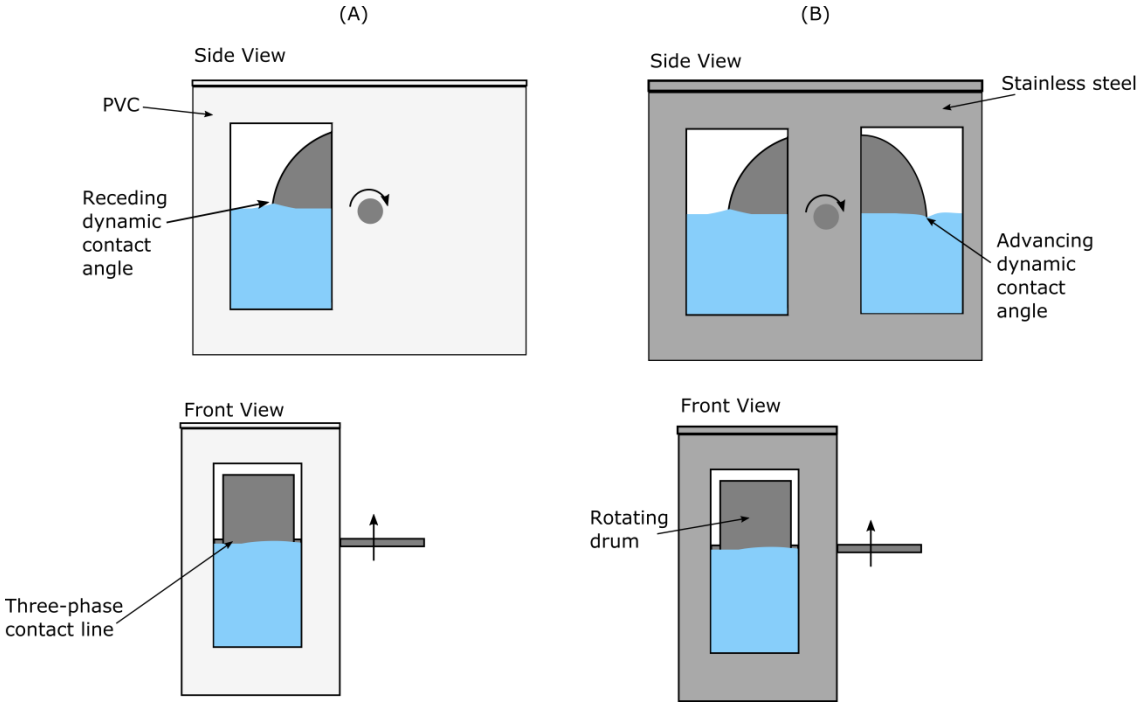

Figure 2.19. Sketches of the old (A) and new (B) rotating drum set ups. With both it is possible to observe the movement of 3-phase contact line (front view) or dynamic contact angle (side view).

In both water baths the same stainless steel drum (with diameter of 12 cm) was used. During measurements, it was half-immersed in a liquid, with the axis in the liquid

surface. There are few motors that can be connected to the cylinder, with which it is possible to have a large range of velocity, between 10^{-4} to 1 m/s. It is also possible to change the direction of rotation of the motors, giving an opportunity to measure both advancing and receding dynamic contact angle.

2.1.11 Change of the dynamic contact angles vs velocity

It was shown in previous works[1-4], that adding surfactants has an influence on the dynamic wetting behaviour. Resulting in a decrease in the dynamic contact angles in comparison to one of pure water already at concentration well below the CMC (Figure 2.20). In case of CTAB only 5,10 or 15 %CMC resulted in a decrease in the dynamic contact angle[1-4]. In case of others surfactant, the amount will differ but it is always below the CMC. The changes continue to increase with increasing concentration of the surfactant. In case of advancing dynamic contact angle the changes in the dynamic contact angle are not as strong as for the receding dynamic contact angle.

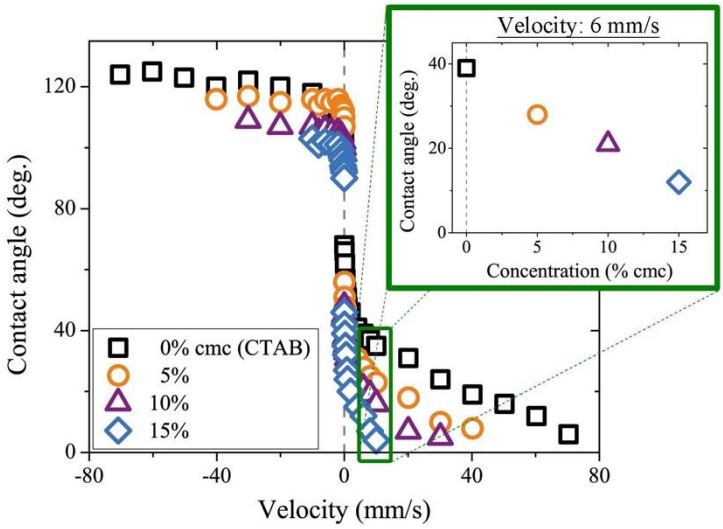

Figure. 2.20 Dynamic contact angles at different velocities for CTAB. Already at concentration below the CMC the dynamic contact angles are reduced in comparison to the ones from water. The receding dynamic contact angle is much more affected by the presence of the surfactant than the advancing. Reprint from PhD thesis of Daniela Fell.[1].

The mechanism behind the change in the dynamic contact angle for surfactant solution is still under investigation. In the proposed model the change in the dynamic contact angle is dependent on the local gradient of the surface tension close to the 3-phase

contact line[4] (Figure 2.21). While the drum is rotating, it pulls the liquid, which results in a fresh surface being created at the three-phase contact line. In this fresh surface, the concentration of surfactant is smaller than far away from the contact line. This difference in surfactant concentrations results in a gradient in surface tension. This difference is equilibrated by the surfactant in the bulk. The process of surfactant coming into the air-liquid interface consists of two steps. The first one is the advection and diffusion of the surfactants from the bulk. The second step is the adsorption of those surfactants into the air-liquid interface. The time to reach equilibrium will depend on different factors, such as diffusion. For surfactants with faster diffusion it is expected that the equilibration of the surface tension will be faster. This gradient in surface tension results in a Marangoni force in the direction of the contact line. The Marangoni force is in the opposite direction to the surface flow. This then leads to a change in the dynamic contact angle [1-4].

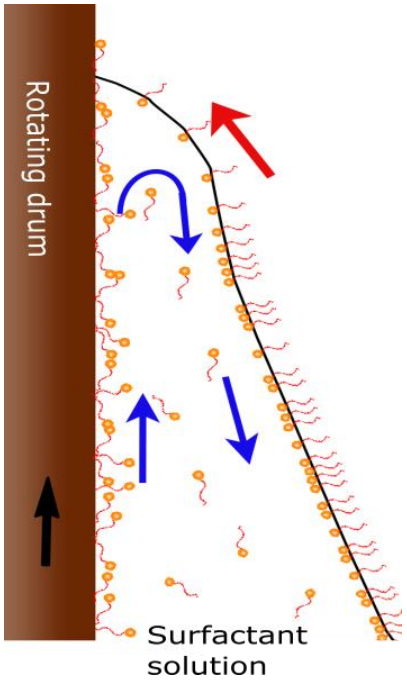

Figure 2.21. Sketch of the flow profile (blue arrows) near the three-phase contact line during forced dynamic dewetting. The liquid is being pulled up by the drum and a new surface close to the contact line. In the newly created surface there are less surfactants than in the bulk, which results in a Marangoni force in the direction of the contact line (red arrow). This results in a change in the dynamic contact angle. Picture reprinted from Truszkowska et al.[65].

2.1.12 Transport in the water bath

Fell et al.[1,2] have shown that in surfactant solutions depending if the surfactant transport is possible or not the dynamic wetting behaviour differs. When the transport of the surfactant is unavailable the change of the dynamic contact angle is stronger than when the transport is allowed. Surfactant in the solution can either diffuse due to a local concentration gradient or be advected by bulk flow resulting from the rotating drum. It is possible for surfactant to diffuse through the air-liquid interface and through the bulk. Advection of the surfactant can happen through bulk or interface. When both diffusion, through air-liquid interface and bulk, as well as advection are possible (Figure 2.22 A) the dynamic contact angle and the critical velocity for film formation are higher than when transport is only possible through the bulk diffusion or advection (Figure 2.22 B) or transport is completely hindered (Figure 2.22 C). This can be also connected to the hypothesis of the flow close to the three-phase contact line described in 2.1.11. The Marangoni force is a result of the surface tension gradient close to the three-phase contact line. This results in a decrease of the dynamic contact angle. When the transport of surfactants is unlimited, the surfactants diffused faster from the receding side to the advancing side. This then again means that the gradient close to the three-phase contact angle is smaller, resulting in a smaller dynamic contact angle than when the transport is limited.

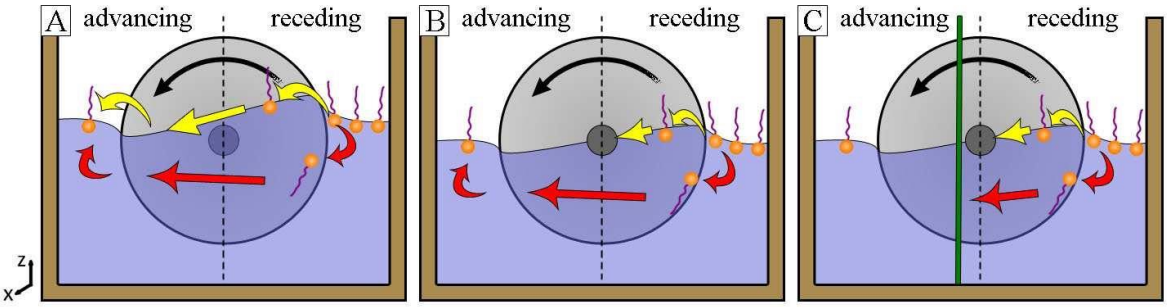

Figure 2.22. Sketch of different transport mechanism of surfactant. When liquid is filled above the axis (A), both surface and bulk transport is allowed. In case liquid is filled up to axis only bulk transport is possible (B). Nor surface or bulk transport is allowed in a case when there is external barrier added into the water bath (C). This figure is repost from PhD thesis of Daniela Fell[1].

2.1.13 Charge of a surfactant

As mentioned in chapter 2.1.1 surfactants can be divided into groups depending on the

charge. They can be ionic (cationic or anionic), non-ionic or amphoteric. Previous works[1-4] did study the change in the dynamic contact angle in solution of surfactants that were nonionic or ionic (cationic or anionic), Those works showed that independent of the charge, the addition of surfactants always resulted in a decrease in the dynamic contact angle (Figure 2.23). Additionally, the charge of the surfactant is not responsible for the difference between different surfactant, such as why some surfactants reduce the dynamic contact angle more than others.

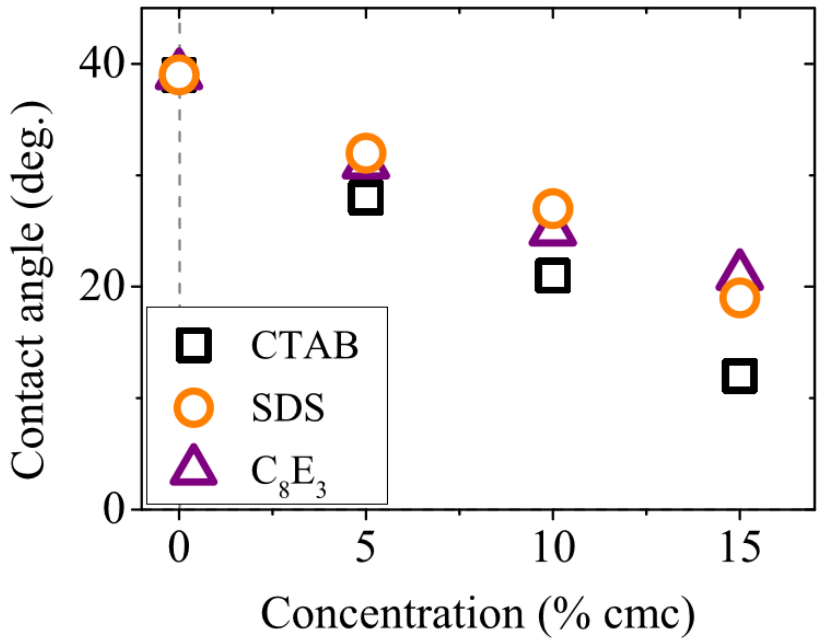

Figure 2.23. Change in the dynamic contact angle at different % CMC. In this work surfactants with different charges were studied. Triethoxy monooctyether (C8E3) is a nonionic surfactant. CTAB and sodium dodecyl sulfate (SDS) are ionic surfactants. SDS is anionic, while CTAB is cationic. Regardless of the charge of the surfactant all of result in a decrease in the dynamic contact angle with increasing concentration. Repost from the PhD thesis of D. Fell.[1]

2.1.14 Fluorescence correlation spectroscopy

With fluorescence correlation spectroscopy (FCS) it is possible to measure the diffusion coefficient, hydrodynamic radius and more of fluorescent molecules[66,67]. It is a highly sensitive method, making it possible to measure even at very low concentrations. FCS is based on measuring the intensity fluctuation caused by fluorescent molecules moving freely through small detection volume. Those fluctuations are then quantified with the

autocorrelation of the intensity signal. The autocorrelation is a measure for the similarity of the intensity δI at a time t and a delayed time, t+τ. It is defined as:

$$g(\tau) = \frac{\langle \delta I(t) - \delta I(t+\tau) \rangle}{\langle I(t) \rangle^2} \quad (2.22)$$

Depending on the size of the molecules the autocorrelation function will be different. From the decay time of this function it is possible to calculate the hydrodynamic radius, R, of studied molecule using Stokes-Einstein equation:

$$\mathrm{D} = \frac{\mathrm{K_b T}}{6\Pi\eta\mathrm{R}} \quad (2.23)$$

Where K_b is the Boltzmann Constant. T and η are temperature and viscosity, respectively. With this equation, it is only possible to calculate the hydrodynamic radius of spherical particle.

2.1.15 MALDI-TOF MS

MALDI, stands for matrix-assisted laser desorption/ionization[74]. In this method, the tested analyte is mixed with large quantity of matrix. Afterwards a laser, usually nitrogen laser (λ=337 nm), is directed at the analyte/matrix mixture. The analytic/matrix mixture absorbs the ultraviolet light and vaporizes it. TOF MS[75] is the abbreviation of time of flight mass spectrometry. This method relies on measuring the time of flight of tested ions. In this case, the ions realised from the analyte/matrix mixture fly through field-free drift region at which end there is a detector. All ions have the same kinetic energy but depending on the mass to charge ratio (m/z) the velocity differs. The smaller the m/z ratio is the faster is the velocity. Thus, as they travel through the analyser they separate and reach the detector with different time. The velocity of the ions, *SWD*, is:

$$v = \left(\frac{2E_k}{m}\right)^{1/2} \quad (2.24)$$

E_k is the kinetic energy and m is the mass of the traveling ions. The flight time, T_f, of the traveling ions through a given distance, d, can be described as:

$$T_F = \frac{d}{v} = d\sqrt{\frac{m}{2E_k}} \quad (2.25)$$

As a result it is possible to calculate the mass values from the given set of flight times. The peak does show the molecular weight of the studied molecule. The height of the peak does not correspond to the amount of the substance.

2.2. Drop impact at high speeds and low temperatures

2.2.1 Wind tunnel

Wind tunnels are used to study the effects of air flow or resistance to the air flow on objects[27]. The air speed can be controlled and depending on the type of the wind tunnel those speeds differ. The simplest classification is between low-speed (subsonic) and high-speed (supersonic, hypersonic).

For many years wind tunnels were used to study various topics. The main focus was on studying aerodynamics of various surfaces[68,69], which is important in different industries. Such as when designing new airplanes or parts for airplanes and testing the resistance of internal structure to incoming wind in civil engineering. Some of the wind tunnels also have the possibility to control the temperature inside the test chamber. This enables the study of icing on different surfaces[27]. This is especially interesting in aerospace industry. In which case the in-flight icing not only reduced the performance of the aircraft but also poses a serious threat to the flight safety. In-flight icing occurs especially at specific weather conditions at altitudes between 9000-20000 ft (2.7-6 km): at temperatures between 0 and -15^{o}C[5].

2.2.2 Super cooled water

The flight altitude for most passenger aircrafts vary between 30000-40000 ft (9-10 km). During winter months, the airplane while ascending to this altitude the aircrafts must fly through several clouds. Those clouds contain large amounts of water droplets and have a lack of nucleation centers. Meaning that the water droplets do not form ice crystals even though the temperature is below freezing. However, the moment those water droplets impact with the surface of the airplane they freeze and create a layer of ice. This phenomenon is known as super cooled liquid. In this state, water is in a liquid state even though it is below the freezing temperature[70].The system is in a metastable state and cannot reach a thermodynamic equilibrium due to lack of nucleation centers.

However, the moment those seed crystals are introduced to the system it immediately changes into the thermodynamically preferable state and it freezes over.

In some cases super cooled water droplets (SWD) can exist even at the temperatures below -35^{o}C [71]. Super cooled large droplets (SLD) have a diameter larger than 50 μm[72]. However, in specific conditions they can even reach up to 500 μm. For droplets of this size, it is possible to splash after impact with the surface of an airplane, rebound of the surface just like smaller droplets and reattach just to freeze at different part of the surface.

2.2.3 Weber number

The way a droplet impacts with a surface depends on various parameters, such as the type of surface the drop is impacting, the impacting velocity, *v*, and the size of the drop r_d. A widely used parameter used for describing this dependency is the dimensionless Weber number. It describes the ratio between the deforming inertial forces and the stabilizing surface tension force, γ.

$$We = \frac{\rho v^2 r_d}{\gamma} \tag{2.26}$$

where ρ is the density of the impacting droplet.

Through the Weber number it is possible to indicate whether the kinetic or surface tension is dominant during impact. In case of high Weber numbers the kinetic energy is dominant, while for lower Weber numbers the dominant are the surface tension forces[73].

3. Dewetting of high molecular surfactants

Part of this chapter is based on my publication "Forced dewetting dynamics of high molecular weight surfactant solutions"[65], which was written under my maiden name, Dorota Truszkowska.

In previous years there have been studies concerning the dynamic wetting behavior of surfactants solutions[1-4]. These studies have shown that at concentration below the critical micelle concentration (CMC), 5-15 %CMC, the dynamic contact angle changes. While the advancing dynamic contact angle is only slightly influenced by the presence of the surfactant. The receding dynamic contact angle is significantly reduced in comparison to pure water, it is explain in detail in chapter 2.1.11. These studies focused on surfactants with molecular weight between 200-500 g/mol, like cetyltrimethylammonium bromid (CTAB) or pentaethylene glycol monododecyl ether (C12E5). Connected to these studies[1-4], there is a hypothesis of a flow-profile near the 3-phase contact line, which is explained in detail in chapter 2.1.11. This hypothesis is based on the existence of surface tension gradients between the bulk and freshly created surface close to the three-phase contact line. This difference in surface tension is equilibrated by the surfactants in the bulk. The time that is needed to reach equilibrium depends on different factors, for example diffusion. For surfactants with faster diffusion reaching the equilibrium should be faster than for molecules with slower diffusion. Much less attention has been given to surfactants with higher molecular weight, that have a slower diffusion rate. This chapter investigates the dynamic wetting of high molecular weight polymer surfactants, a {polyethylene-oxide} – {polypropylene-oxide} -{polyethylene-oxide} (PEO-PPO-PEO) triblock copolymer called Pluronic. Just like a surfactant, Pluronics are amphiphilic. That means they have both hydrophobic (PPO) and hydrophilic (PEO) part. Additionally, Pluronics come in a large variety of molecular weight. In this thesis Pluronics with molecular weight between 2000- 13600 g/mol, were studied. Additionally, Pluronic can have various PPO:PEO ratio. Making it possible to study the influence of the building blocks (PEO and PPO) of Pluronic on the dynamic wetting.

3.1. Material

3.1.1. Pluronic

Due to a large variety of different molecular weight and ratios of hydrophobic {polypropylene-oxide} PPO to hydrophilic {polyethylene-oxide} PEO block, Pluronic was chosen as the high molecular weight surfactant in this study. This work was focused on 6 different Pluronics (Table 3.1). More information about Pluronic can be found in chapter 2.1.1.

In this work, instead of using the industrial name of Pluronic, which was explained in detail in chapter 2.1.1., we developed our own system. In our system, it is possible to calculate the molecular weight, in g/mol, and %PPO of overall molecular weight of the Pluronic from the name.

In this system, the name of Pluronic can be divided into two parts. The first one indicates the molecular weight while the second one shows how much hydrophobic PPO is in the polymer. The letter "P" at the beginning stands for Pluronic. It is then follow either by 2 or 3 digits, which indicate the molecular weight in g/mol by 100. The second part of the name indicates the %PPO. It starts with letters "PG", which stands for polypropylene oxide (PPO). The folloairfoil numbers just show the %PPO. For example, Pluronic F-127 has molecular weight of 13 600 g/mol and 26% PPG so its name in our naming system will be P136PG26. Both industrial names as well the corresponding names in our naming system for each Pluronic can be found in Table 3.1.

Used Pluronics have been carefully chosen depending on the molecular weight and amount of PPO and PEO. The molecular weight varied between 1900 – 13 600 g/mol. The used Pluronic are not monodisperse, so the molecular weight of each Pluronic slightly varies. The molecular weight of each Pluronic was later measured using MALDI-ToF, this is further described in chapter 3.2. Additionally, two pairs of Pluronic were made that have similar molecular weight but differ in the PPO:PEO ratio (P19PG40:P20PG88 and P54PG53:P55PG53). The second important parameter was the ratio of hydrophobic PPO to hydrophilic PEO. In this case the Pluronic the amount of PPO varied between 17-88 % of overall mass in g/mol. So it was easy to divide all studied Pluronic into two groups. The first group has Pluronics with small %PPO (P19PG40, PG54PG53, PG84PG17 and P136PG26). The second group consists of Pluronic, P55PG88 and P20PG88, which have much larger %PPO.

Also the length of PPO blocks was taken under consideration. In this way there are two pairs of Pluronic that have the similar length of PPO but different length of PEO. The first pair is P84PG17:P20PG88, which both have approximately 30 PPO blocks in the middle. The second is the P136PG26:P55PG88, which middle part consists of about 75 PPO blocks. The lengths of PPO and PEO blocks given in table 3.1 are given from the manufacture, Sigma-Aldrich. However, Pluronic are not monodisperse. That means that the lengths of the PEO and PPO blocks of Pluronic in the same batch will differ from each other. Some Pluronic might have slightly longer or shorter PEO or PPO blocks. However, in this work we will use the mentioned by manufacture length of blocks to compare different Pluronic with each other. The polymers were also used without any further purification.

Pluronic	P19PG40	P20PG88	P54PG53	P55PG88	P84PG17	P136PG26
Industrial name	L-35	L-61	P-84	L-121	F-68	F-127
PEO-PPO-PEO	12-16-12	2-30-2	19-43-19	5-70-5	75-30-75	100-70-100
Molecular weight (g/mol)	1900	2000	5400	5500	8400	13600
%PPO	40	88	53	88	17	26
CMC (μmol/l)	1800	20	2000	5	2100	2000
CFSC(μmol/l)	10	0.3	2	0.15	3.5	1
Diffusion constant (m^2/s)	$8.43*10^{-18}$ - $-1.72*10^{-17}$	$1.68*10^{-17}$	$6.23*10^{-18}$- $-1.19*10^{-17}$	$1.67*10^{-17}$	$4.68*10^{-18}$ - $1.32*10^{-17}$	$4.59*10^{-18}$- $-9.18*10^{-18}$
Surface tension at CMC (mN/m)	46.20	45.15	33.26	33.53	38.14	35.99
Surface tension at CFSC (mN/m)	50.22	51.34	39.81	43.08	48.26	44.97
Smaller molecular weight impurity (g/mol)	---	---	1400-1600	1000-1300	1800-2000	5000-5200

Table 3.1. List of Pluronic used in this study, with their molecular weight, length of PEO and PPO blocks, % of hydrophobic polypropylene oxide (PPO) to overall molecular weight of the whole Pluronic, critical micelle concentration (CMC), concentration of full surface coverage (CFSC), diffusion coefficient and surface tension at CMC and CFSC. The explanation for diffusion coefficient can be found in chapter 3.4.3. Pluronic are not monodisperse, so there will be differences in the molecular weight and length of PEO and PPO of the same Pluronic molecules in one batch. In this work, the used PPO block length is the one mentioned by the producer. For Pluronic with high molecular weight The MALDI-TOF MS measurements detected additional peak at lower molecular weight. This means that apart from Pluronic there is additional small molecular weight impurity. This was further discussed in chapter 3.2.

3.1.2. Small molecular weight surfactants

As for the small molecular weight surfactants, cationic cetyl trimethyloammonium bromide (CTAB) and nonionic pentaethylene glycol monododecyl ether (C12E5). They have similar molecular weight, CTAB is 364,45 g/mol and C12E5 is 406 g/mol, which is much smaller than the one of studied Pluronics. However, there are some differences between them, e.g., the CMCs for CTAB and C12E51000 μmol/l and 7 μmol/l, respectively.

3.2. Molecular weight of Pluronic

3.2.1. MALDI-ToF set-up

The measurements were done by J. Raeder using a Bruker Reflex II MALDI-ToF mass spectrometer (Bremen, Germany) accompanied with a N_2 laser (λ=337 nm) which operates with a pulse rate of 3Hz. A pulsed ion extractor (PIE design from Bruker) using a Voltage of 20 kV accelerated the ions, which were later detected by a Bruker HIMAS^{TM} analyser, which was operated in linear mode. This ensured the highest sensitivity for polymer analysis. For each spectrum a total of 60 shots were accumulated. Before the measurement, the equipment was calibrated with polyethylene glycol (PEG), with a mass range up to 20 000 g/mol.

3.2.2. Sample preparation

Samples preparation was done by J. Raeder. The samples were prepared by a solvent-free sample preparation. In this case powder 2.5-dihydroxy benzoic acid (2.5-DHB), purchased from Sigma-Aldrich was used as matrix. The Pluronic were mixed in weight ratio of 1:20 with 2,5-DHB. To ensure that the solution is homogeneous it was shaken for 10 minutes in a ball mill MM2000 from F. Kurt Retsch GmbH & Co. KG (Haan, Germany). The fine powder, obtained from this method, was afterwards crushed on the stainless steel MALDI target.

3.2.3. Mass spectra

The mass spectra showed that the molecular weight of Pluronic correspond well with the values provided by the manufacturer. For P19PG40, P20PG88 and P84PG17 the molecular weight obtained was the exact same as the one stated by Sigma-Aldrich. For the other Pluronic the mass spectra showed polymer distribution at slightly higher values, by around a 1000 g/mol more than in the specifications. Additionally, the measurements also showed an additional polymer distribution at lower molecular weight for Pluronic that have large molecular weight (≥5400 g/mol). This indicates that

apart from the large Pluronic molecule there is another species with lower molecular weight, the molecular weight of the low molecular weight species can be found in table 3.1. For example for P136PG26 there is a narrow polymer distribution at 13 600 g/mol, which is close the molecular weight (12 600 g/mol) provided by Sigma-Aldrich. There was a second narrow polymer distribution with molecular weight of 5200 g/mol. The smaller peak can be either a Pluronic with a lower molecular weight, shorter PEO-PPO diblock copolymer or a PEO or PPO homopolymer. The height of the peaks in the spectrum (Figure 3.1) does not correspond to the exact amount of Pluronic and small molecular weight species in the sample. Small molecular weight species have shorter flying time (equation 2.25) than larger Pluronic. This means that in the measurements time more small molecular weight species molecules than large Pluronic will hit to the detector. As a result the height of its peak for the small molecules is higher than for the large ones.

There is no way of distinguishing, which type of small molecular weight species is present. Since all of them can have a similar molecular weight and are indistinguishable using this method. Probably the molecules in the second peak came from the Pluronic synthesis process. The exact way of the synthesis of Pluronic is unknown. However, in the process of polymerisation few things may happen leading to the creation of the earlier mentioned low molecular weight species. As mentioned before Pluronic is a triblock copolymer made of PEO-PPO-PEO blocks. It might be that for unknown reason the polymerization stopped too earlier for some molecules, which would result in a part of Pluronic to be smaller than they should. It is also possible that during polymerization process for some reason one of the outside PEO blocks would not attach to the PPO-PEO blocks. Thus, resulting in a shorter PPO-PEO diblock copolymer apart from Pluronic. It might happen that either PPO or PEO block would not attach to each other for unkown reasons, which results in a PEO or PPO homopolymer next to the correctly sized Pluronic. Lastly, it might be that the PEO or PPO block breaks after the end of polymerization process. Thus, resulting in any of the mentioned low molecular weight species.

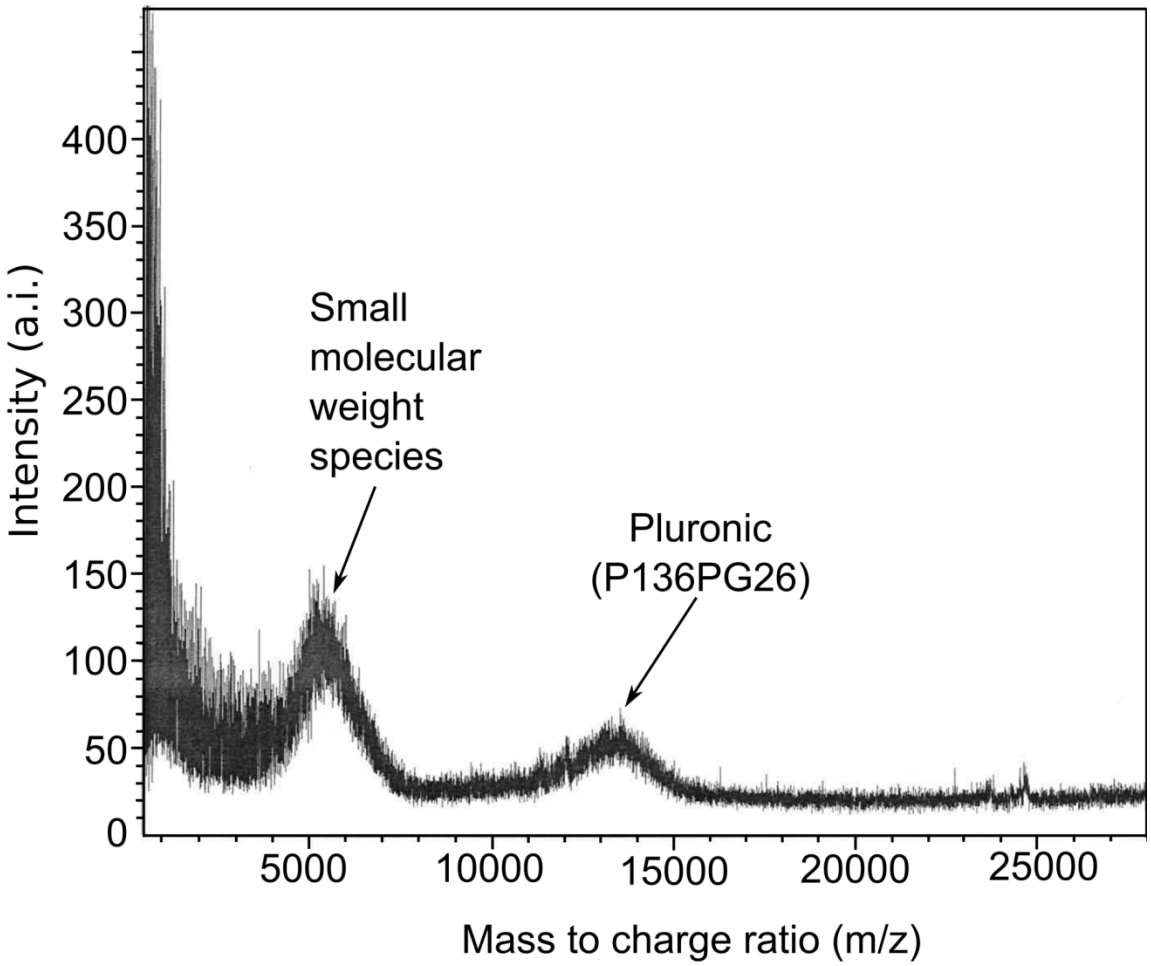

Figure 3.1. Example of MALDI-Tof spectrum for Pluronic. In this case it is of P136PG26. There are two peaks visible, which means that apart from Pluronic tested Pluronic there is an additional lower molecular weight species present. This peak at low molecular weight can be either Pluronic with a lower molecular weight, shorter PEO-PPO diblock copolymer or a PEO or PPO homopolymer. The higher peak at low molecular weight does not mean that there is a larger amount of small molecular weight species than Pluronic polymer in the sample.

3.3. Methods for dynamic measurements

3.3.1. Sample preparation

All the samples were prepared in the same way. The applicable amount of chosen Pluronic was added to ultrapure water (prepared with an Arium® pro VF/UF& DI/UV (Sartorius); electrical resistivity 18.2 MΩ). The samples were then left stirring for few hours at room temperature and used directly after preparation.

The samples containing PEO (Sigma-Aldrich) and PPO (Sigma-Aldrich) used for surface tension measurements were also used immediately.

3.3.2. Tensiometer

Surface tensions for different Pluronic solutions were measured using a tensiometer (DCAT 11, DataPhysic, Germany) using the Wilhelmy Plate method. Before each measurement, the glass beaker as well magnetic mixers were cleaned using 4:1 isopropanol:water solution in an ultrasonic cleaner for 30 minutes. Afterwards all materials were rinsed with ultrapure water (prepared with an Arium® pro VF/UF& DI/UV (Sartorius); electrical resistivity 18.2 MΩ) and dried using dry nitrogen. This procedure was followed to ensure that there were no contaminations on the beaker or magnetic stirrer.

The surface tension of ultrapure water, without any contaminations, is 72 mN/m. Each measurement set started with measurement of ultrapure water. Only when the surface tension of ultrapure water was 72 mN/m an appropriate amount of stock solution of Pluronic was added. After each of the addition the mixture was stirred for 2 minutes. Then either 1,2, or 5 minutes waiting time before the measurement was given. In all cases the surface tension results were independent from the waiting time if it was longer than 1 minute.

It was shown before that the CMC for Pluronic decreases with increasing temperature[34,38,43]. In this work all the surface tension measurements were done at room temperature.

3.3.3. Oscillating Drop Generator (ODG)

The dilational interfacial rheology, described in detail in chapter 2.14, measurements were done using the Oscillating Drop Generator (ODG, DataPhysic, Germany), connected to a goniometer OCA35 (DataPhysic, Germany). In this thesis, we used volume oscillations, which mean that the volume of the droplet was changing with a fixed frequency during the measurements. Before the measurements, the whole set-up was first cleaned with isopropanol and afterwards rinsed with ultrapure water. This was done until any surfactant or other contaminations were removed. This was tested by measuring surface tension of ultrapure water using the pendant drop method, described in chapter 2.1.4.2. Only when the surface tension of ultrapure water was 72 mN/m the measurements were done.

Just before the measurements, the set-up as well as the used syringe and needle were rinsed for 15 minutes with the specific Pluronic solution. This was done to ensure that their surfaces were in adsorption equilibrium with the measured solution. Just before the oscillations begun the drop was left pending for 5 minutes. It was assumed that after this time an adsorption equilibrium of the surfactant to the surface was reached. It was shown in chapter 3.2.2, using the Wilhelmy Plate method, that the time was enough for the surface tension to be constant. The frequency range used in this work was between 0.01-0.125 Hz. The volume of the droplets was between 15-20 μl. Droplets with this volume had an oblong shape, needed for PAT analysis, described in detail in chapter 2.1.4.2. At this volume, the drop was on the verge of separating from the needle tip. During the measurements length of the droplet varied due to the oscillations, leading to an increase and decrease in the volume. The amount the volume of the droplet changes is called surface amplitude by the manufacturer and given in mm for the change in length of the droplet. All the measurements were done with a surface amplitude of 0.1 mm as recommended by the manufacture (DataPhysic, Germany). To prevent evaporation of the drop during the measurements the oscillations were done in saturated atmosphere.

3.3.4. Rotating drum set-up

In this work, both home-made rotating drum set-ups, described in 2.1.10.2, were used to measure the dynamic contact angles. However, independent from the used water-bath the treatment of the drum and the way the contact angles were measured was identical.

3.3.4.1.Surface preparation of the drum

Before the measurements, the surface of the drum was coated by anionically polymerized polystyrene (Molecular weight of 300 kg/mol). For coating, the drum rotated in a 0.8 wt% solution of polystyrene in tetrahydrofuran (THS, Sigma-Aldrich) for 5 minutes. Thereafter the polystrytol-THF solution was quickly removed. The drum was left to dry for 1 hour in ambient condition and subsequently for 16 hours at 60 ^{o}C. To prevent dust deposition on the surface of the drum, it was stored in a closed chamber.

Before the measurements, the drum was put under ultrapure water (Arium® pro VF/UF& DI/UV (Sartorius); electrical resistivity 18.2 MΩ) for 1 hour to ensure the set-up was clean. The cleanliness of the set-up was checked in two ways. The first way was

by measuring the dynamic contact angle of water and comparing it to measurements done previously in a clean set-up. The second way was by measuring the surface tension of ultrapure water that was inside the water bath after rinsing it for 1 hour. When the surface tension of ultrapure water was 72.2 mN/m, the set-up is clean.

3.3.4.2.Measuring the dynamic contact angle

For the measurements, the rotating drum-set up (Figure 3.2) was filled up to the x-axis (corresponding to ~ 900 ml in the old set-up and ~ 1000 ml in the new one). This was done to prevent a surface transport of the surfactant in the water bath (compare chapter 2.1.12). After the drum was immersed in the studied liquid and the set-up was closed. Afterwards the drum was rotated for at least 45 minutes alloairfoil for the water vapor to saturate the air inside the water bath. This time ensured that adsorption equilibrium of the surfactants to the surface of the drum was reached.

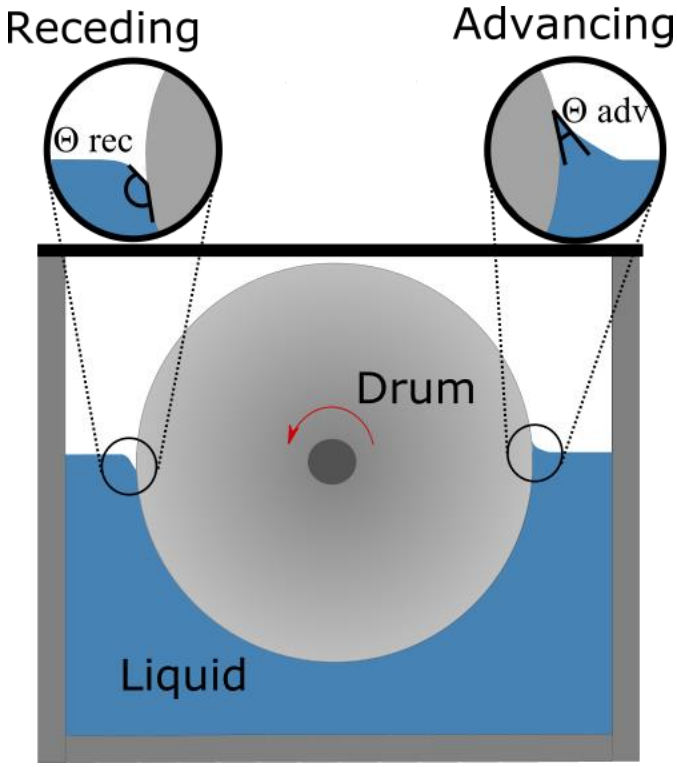

Figure 3.2. Sketch of the rotating drum set-up. It is possible to measure the advancing (θ_{adv}) and receding (θ_{rec}) from the side view.

Videos of the dynamic contact angles were recorded using a High Speed Camera (Photron, Fastcam SA-1, equipped with 12 x magnification optics with working distance about 30 cm) with a frame rate of 250 fps. The dynamic contact angles were measured from the recorded videos using ImageJ (Figure 3.3). The dynamic contact

angle was calculated by averaging 10 independent dynamic contact angle measurements from each video. The uncertainty of the contact angle is given as the standard deviation of the 10 independent measurements.

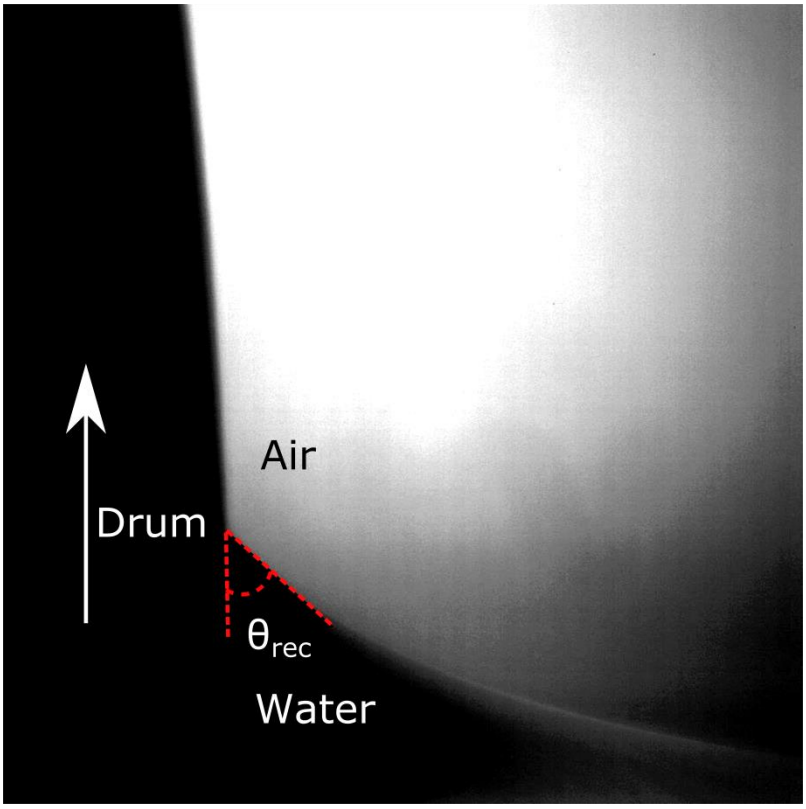

Figure 3.3. Picture of the receding dynamic contact angle, θ_{rec}, of water measured using rotating drum set-up. The drum was rotating with velocity of 27 mm/s. The arrow shows the direction of rotation.

3.3.5. Fluorescence correlation spectroscopy (FCS)

The aggregation behavior of Pluronic P136PG26 was measured by fluorescence correlation spectroscopy (FCS). This measurement was done in cooperation with Dr. K. Koynov and J. Schultze.

In this case, a commercial set-up (Zeiss, Germany) was used. It consists of a module ConfoCor 2 and an inverted microscope model Axiovert 200 with a Zeiss C-Apochromat water immersion objective with magnification 40x. The fluorescence light was first filtered (BP560-615 bands pass emission filter) and afterwards collected by an avalanche photodiode, which enables single-photon counting. As a sample cell an eight-well polystyrene-chambered cover glass (Laboratory-Tek, Nalge Nunc International) was used. The measured solutions of P136PG26 at various concentrations

contained Rhodamine 6G (Rh6G) at concentration ~10 nmol/l. For each of the samples a series of 20 measurements (each lasting 10 sec) were done and then the average of them was used in further analysis. The autocorrelation functions, obtained from the experiments, were fitted with a single component free 3D diffusion analytical function[76]. In this way the diffusion coefficient was obtained. With it was possible to calculate using Stokes-Einstein equation (equation 2.24) the hydrodynamic radius of the fluorescent species. For calibration of the confocal observation volume Rh6G was used as reference dye, since it diffusion coefficient is known.

3.3.6. NMR spectroscopy

All samples were prepared by adding applicable amount of the chosen Pluronic in deuterated water. Then they were mixed until the Pluronic was fully dissolved. All the used concentrations were below the critical micelle concentration (CMC). In most cases, the concentration was close to the concentration of full surface coverage (CFSC). CFSC is the concentration at which the whole surface is fully covered with surfactants but no micelles are present in the bulk. It is further explained in chapter 3.4.1.1. This was done to ensure that in the solutions there were no micelles present and only the diffusion of free surfactant was measured.

These measurements were done by M. Wagner using a 5 mm TXI $^{1}H/^{13}C/^{15}N$ z-gradient on the 850 MHz spectrometer equip with a Bruker Avance III system. In case of ^{1}H NMR spectrum between 16 and 1024 transients were used with a 9 μs long 90^{o} pulse. The 17000 Hz spectral width together with a recycling delay was between 5 and 10 seconds. Measurements using Diffusion Ordered NMR Spectroscopy (DOSY-NMR) were done using a 5 mm TXI $^{1}H/^{13}C,^{15}N$ z-gradient probe, that has a gradient strength of 5.350 G/mm on a Bruker Avance-III 850 NMR spectrometer. Calibration of the gradient strength of the probes was done by analysis of a sample of $^{2}H_2O/^{1}H_2O$ at a 298.3 K and then compared with the theoretical diffusion coefficient of $^{2}H_2O/^{1}H_2O$ at the same temperature. The theoretical value was taken from the Bruker diffusion manual. During the measurements the temperature was kept constant at $25^{o}C$. The temperature was controlled by a VTU (variable temperature unit), with accuracy of +/ 0.1K, which was check using standard Bruker Topspin 3.1 software.

The diffusion time was optimized for the TXI probe to 50 ms and the gradient pulse length was 1.4 ms. The optimization was performed by comparison of the remaining

signal intensity at 2 and 95% gradient strength. In this case, the intensity loss of the echo was in the range of 90%. Due to a short spin lattice relation time (T_1), longer diffusion time results in a loss of signal intensity. The T_1 was measured using the inversion recovery method[77]. It was done before the diffusion coefficient of Pluronic was measured. They were done using a 2D DOSY [78] sequence by incrementing in 32 linear steps from 2 to 100% with the TXI probe as well as 16 gradient linear steps with the diffusion probe. The 2D NMR sequences used for measuring diffusion coefficient using echoes for convection compensation and longitudinal eddy current delays to store the magnetization in the z-axis. It also was only dependent on T_1-relaxation. The diffusion coefficient was automatically calculated with the mono exponential function[63]:

$$\ln\left(\frac{I(G)}{I(0)}\right) = -\Upsilon^2\delta^2G^2\left(\Delta - \frac{\delta}{3}\right)D \qquad (3.1)$$

Here *I(G)* and *I(0)* corresponds to the intensities of the signal with and without gradient. Υ is the gyromagnetic ratio of the nucleus, here ^{1}H. *G* is the gradient strength, while δ is the duration of the pulse field gradient. *D* is the diffusion coefficient in m^2/s, while Δ is the "diffusion time" of the molecule between the beginning of the two gradient pulses. In this case, the relaxation delay between the scans was 2 seconds.

The 2D sequence, used for these diffusion measurements, used double stimulated echo with three spoil gradients for convection compensation and with an eddy current delay of 5 ms for reduction[79].

3.4. Results

3.4.1. Surface tension

3.4.1.1. High molecular weight surfactant vs. low molecular weight surfactants

Similar to low molecular weight surfactants the surface tension decreases with increasing concentration of Pluronic. With increasing concentrations, this continues until a plateau is reached. This concentration is known as critical micelle concentration (CMC). It is a concentration, at which the whole air-water interface is covered with surfactants. At the same time in the bulk 50% of surfactants molecules are in micelles. The critical micelle concentration is described in detail in chapter 2.1.3. However, in comparison to low molecular surfactants, e.g. CTAB, the concentration range in which the surface tension decreases is much wider in case of Pluronic. Pluronic changes the

surface tension from nano-molar to milli-molar concentration (Figure 3.4). Unlike the CTAB surface tension curve in case of Pluronic the curves show two separate slopes, as can be seen by the two separate fits in the decreasing regime (Figure 3.4). At low concentrations, the decrease of the surface tension with increasing concentration is stronger than at higher concentration. At a specific concentration (in case of P136PG26 it is around 1 μmol/l) the curve becomes less steep. The decrease in the surface tension then continues until the CMC is reached. At higher concentrations, the surface tension is constant.

This unusual shape of the surface tension curve can be explained by the conformation change of the Pluronic molecules at the surface[44,47,65]. At low concentrations, the Pluronic molecule adsorbs fully, i.e. the PEO and PPO blocks, to the surface (A) (Figure 3.4 A). At point (B) the surface is fully covered with Pluronic (Figure 3.4 B). With increasing concentration, the more hydrophilic PEO blocks are moved from the surface into the bulk liquid and are replaced by more hydrophobic PPO blocks (C) (Figure 3.4 C). This process continues until the whole surface is covered with PPG blocks (D) (Figure 3.4 D). Only then aggregates starts forming in the bulk. The point B (Figure 3.4 B) is the concentration of the full coverage (CFSC) and D (Figure 3.4 D) is the critical micelle concentration (CMC).

For low molecular size surfactants those two characteristic concentrations are equal. While for Pluronic they are a different by a few orders of magnitude. This can explain why the reported CMC for Pluronic varies largely in literature. Just for the P136PG26 the CMC varies between 2.8 μmol/l[80,81] to around 3 mmol/l[31,34].

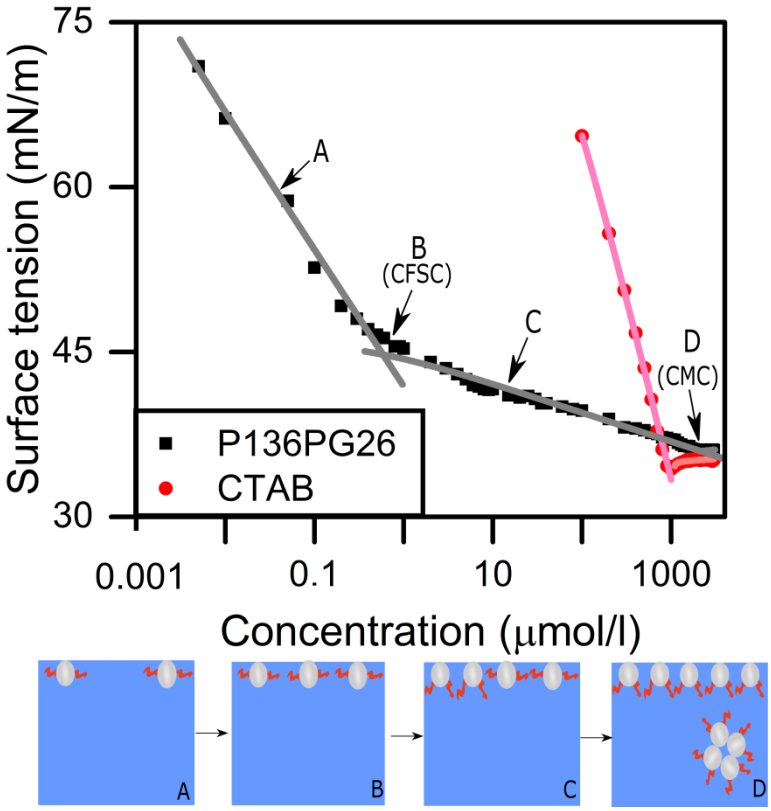

Figure 3.4 Surface tension curves for P136PG26 and CTAB. The points A-D agree with the stages of the proposed model of surface coverage[44,47,65] *At lower concentration the Pluronic adsorbs entirely to the surface (A), which continues until the hole surface is covered with them (B). With increasing concentration part of the PEO block of Pluronic is moved from the surface into the bulk liquid and replaced by PPO (C). Only when the whole surface is filled with the bended Pluronic molecules there are aggregates in the bulk (D). Reprint from Truszkowska et al*[65].

3.4.1.2.Polypropylene oxide (PPO) and Polyethylene oxide (PEO)

The proposed model of surface coverage assumes that the hydrophilic PEO blocks are moved from the air-water interface to the bulk liquid by the more hydrophobic PPO blocks. This should also happen when the PEO and PPO blocks are unconnected. To check that, at first the surface tension of PEO was measured (Figure 3.5.). When PEO is slightly active, this results in a slight decrease in the surface tension with increasing concentration. For the next step, PPO was added to the solution that already contained PEO (Figure 3.5.). This resulted in a strong reduction of the surface tension, which indicated that the PPO can replace PEO at the surface. This result fits the proposed model of surface coverage (Figure 3.4).

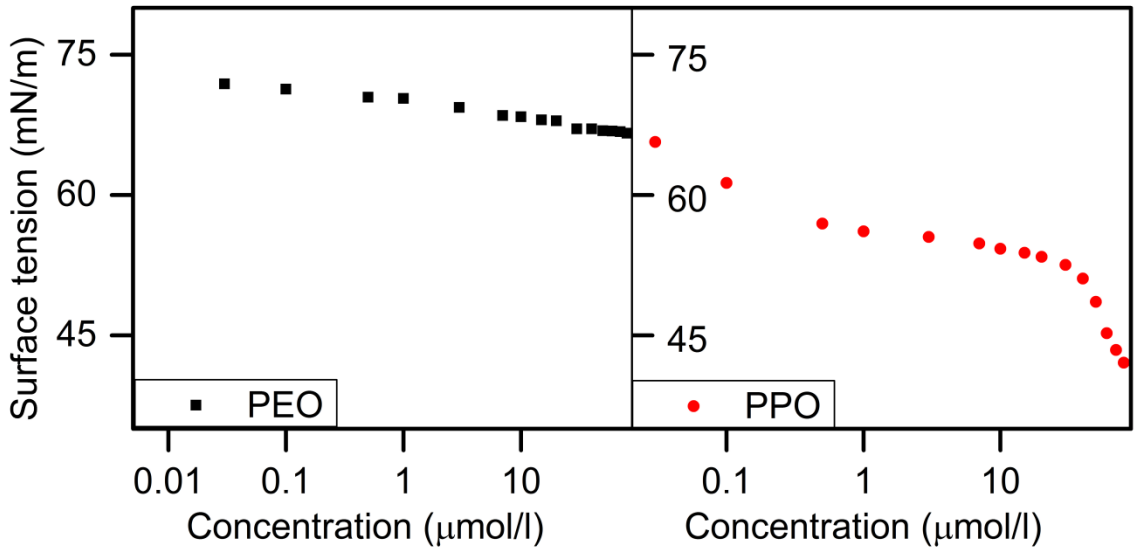

Figure 3.5. Surface tension vs concentration of PEO (■) and PPO (●). PEO results in a slight decrease of surface tension with increasing concentration. When PPO is added the surface tension strongly decreases. It indicates that PPO replaces PEO at the surface. Reprint from Truszkowska et al.[65]

3.4.1.3.Surface tension PEO:PPO ratio

The existence of two characteristic concentrations can be also shown for the other tested Pluronics (Figure 3.6). However, there are two groups visible depending on the amount of hydrophobic PPO. The surface tension for Pluronics with large %PPO, P20PG88 and P55PG88, shows a decrease in a surface tension over a smaller range of concentration (nano-molar to micro-molar) than the Pluronic with small % PPO, P19PG40; P54PG53, P84PG17 and P136PG26, where it was between nano-molar and milli-molar.

Alexandritis et al.[34] have shown that the amount of PPO and PEO as well the molecular weight of Pluronic influences the CMC. In case when Pluronic have the same amount of PEO an increasing amount of PPO will decrease the CMC. In the opposite situation when number of PPO is constant, an increase in amount of PEO slightly increases the CMC. While for Pluronic with the same ratio of PEO: PPO, the CMC will decrease with increasing molecular weight.

Since all the studied Pluronics, Table 3.1, have different length of the outside PEO blocks, it is impossible to look into the influence of the PPO on the CMC. However, there are two pairs of Pluronic, that have the same length of middle PPO block but different length of PEO blocks (P84PG17:P20PG88 that have 30 PPO blocks and

P136PG26:P55PG88 with 75 PPO blocks). The CMC of P20PG88, 2 PEO blocks on each side, is 20 μmol/l. While the CMC of P84PG17, 75 outside PEO blocks, is 2100 μmol/l. It is similar for the second pair of Pluronic with the same length of PPO blocks. The CMC for P55PG88 is 5 μmol/l and for P136PG26 is 2000 μmol/l. P55PG88 and P136PG26 has 5 and 100 outside PEO blocks. This fits with the influence of PEO blocks described by Alexandritis et al.[34] Additionally, there are two Pluronics that have the same ratio of PEO:PPO but different molecular weight (P20PG88 and P55PG88). Alexandritis et al[34] mentions that in this case with increasing molecular weight the CMC decreases and it is true for the tested Pluronics.

From the surface tension curve, it was possible to determinate both the CFSC and CMC of the Pluronics (Figure 3.6). Each of the curves can be divided into three parts:

1. Steeply decreasing part at concentrations below the CFSC
2. Less steep decrease at concentration between CFSC and CMC
3. Constant surface tension at concentration higher than CMC

For each of the curves it was possible to do a logarithmic fit ($y = a - b\ln(x + c)$). For the fit the concentration at which each of the part started and ended was chosen depending on the surface tension. For the fit of Part 1 the range of concentration was chosen until a concentration at which the change in surface tension became less steep. This point overlaps with the concentration range for part 2, which continues until the concentration at which the plateau in surface tension started. This is also the point at which the part 3 starts. The CFSC and CMC correspond to the points at which the curves intersect with each other. The CFSC is the intersection between part 1 and part 2, while the CMC is the intersection between part 2 and part 3. The points at which each of the parts, thus the CFSC and CMC, was slightly harder to distinguish for P19PG40 and P54PG53. For P19PG40 the end of one part and start of the next one is not as defined as for others Pluronic. Making it harder to determine the CFSC and CMC. For P54PG53 between part 1 and part 2 there is a kink, making it also harder to pinpoint the exact concentration at which part 1 ends and part 2 begins. This again influences the measured CFSC. For the fit the points at the kink were cut out. From the fit the CFSC was measured. This means that the CFSC and CMC for those two Pluronic have higher uncertainty then for the others. The exact value of CFSC and CMC for each Pluronic are given in table 3.1.

The CFSC is influenced by the molecular weight and length of PEO blocks in the same way the CMC is[34]. For P20PG88 and P55PG88, that have the same PEO: PPO ratio, the CFSC, just like the CMC, decreases with increasing molecular weight. As mentioned before the CMC is influenced by the length of PEO blocks. In the case of Pluronic with the same length of the middle PPO blocks, the CMC and the CFSC increases with increasing length of PEO. As mentioned before it is impossible to investigate the influence of the length of the PPO blocks as Pluronic used in this study have different length of PEO blocks.

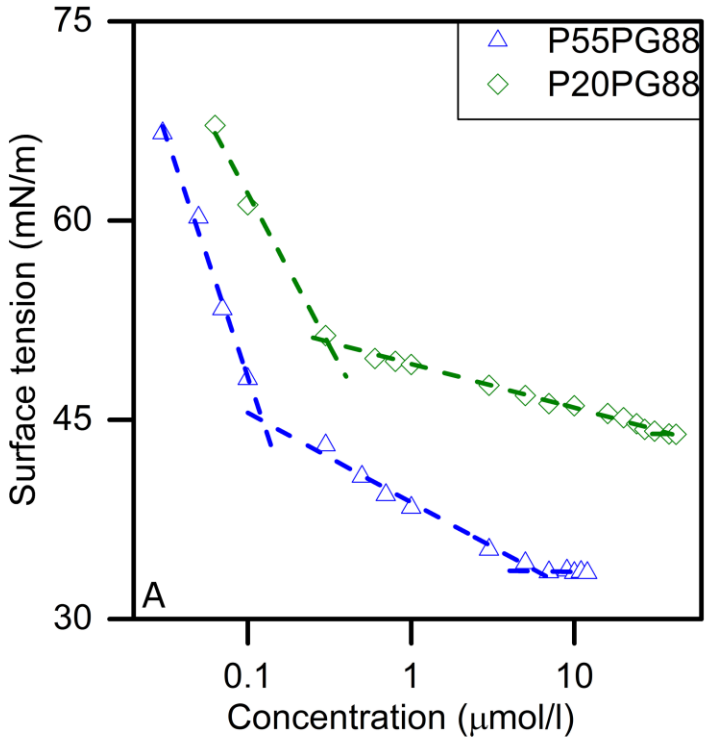

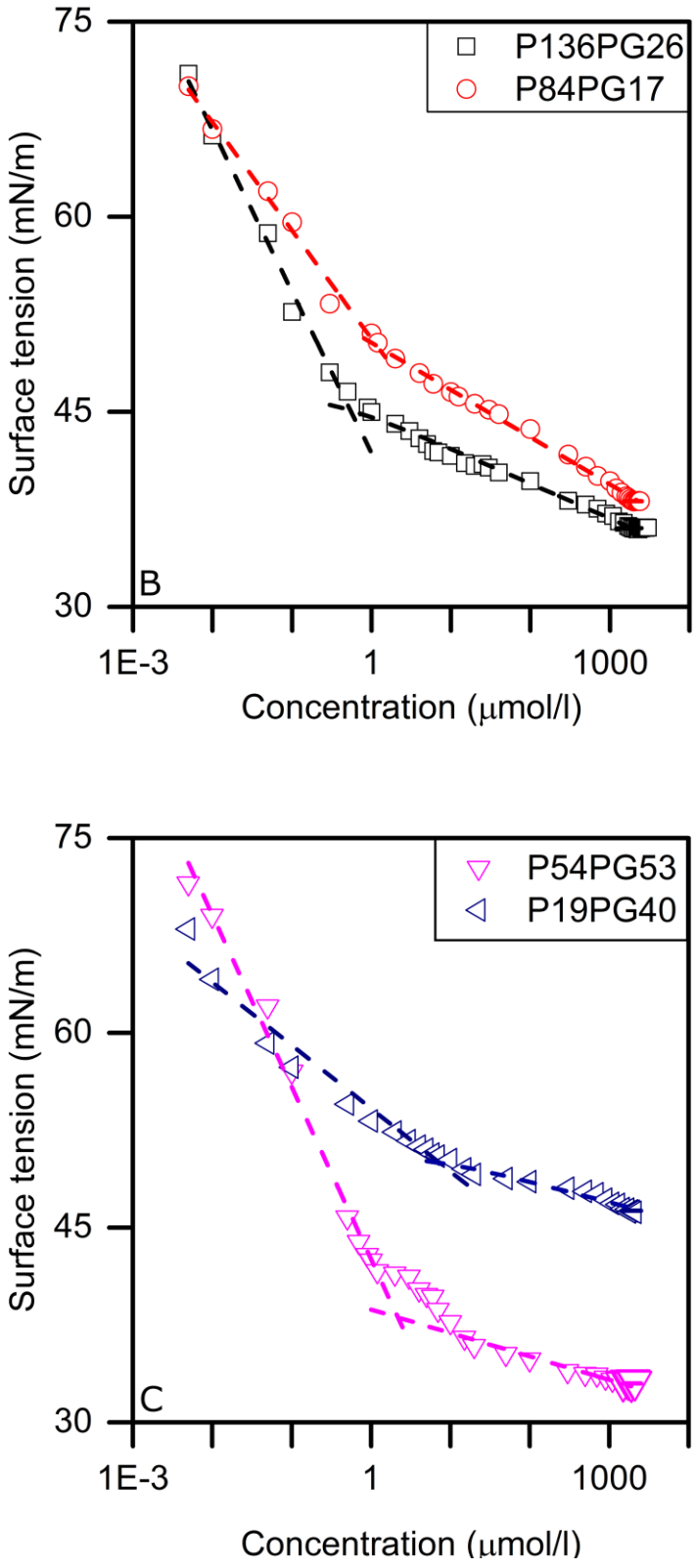

Figure 3.6. Surface tension curves of Pluronic with large %PPO (A) and small % PPO (B, C). All of them show the same shape of the surface tension curve. Indicating that all Pluronic have both CFSC and CMC and between them there are few orders of magnitude.

3.4.1.4. Surface excess

Every two-component system can be divided into two bulk phases with specific volume, V^{α} and V^{β}, and the interface σ[53]. In the Gibbs model, all the extensive thermodynamic quantities can be written as a sum of three components. However, at the interface there is a change in molecular composition. The actual number of molecules N_i of component *i* at the interface will be shown as

$$N_i^{\sigma} = N_i - c_i^{\alpha} V^{\alpha} - c_i^{\beta} V^{\beta} \qquad (3.2)$$

Where c_i^{α} and c_i^{β} are the concentration of the *i*th component in the two phases, and N_i is the total number of molecules of component *i*. From this equation it is possible to estimate an interfacial excess Γ_i, which is the amount of component actually present in the system close to the interface in comparison to a reference system:

$$\Gamma_i = \frac{N_i^{\sigma}}{A} \qquad (3.3)$$

A is in this case the interfacial area. The interfacial excess is described either as a number of molecules per area or in mol/m^2. Two component system, with a solvent 1 and solute 2, is the easiest application of the Gibbs adsorption isotherm. The change in surface tension can be described as

$$d\gamma = -\Gamma_1 d\mu_1 - \Gamma_2 d\mu_2 \qquad (3.4)$$

where the Γ_1 and Γ_2 represent the surface excess of the solvent and solute. μ_1 and μ_2 is the chemical potential of the solvent and solute. In a situation when the ideal interface is defined, the surface excess of solvent, $\Gamma_1=0$, the equation (3.4) can be described as:

$$d\gamma = -\Gamma_2^{(1)} d\mu_2 \qquad (3.5)$$

the superscript (1) indicates that a special interface was chosen. The chemical potential of the solute, μ_2, is:

$$\mu_2 = \mu_2^0 + RT \ln \frac{a}{a_0} \qquad (3.6)$$

Where $\mu_2{}^0$ is the standard state chemical potential. *a* is the activity of the surfactant and a_0 is the standard activity of 1 mol/L. For ion-ion and ion-H_20 the number of ions that can react chemically ("free" ions) is sometimes less than the concentration states. *a*

corresponds to the number of "free" ions. The concentration, *c*, and *a* is connected to each other through activity coefficient, *α*.

$$a = \alpha c \tag{3.7}$$

When the concentration and activity are equal then $\alpha=1$. *R* and *T* are the gas constant and temperature. At constant temperature with respect to a/a_0 it is possible to differentiate equation (3.6) at constant temperature with respect to a/a_0 to:

$$d\mu_2 = RT\,\frac{d(a/a_0)}{a/a_0} = RT\,\frac{da}{a} \tag{3.8}$$

When substituting equation (3.7) into equation (3.5) it leads to

$$\Gamma_2^{(1)} = -\frac{a}{RT}\frac{\partial \gamma}{\partial a} \tag{3.9}$$

In a situation when the solute at the interface is enriched, $\Gamma^{(1)}>0$, the surface tension will decrease with increasing concentration. The interface excess values calculated for Pluronic are in similar range to the ones from the small molecular weight surfactants, CTAB and C12E5 (Figure 3.7.). The difference between them is the charge. CTAB is a cationic surfactant while C12E5 is nonionic.

For all surfactants, Pluronic, CTAB and C12E5, with increasing concentration the surface excess increases until the CMC. Afterwards the surface excess remains contact. It is rather surprising, considering the size of tested Pluronic. Just looking at the molecular weight, which varied between 1900 – 13 600 g/mol, it was rather expected that the surface excess should differ more between the Pluronic.

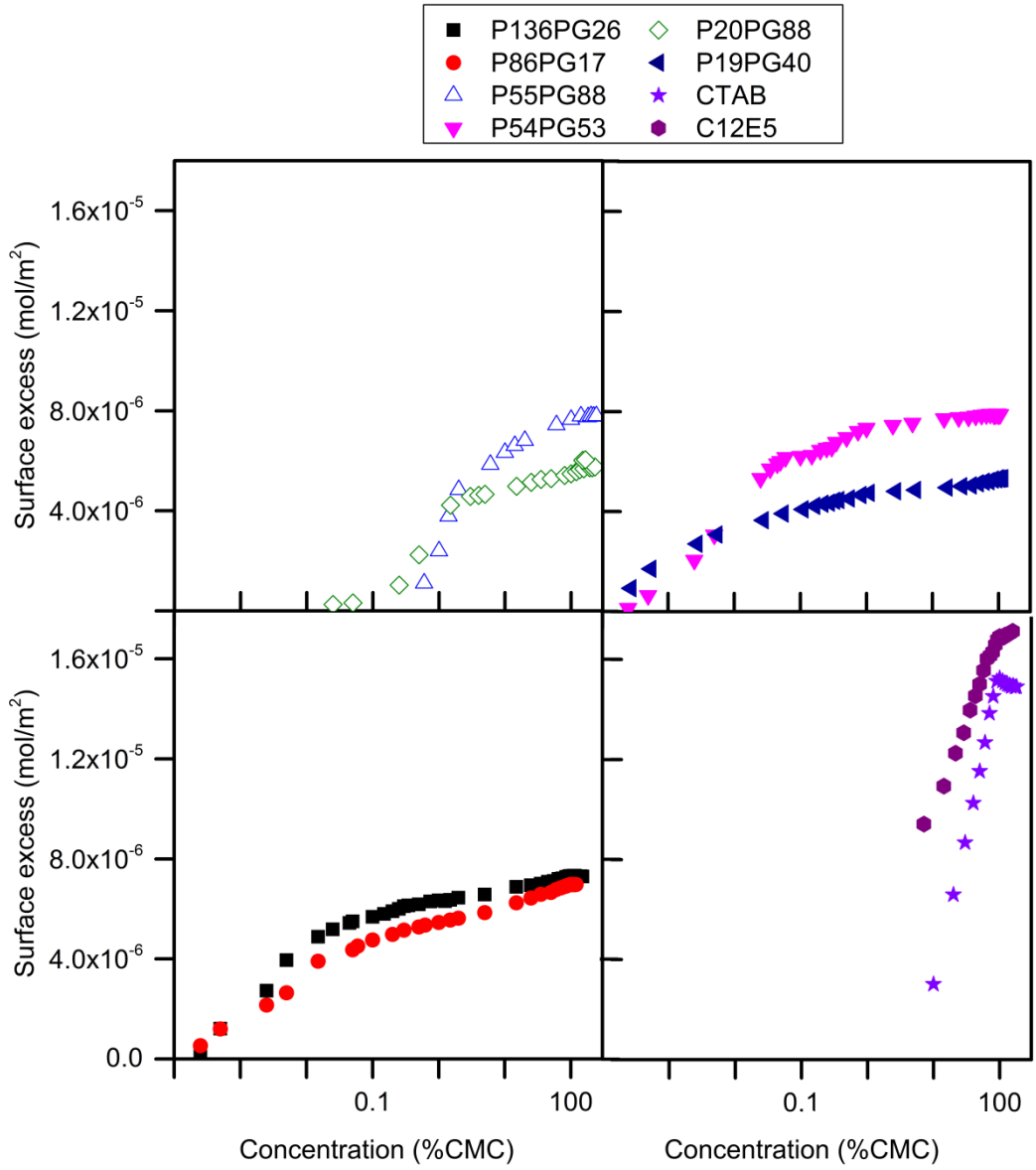

Figure 3.7. Surface excess, calculated using equation 3.3, at different %CMC for different Pluronic and two small molecular weight surfactants, CTAB and C12E5. For all surfactants the surface excess increases with increasing concentration. The surface excess for different Pluronic is similar to each other.

3.4.1.5.Area pro molecule

From the surface excess, Γ, it is possible to estimate the area the molecule is taking at the surface, A:

$$A = \frac{1}{N_A \Gamma} \qquad (3.10)$$

Here, N_A, is the Avogadro constant. The calculated area per molecule for different Pluronic does not differ so much from the one for smaller surfactants (Figure 3.8). In this case, the smaller size surfactants are CTAB and C12E5. This result is rather unusual since the smallest used Pluronic, P19PG40, is already around 5 times larger than CTAB and C12E5. Even in case of Pluronic, which molecular weight varies between 1900-13600 g/mol, the calculated area per molecule is similar to each other. This shows that the Pluronic adsorb to the surface not as a whole molecule. It rather absorbs in parts. First absorb the hydrophobic PPO blocks and then hydrophilic PEO blocks. The PPO and PEO blocks also probably do not absorb as one block. They rather absorb piece by piece to the surface.

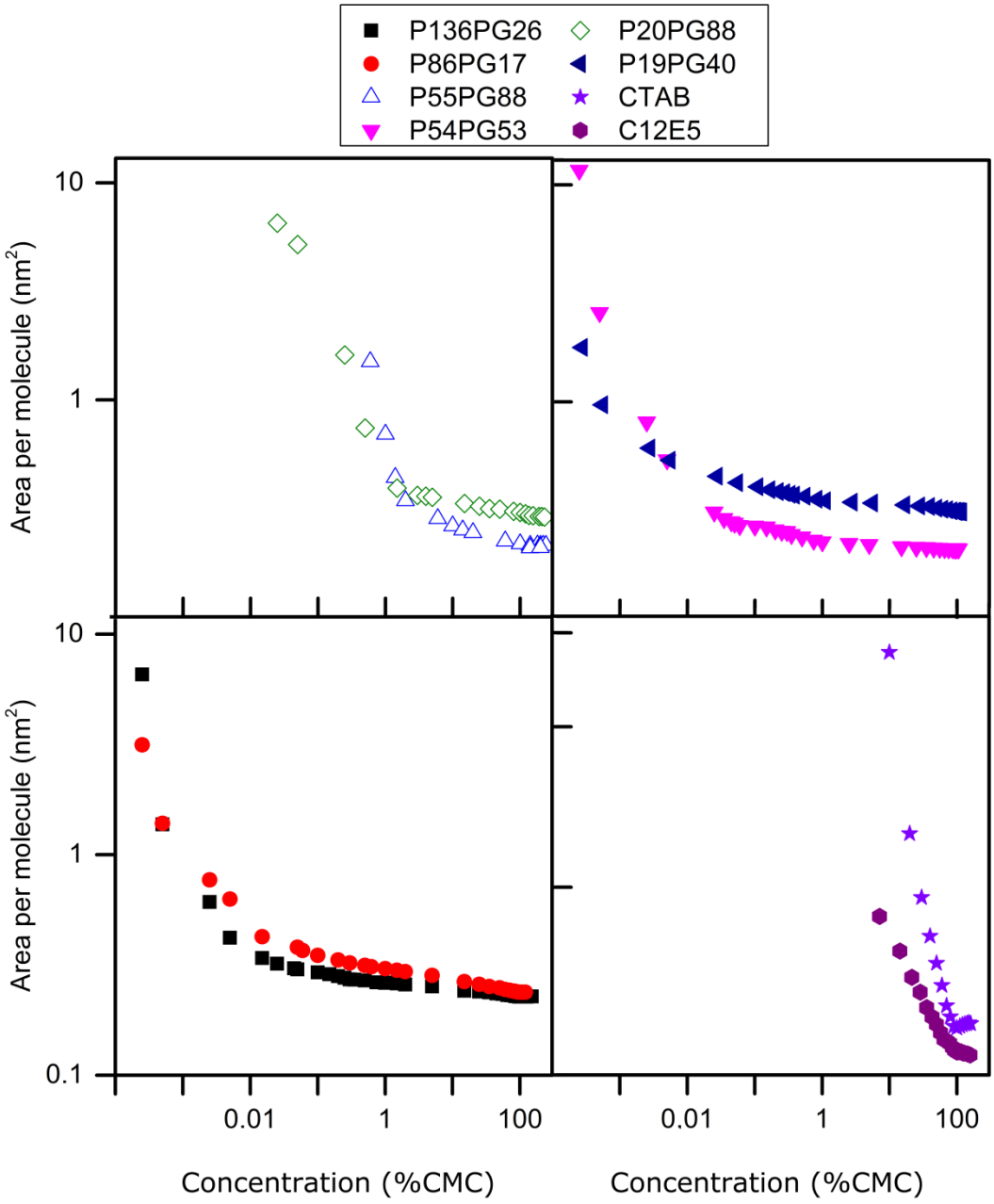

Figure 3.8. Area per molecule at the surface for different Pluronic as well as CTAB and C12E5. Even though there is a large differenc between the size of different Pluronic and CTAB or C12E5 the calculated area per molecule is similar.

3.4.2. Aggregation behavior

This part was done in cooperation with Dr. K. Koynov and the measurements were performed by J. Schultze. The description of the fluorescence correlation spectroscopy (FCS) can be found in chapter 2.1.14.

For Pluronic there are two characteristic concentrations, CFSC and CMC, see chapter 3.4.1.1. In both the air-water interface is fully covered by the differently oriented

Pluronic molecules. At CFSC Pluronic are flatly oriented at the surface (Figure 3.4.). With increasing concentration the hydrophilic PEO blocks of the Pluronic molecule bends into the bulk and the PPO blocks remain at the air-water interface. This process continues until the CMC is reached, where the whole surface is covered by bended Pluronic. However, the question remains, at which concentrations aggregates form in the bulk. To answer this question, the aggregation behavior in the bulk was studied using fluorescence correlation spectroscopy (FCS). The principals of FCS were described in detail in chapter 2.16. Due to high sensitivity of this method it is suitable for looking into micelle formation[82-84]in system with very low CMC. The aggregation behavior was measured by a method first suggested by Horn et al[82]. In this method, a small amount of Rhodamine 6G (Rh6G) was added to a solution of P136PG26 with a specific concentration. This allowed to estimate the apparent hydrodynamic radius of R_{app} of Rh6G at different concentration of P1236PG26. Rh6G is amphiphilic. This means that when micelles are present, the Rh6G would be situated inside the micelle. This would result in an increase in the R_{app} of Rh6G in comparison to the R_{app} for free Rh6G in micelles. In Figure 3.8 shows the measured autocorrelation function. At concentrations below CMC the hydrodynamic radius of Rh6G is the same as the hydrodynamic radius of a single Rh6G molecule. Only at concentration higher than CMC the measured apparent hydrodynamic radius of Rh6G increases, which indicates presence of micelles in the bulk. This data (Figure 3.9) clearly shows that in case of P136PG26 micelles are only present above the CMC. This suggests that the conformation change of Pluronic at the surface above CFSC is only a surface feature and does not influence any changes in the bulk properties.

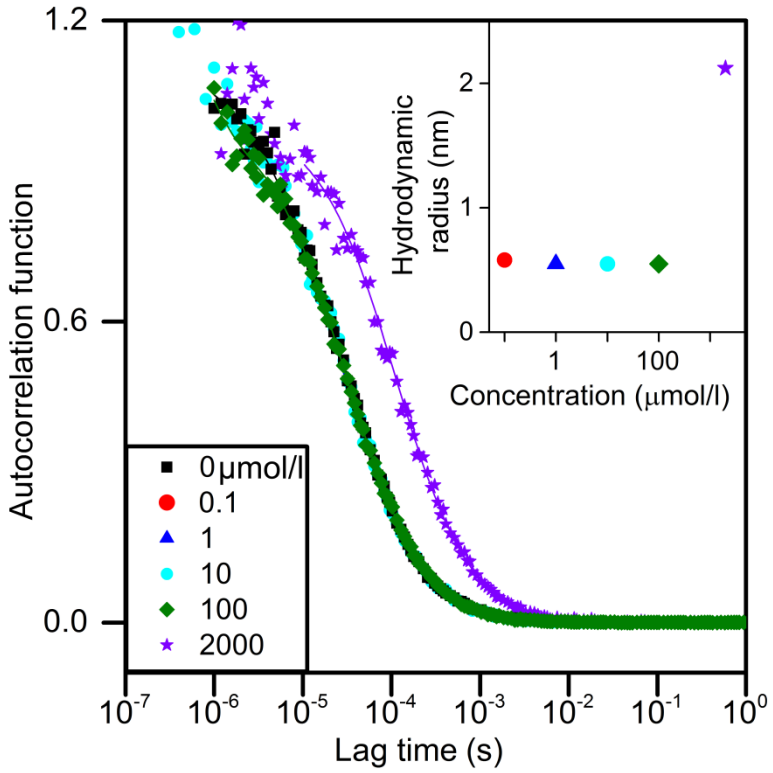

Figure 3.9 FCS autocorrelation curves for mixtures of Rhodamine 6G in water or in Pluronic P136PG26. For Rhodamine 6G: water and Rhodamine solutions at low concentrations the autocorrelation functions overlap. At these concentrations, there are no micelles present. Only at concentration higher than CMC, in this case 2000 µmol/l micelles are present. This figure was adapted from Truszkowska et al[65].

3.4.3. Diffusion coefficient of Pluronic

The diffusion coefficient for Pluronic at different concentrations (Figure 3.10) was measured by M. Wagner. All of the used concentrations were measured below the (CMC). The used concentrations were either below or higher than the CFSC. The exact values for both CMC and CFSC can be found in table 3.1.

The FCS measurements, described in chapter 3.4.2, indicates that there no micelles present at concentration below the CMC. However, it is possible that at those concentrations Pluronic forms aggregates in the bulk. It is impossible to tell it using FCS, since it measures the hydrodynamic radius of Rh6G and not of Pluronic. The measured diffusion coefficient should correspond only to single Pluronic molecules.

In case of P55PG88, Pluronic with large %PPO, the diffusion does not change with increasing concentration. While for the Pluronic with small %PPO, P19PG40; P54PG53; P84PG17 and P136PG26, the diffusion coefficient changes depending on concentration. From the measured diffusion coefficient, *D*, it was possible to calculate the hydrodynamic radius, *R*, of Pluronic using Stokes-Einstein equation (equation 2.23), mentioned in chapter 2.1.14.

Unfortunately for Pluronic, P20PG88, it was possible only to measure one concentration below the CMC. It was because both the CMC and molecular weight of this Pluronic is very low. It was only possible to measure one sample, that had a concentration close to the CMC. There was no signal at lower concentrations. Making it impossible to measure any further samples with lower concentrations. The focus of this work was on the bulk behavior of Pluronic in the bulk at concentrations below the CMC. For this reason, no further samples with concentrations larger than CMC were measured. For concentrations above the CMC the measured diffusion would be for Pluronic micelles and not Pluronic molecules.

For P55PG88 the hydrodynamic radius is similar in both concentrations tested, around 0.5 nm. While for the other Pluronic, all with small % PPO, the calculated hydrodynamic radius is different at different concentrations, varied between 0.6-1.6 nm. This can be explained by different forms Pluronic can have in a bulk (Figure 2.5).

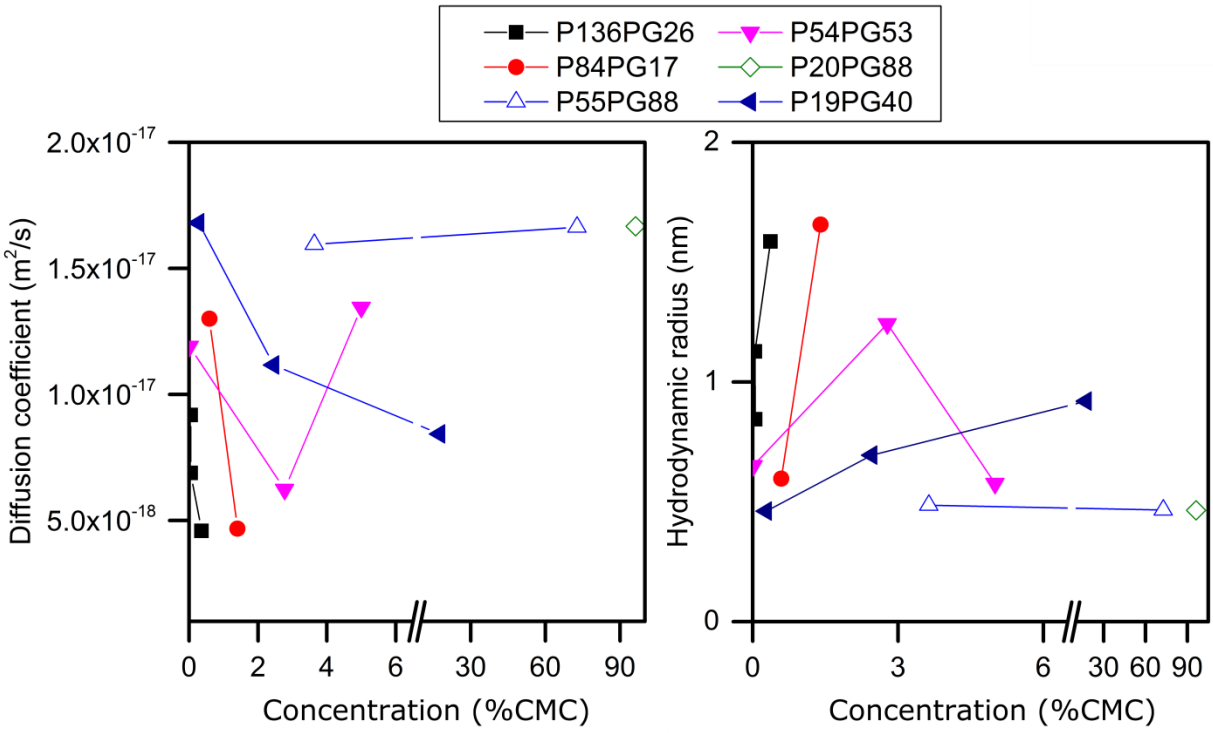

Figure 3.10. Diffusion coefficient and hydrodynamic radius for studied Pluronic at different concentration below the CMC. In the bulk at these concentrations no micelles are present. In case of Pluronic the diffusion constant for Pluronic with large %PPO is independent from the concentration. While for Pluronic with small %PPO, the diffusion coefficient differs in different concentration. This indicates that in the bulk there might be aggregates made from two or more Pluronic molecules present.

For most Pluronic the diffusion coefficient decreases with increasing concentration. For P54PG53 the curve looks slightly different. Just like other Plutonic, at the beginning the curve for P54PG53 decreases with increasing concentration. However, then with increasing concentration the diffusion coefficient increases, unlike the curves for other Pluronic. At this point, I am unable to exactly say which of those molecular species are present in the bulk at specific concentrations. Based on the diffusion coefficients, aggregates are more likely than micelles. However, it is difficult to verify this working hypothesis based solely on hydrodynamic radius measurements.

The hydrodynamic radius measured from the FCS and NMR for P136PG26 differs from each other. During FSC and at concentrations above CMC, the Rh6G is only present inside micelles and the hydrodynamic radius measured corresponds to the micelles, as can also be seen in Figure 3.10. In NMR measurements, the measured hydrodynamic

radius corresponds to free P136PG26 or small aggregates of P136PG26, as the concentration used does not allow for micelles. The measurements point at a positive correlation between size and hydrodynamic radius, as expected.

Similar to small molecular weight surfactants at concentration higher than the CMC Pluronic form micelles. However, in lower concentration the Pluronic can have different forms in the bulk (Figure 2.5.), as mentioned in chapter 2.1.2. At lower concentration, Pluronic can either adsorb into the air-water interface or be in the bulk in a form of free surfactants. Apart from that, Pluronic can also be in a form of a unimer, where the hydrophilic PEO blocks create a shell around the middle hydrophobic PPO blocks[34,35,38,48,49]. This is only possible for Pluronic with long outside PEO blocks. When the PEO block, is much shorter than the middle PPO block it is unable to create a shell around the middle blocks. It is also possible for Pluronic to form aggregates at higher concentrations. They are made from two or more Pluronic molecules. All of this can explain why the diffusion coefficient changes with increasing concentration (Figure 3.10). Since those aggregates are bigger than the unimer or free Pluronic. At this point, it is unable to exactly say which of those molecular species are present in the bulk at specific concentration. To do it further work would have to be done.

3.4.4 Surface Rheology

The hypothesis of the flow profile close to the 3-phase contact line, described in 2.11, makes a connection between surface tension gradients and creation of liquid-air interface close to the three-phase contact line. The hypothesis implies a fresh build liquid-air surface is created close to the three-phase contact line. The creation of this new surface is a similar process to surface expansion. One parameter connected to surface expansion is surface elasticity. A way to describe the surface elasticity is to look into the interfacial viscoelastic modulus, using the oscillating drop method (ODG). The theoretical background of this method is discussed in detail in chapter 2.14. In this work, we measure the viscoelastic modulus of Pluronic solutions as a function of frequency and concentration.

In this experiment, I look at changes of the surface tension, $\delta\gamma$, as a function of the change in the relative interfacial area of the droplet $\delta \ln A$. Previous works[41,85] showed that for small molecular weight surfactants the peak of viscoelastic modulus corresponds with the CMC, concentration at which the whole surface should be fully

covered by the surfactants. Thereby follow that the oscillating drop method is able to measure the concentration at which the whole air-liquid interface is fully covered with surfactants. For Pluronic the viscoelastic modulus curve looks different than for the one of small molecular weight surfactants (Figure 3.11 and 3.12), where there are two peaks present. The peak at lower concentrations corresponds to CFSC, while the second one corresponds to CMC.

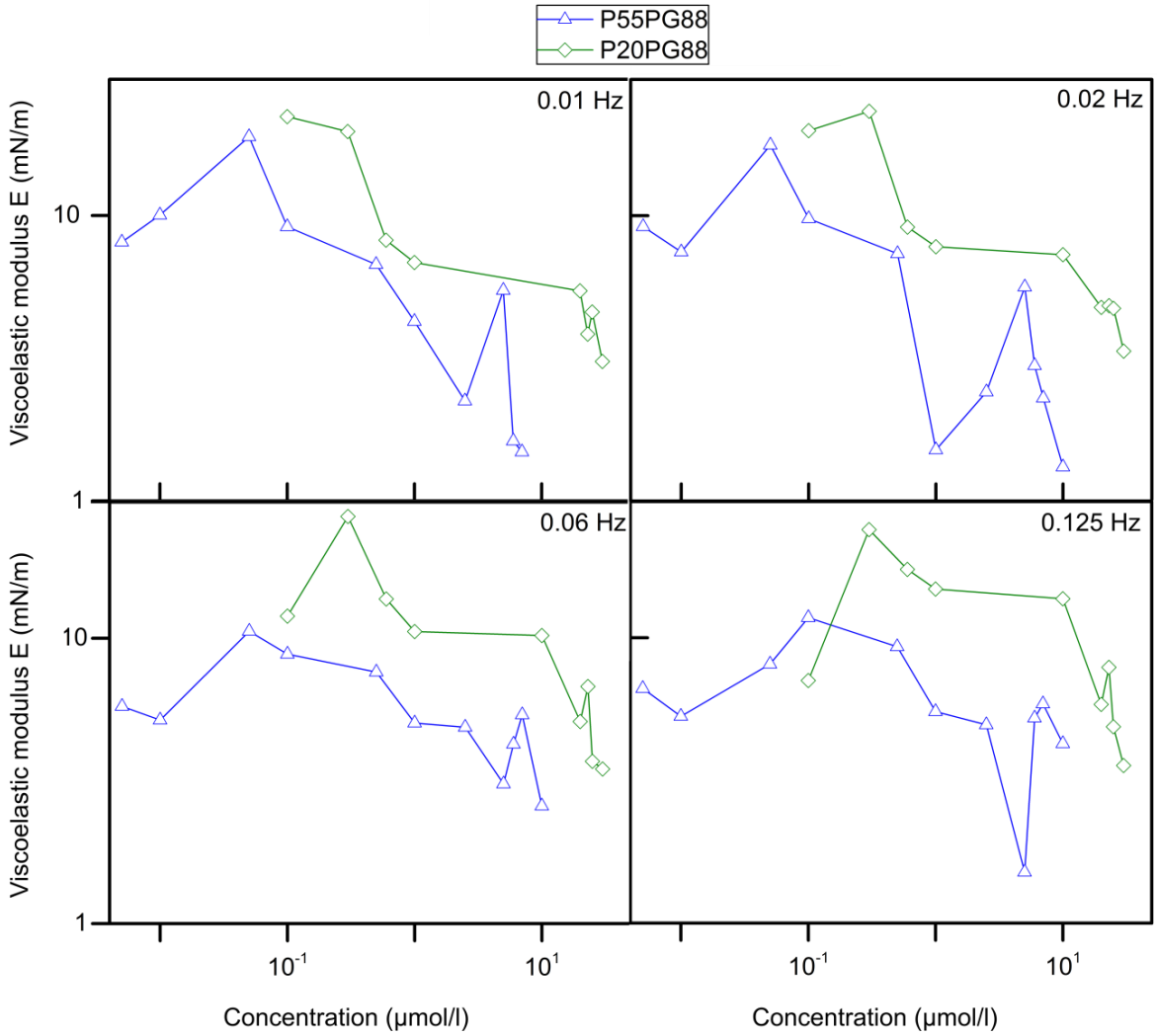

Figure 3.11. Viscoelastic modulus for Pluronic with large %PPO at different concentrations at frequencies between 0.01-0.125 Hz. Similar to Pluronic with small %PPO two peaks are visible. The concentration at which the viscoelastic modulus has a peak is the concentration corresponding to concentration at which the surface is fully taken by surfactants. The one at lower concentrations corresponds with the CFSC and the second peak corresponds with CMC. Both CMC and CFSC estimated from this method fit with the ones measured from surface tension (Figure 3.5).

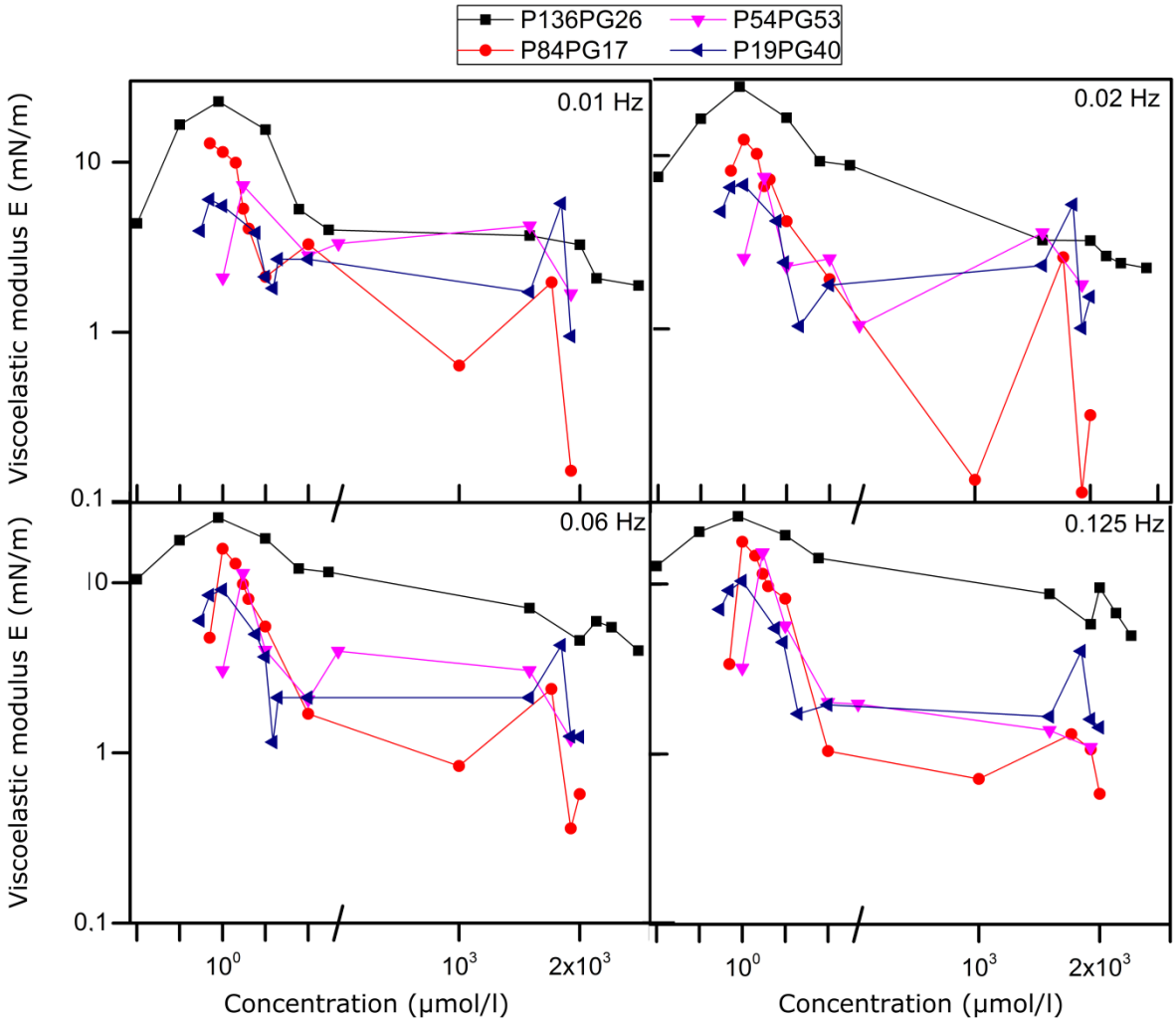

Figure 3.12 Viscoelastic modulus for Pluronic with small %PPO at different concentrations at frequencies between 0.01-0.125 Hz. In case all cases there are two peaks visible. The concentration at which the viscoelastic modulus has a peak is the concentration corresponding to concentration at which the surface is fully taken by surfactants. First one is at lower concentrations and the second one is at higher concentration. These peaks correspond with the CFSC and CMC. Furthermore, both CFSC and CMC measured with this method correspond with the one measured from surface tension measurements.

For the Pluronic with small % PPO this is shown in Figure 3.11 and for the big % PPO in Figure 3.10. The presence of two peaks clearly indicates that there are two

independent concentrations at which the whole surface is fully occupied by a layer of surfactants. This clearly fits with the proposed model of surface coverage for Pluronic (Figure 3.3.). The first characteristic concentration is the CFSC, at which the whole surface is fully taken by flatly oriented Pluronic. With increasing concentration, parts of the Pluronic (hydrophilic PEO blocks) bend into the direction of the bulk and the hydrophobic PPO blocks stay at the interface. As a result, the layer of Pluronic at the air-water interface is not uniform. This results in a decrease in the viscoelasticity. However, the viscoelastic modulus does not reduce completely, like it does for pure water. This means that the surface still has some elasticity. It is due to PEO chain not being entirely folded in the direction of the bulk. This trend continues until the CMC is reached and another peak is visible. At the CMC, the whole air-water interface is occupied by bended Pluronic (Figure 3.4). Furthermore, for all Pluronics the CFSC and CMC measured with the oscillating drop method are close to the ones measured by surface tension measurements (Table 3.2.). CFSC of P20PG88 or CMC of P55PG88 and P136PG26, the values are identical. For others Pluronics the differences are larger. For example, for P84PG17 both CFSC and CMC measured through ODG varies from the one measured from surface tension. For this Pluronic using ODG, measured CFSC at 1 μmol/l and CMC at 1800 μmol/l, while from surface tension measurements CFSC and C'MC are 3.5 μmol/l and 2100 μmol/l respectively. The difference can is within the accuracy of the equipment. There is one Pluronic (P19PG40), for which the CFSC measuring using the ODG and surface tension had an even larger difference. For P19PG40 the CFSC measured through surface tension is 10 μmol/l, while the one measured from ODG is around 2 μmol/l. However, even though there are small differences between the CFSC and CMC values depending on the measuring method, the ODG can be used as an alternative for measuring the CFSC and CMC for surfactant solutions.

Pluronic	CFSC (μmol/l)		CMC (μmol/l)	
	Surface tension	Surface rheology	Surface tension	Surface rheology
P19PG40	10	2	1800	1800
P20PG88	0.3	0.3	20	23
P54PG53	2	4	2000	1800
P55PG88	0.15	0.05	5	5
P84PG17	3.5	1	2100	1800
P136PG26	1	0.8	2000	2000

Table 3.2. CFSC and CMC measured through surface tension measurements and ODG method at exemplary at 0.02 Hz. In case of ODG CFSC and CMC were measured by measuring the peak in viscoelastic modulus (Figure 3.10 and Figure 3.11). Both CFSC and CMC measured from those two methods are close to each other.

3.4.5. Rotating Drum

3.4.5.1 Receding dynamic contact angle

Using the rotating drum set-up described earlier in sections 2.1.10.2 and 3.3.4, the dynamic contact angle was measured in a range of velocities between 0-200 mm/s. The receding dynamic contact angles decrease with increasing velocity. Previous studies[1-4] showed that already at concentrations below the CMC, 5-15%CMC, the dynamic contact angle decreases in comparison to the one of pure water. These works[1-4] have also shown that the advancing dynamic contact angle is not as strongly affected by surfactants as the receding dynamic contact angle. For that reason, the focus of this work is the receding dynamic contact angle. Also the influence of adsorption and desorption kinetics of surfactant to and from the surface have been discussed before[1-3].

In those works, it was argued that these processes are not the limiting factor for the dynamic wetting of surfactants solutions. In that case a non-local process, such as diffusion of surfactant to the surface, seems to have a larger significance.

Also for Pluronic already a small amount of surfactant results in a change in the dynamic contact angle (Figure 3.13). The fundamental difference between the small sized surfactants and Pluronics is, however, the amount of surfactant added. For most of the small sized surfactants, significant changes in the dynamic contact angles were observed for surfactant concentrations between 5 %CMC and 15 %CMC[1-4]. In case of Pluronic the concentrations were much smaller. For P136PG26 already a concentration of 0.0004% CMC, which is around 0.08 μmol/l, decreases the receding dynamic contact angle. In case of other Pluronic the minimal concentration needed to cause a reduction in the receding dynamic contact angles differs from each other but is never larger than 0.01% CMC. Similar to low molecular weight surfactants with increasing concentration, the receding dynamic contact angles continue to decrease. At low velocities, till 10 mm/s, the decrease in the dynamic contact angle is stronger than at higher velocities. This is similar for all studied surfactants.

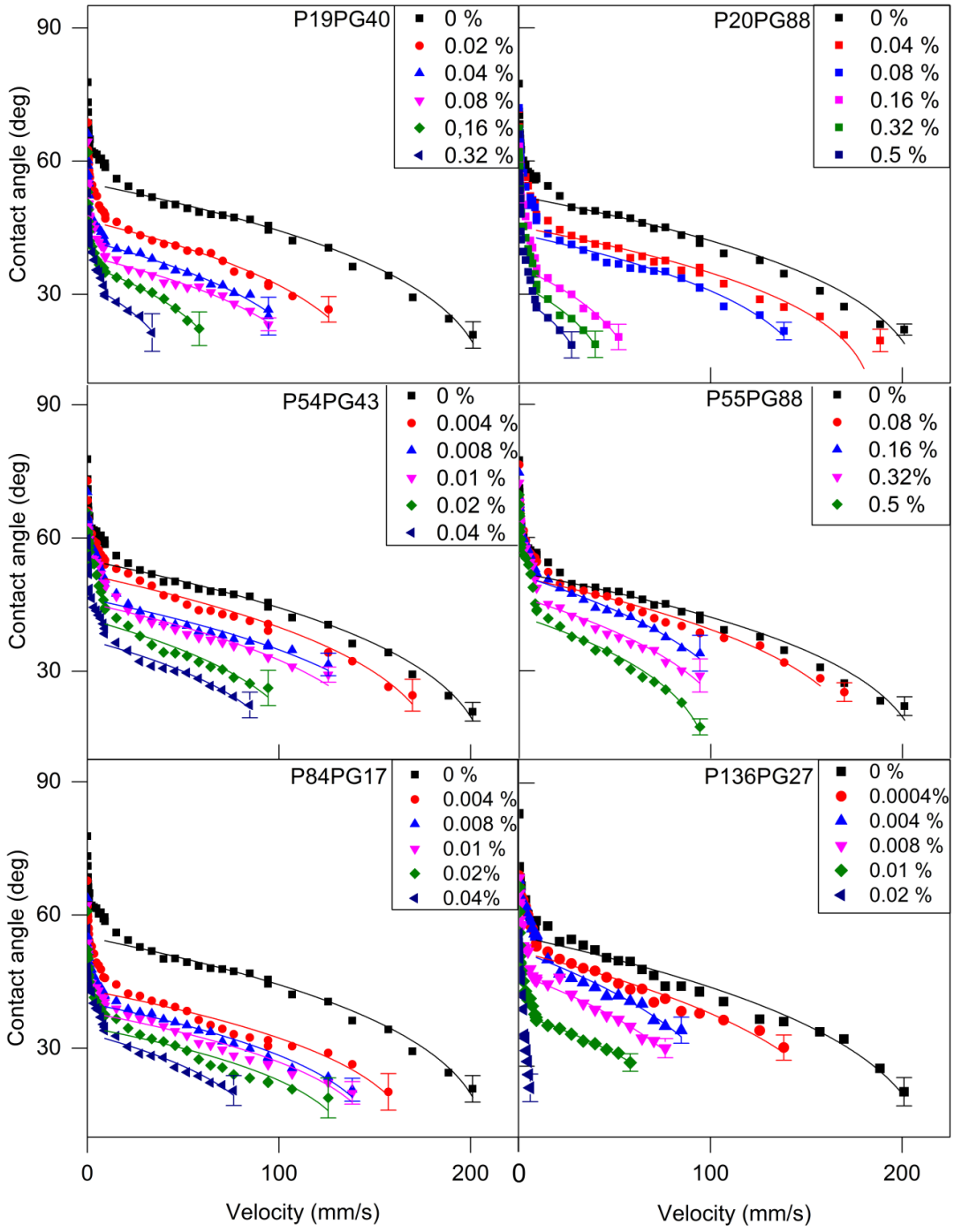

Figure 3.13. The dynamic receding dynamic contact angle for all studied Pluronics as a function of velocity. The concentration is in % CMC, which means that the concentration varies between 0.009 µmol/l-5.8 µmol/l depending on the specific Pluronic. Already a small concentration of surfactant results in a decrease of the receding dynamic contact angle in comparison the ones of pure water (0% CMC). With increasing concentration of Pluronic the dynamic contact angle decreases. The solid lines represent a fit used with equation 3.11. For all curves the fitting only includes the velocities above 9 mm/s. The reason for it is discussed in chapter 3.4.5.2.

The change in the dynamic contact angle seen in Figure 3.13 can be explained by the detailed hypothesis of the flow close to the three-phase contact line explained in chapter 2.1.11 (Figure 2.21). In this model, while the drum is rotating it pulls up the liquid and close to the three-phase contact line a fresh surface is created. In this fresh surface there is a smaller amount of surfactant than in the bulk. In this hypothesis the solution that is far from the surface is considered as the bulk. This results in a gradient in the surface tension close to the three-phase contact line and the bulk. Due to this gradient there is Marangoni force in the direction of the three-phase contact line, thus the contact angle changes. The strength of this surface tension gradient is connected to the surface tension curve (Figure 3.6). However, those curves show rather the equilibrium surface tension. It means that at the moment of measurement the surface and the bulk were at adsorption and desorption equilibrium. However, in the hypothesis of the flow near the three-phase contact line the surface tension is not at equilibrium. Instead there is a stationary state of dynamic surface tension gradients between the freshly created surface close to the three-phase contact line and the bulk. According to the hypothesis (Figure 2.21) it is expected that increasing concentration will result in a larger gradient in surface tension. This then results in an increase in the receding dynamic contact angle.

3.4.5.1 Comparison with the hydrodynamic theory by Cox-Voinov

For all studied Pluronics the curves of the contact angle vs velocities show a couple of similarities (Figure 3.13). As mentioned above at lower velocities the dynamic contact angle changes more than at higher velocities. Depending on studied Pluronic the velocity at which the dynamic contact angle transits from a regime with large change in the contact angle to a regime of small change is slightly different. It depends also on the used surfactant concentration. In this chapter, the focus is on the dynamic contact angles at higher velocities.

As mentioned in chapter 2.1.8 there are different theories that describes the dynamic wetting behavior. In this thesis, the results presented in chapter 3.4.5.1 are compared with the hydrodynamic theory. Therefore, the experimental results at velocities larger than 9 mm/s (lines in Figure 3.13) were fitted with Cox-Voinov relation[61], which is described in section 2.1.8.2:

$$\theta^3 = \theta_0^3 - 9Ca\ ln\left(\frac{\alpha h}{\lambda}\right) \tag{3.11}$$

Where θ is the dynamic contact angle at specific velocity, and θ_0 and $\alpha h/\lambda$ are used as two fitting parameters in the Cox-Voinov relation. θ_0 describes the apparent receding

dynamic contact angle at zero velocity. The parameter *ln ($\alpha h/\lambda$),* corresponds to friction close to the three-phase contact line. A higher value of the "friction parameter" means a larger hydrodynamic dissipation (energy dissipation) close to the three-phase contact line.

It was impossible to fit with Cox-Voinov relation dynamic contact angle below a velocity of 10 mm/s. The stronger decrease at low velocity is yet now well understood. It might depend on the roughness of the drum surface. For that reason, further investigation has to be done to fully understand the dewetting behavior at low velocities.

Henrich et al.[4] had used the Cox-Voinov relation to fit the dynamic contact angle of various small molecular weight surfactants. Among the studied surfactants there were CTAB and C12E5. In that work the θ_0 and friction parameters were used as fitting parameters as well.

Henrich et al. [4] have shown that depending on the charge of the surfactant the friction parameter differs. In case of ionic surfactants, the friction parameter increases with increasing concentration. While for non-ionic surfactants the friction parameter is relatively constant. However, the exact values of the friction parameter for small molecular weight surfactants were shown to largely differ between each other [4]. In this chapter, the friction parameter of Pluronic is compared with the friction parameter of two small molecular weight surfactants, cationic CTAB and non-ionic C12E5. The friction parameters for Pluronic have similar trend to non-ionic surfactants (Figure 3.14 A) and does not increase with increasing concentration like for cationic surfactant CTAB. However, there are two groups of curves present. For P84PG17 and P54PG53 the friction parameter at first decreases with increasing concentration and then remains constant. For P19PG40, P20PG88, P136PG26 and P55PG88 the friction parameter at first decreases with increasing concentration up to a specific concentration at which the behavior is reversed and we observe an increase in friction. The reason why the friction parameter curves for different Pluronic differ from each other is unknown. While some Pluronic with similar molecular weight (P19PG40 and P20PG88) or length of PPO block (P136PG26 and P55PG88) do have similar friction parameter curves. At the moment there is no one clear parameter that would explain this behavior regarding all studied types of Pluronic. The curves are instead a result of a combination of different parameters rather than just one. Further discussion on this can be found in chapter 3.6.4.

The estimated contact angle at zero velocity θ_0 for Pluronic and C12E5 are similar to each other (Figure 3.14 B). They all decrease with increasing surfactant concentration.

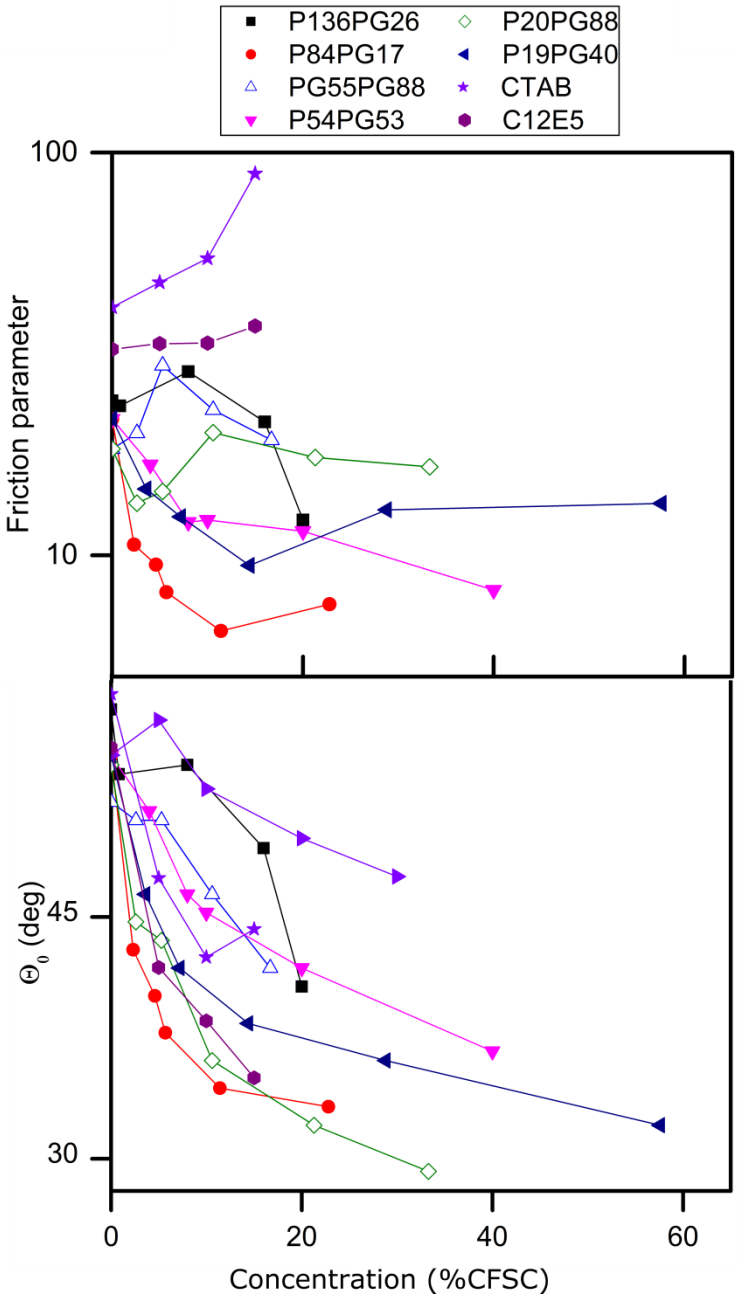

Figure 3.14. The friction parameter (A) and contact angle at zero velocity (B) for different Pluronics and the non-ionic small molecular weight surfactants, nonionic C12E5 and cationic CTAB. The friction parameter for nonionic surfactants, Pluronic and C12E5, differ from the one of cationic CTAB. The friction parameter for C12E5 is slightly larger than for Pluronic samples. However, the shape of the curve is similar to the one of Pluronic. The contact angle at zero velocity is also similar for both large and small size surfactants.

3.4.5.3 Critical micelle concentration (CMC) vs concentration of full surface coverage (CFSC)

In previous works[1-4] concerning the dynamic wetting of surfactant solution the CMC was used as the relevant scale. This was accurate because the focus of those works was small sized surfactants, such as CTAB or C12E5, where the CMC and CFSC are equal. This is different in case of Pluronic, since there is a large difference between those two characteristic concentrations. This raises the question which of those concentrations should be used as the relevant scale for dynamic wetting.

The CMC is a bulk property. It reflects the equilibrium between the molecularly dissolved Pluronic and Pluronic aggregates in the bulk. In contrast, CFSC is a surface property, as it reflects the equilibrium between molecularly dissolved Pluronic and Pluronic adsorbed at water-air interface.

In the hypothesis for the flow near the 3-phase contact line (Figure 2.21), described in detail in chapter 2.1.11, the impact of surface active molecules on the dynamic wetting is the result of creation and/or dilation of the liquid-air interface close to the receding 3-phase contact line [1-4]. For that reason, a high surface activity, which results in a strong reduction in surface tension, is connected to a stronger coupling of the dynamic contact angle. In case of low molecular weight surfactants, the CMC is the concentration at which the surface elasticity is the highest[4,85]. Pluronics have two characteristic concentrations, CFSC and CMC. For them the concentration of the highest surface elasticity is the CFSC not the CMC. Furthermore, between those two concentrations there is a large difference. In some cases, the difference is a few magnitudes.

In the proposed hydrodynamic hypothesis (Figure 2.21), the dynamic contact angle changes due to surface tension gradient between the fresh surface and the bulk volume. That means that processes happening close at the air-liquid interface have stronger influence than aggregation formation in the bulk. As mentioned before the CMC is a bulk property while CFSC is a surface property. Taking this into the CFSC should be used to scale the concentrations instead of the CMC.

To test if the CFSC is the better scaling concentration, I compare the change of the change in dynamic contact angle at 15 mm/s (Fig. 3.15) using the CMC (A) and the CFSC (B) as characteristic concentration. The change in the dynamic contact angle is the difference between the dynamic contact angle at specific velocity and the dynamic

contact angle for water at the same velocity. I compare the change in the dynamic contact angle of Pluronic with two small molecular weight surfactants, CTAB and C12E5 (Figure 3.15). When the CFSC is used to scale the concentration, we observe a change in the concentration dependent contact angle in the same range of % of CFSC, (0% - 30%) for Pluronic and CTAB, while with the CMC as the scaling concentration we observe a change in the dynamic contact angle at below 1 % CMC for Pluronic and around 10% – 30% for CTAB.

Specially taking into consideration the difference in the minimal absolute concentration needed for the change in the dynamic contact angle can be considered. The minimal amount for C12E5 to see a change in the dynamic contact angle is 5%CMC, which is 0.35 μmol/l. For Pluronics, the exact concentration varied between 0.009 μmol/l - 5.8 μmol/l. Those concentrations for Pluronic and C12E5 are rather close to each other. However, when the change in the dynamic contact angle is compared using %CMC as scaling factor there is large difference between the Pluronics and C12E5. Making it impossible to compare them together. But when %CFSC is used as the characteristic concentration all curves are much closer to each other. This shows that the CFSC and not the CMC is the universal and relevant quantity determining the decrease of the receding dynamic contact angle.

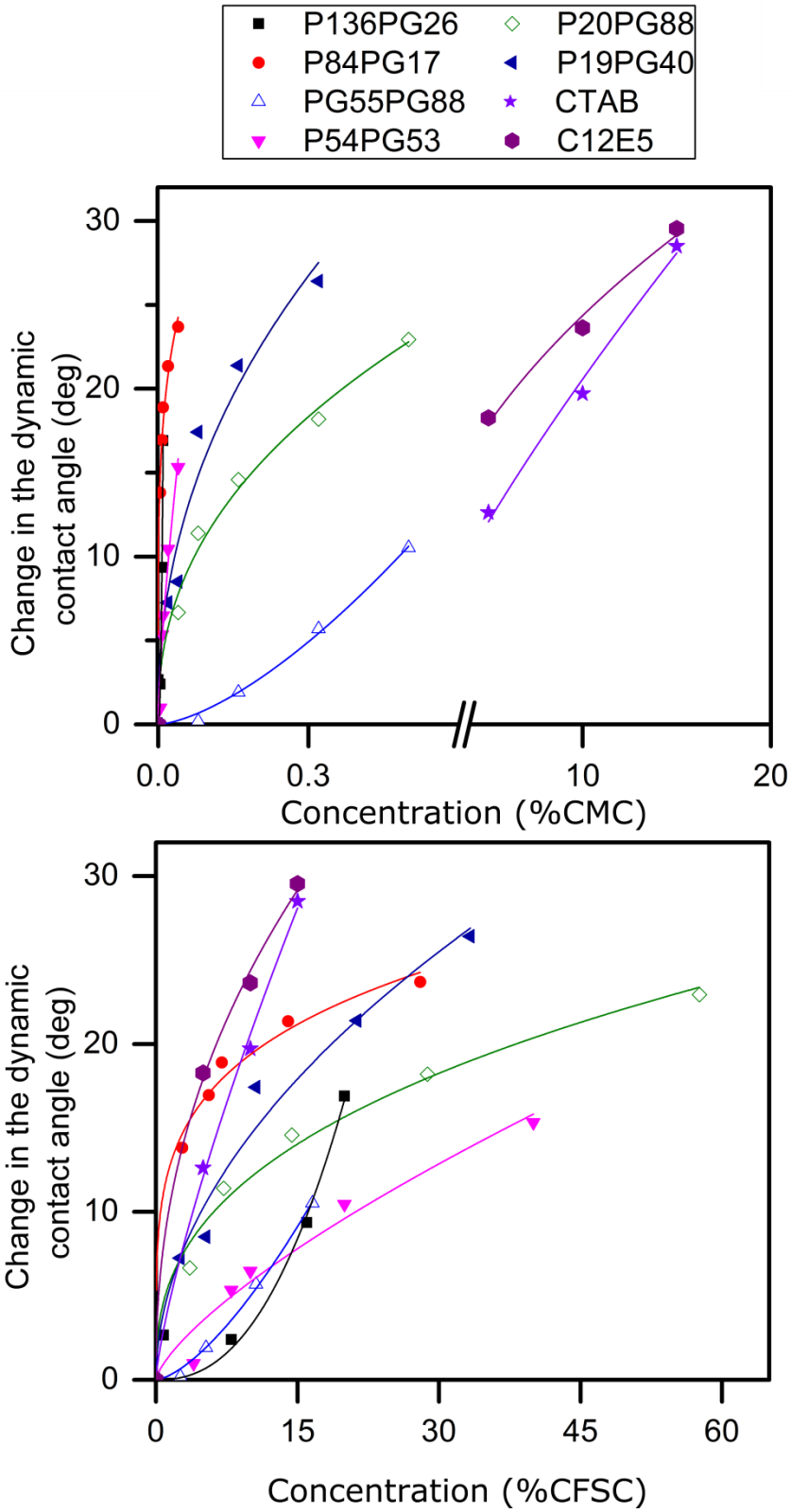

Figure 3.15 Comparison of the change of the receding dynamic contact angle for CTAB, C12E5 and different Pluronic at 15 mm/s scaled by %CMC (A) and %CFSC (B). When % CFSC is used as a scaling concentration for the change in the receding

dynamic contact angle, Pluronic are much more similar to CTAB and C12E5 than when scaled by CMC.

3.4.5.4 Influence of different parameters of Pluronic on dynamic dewetting

Even when the CFSC is used as the characteristic concentration to compare the change in the dynamic contact angle the curves for Pluronic differ from each other. The question then has arisen, what is the reason for these differences. Each of the Pluronic is different, either by the molecular weight or the amount of PPO and PEO. Those differences in Pluronic parameters could potentially explain the difference in the dynamic wetting behavior between them. The group of six Pluronics, were all carefully chosen. The molecular weight varied between 1900 – 13 600 g/mol and additionally there are some Pluronic, that have similar molecular weight but different PEO:PPO ratio (P20PG88:P19PG40 and P55PG88:P54PG53). Also the PPO:PEO ratio was carefully chosen and it varied between 17-88%PPO of overall mass in g/mol. Also the length of PPO and PEO blocks also varied between different Pluronic. There were two pairs of Pluronic that have the same length of middle PPO blocks and different length of outside PEO blocks (P84PG17:P20PG88 with 30 PO blocks and P136PG26:P55PG88 with 75 PO blocks). All information for each Pluronic can be found in Table 3.1.

3.4.5.4.1. Molecular weight

Looking at the change in the dynamic contact angle (Figure 3.15) the molecular weight seems not to have any correlation between them. Since the curves for different Pluronic are not situated in an order corresponding to the molecular weight.

3.4.5.4.2. Diffusion Coefficient

In the proposed hypothesis of the flow profile in close to the 3-phase contact line, described in detail in chapter 2.1.11, during rotation of the drum a fresh surface is being created. Between this fresh surface and the bulk, which in this case is liquid that is far from the air-liquid interface, there is a difference in the surface tension. This difference in the surface tension results in a Marangoni force in the direction of the 3-phase contact line. This results in a change in the dynamic contact angle. The stronger is the gradient in the surface tension the stronger will be the change in the dynamic contact angle. In this case, the diffusion of the surfactants will have an influence on the dynamic wetting behavior. When the diffusion coefficient of surfactant is low, this means that the equilibration of the difference of the surface tension between the bulk and freshly created surface is slower. This results in a larger change in the dynamic

contact angle. As a result the change in the dynamic contact angles for slowly diffusing surfactant should be larger than for surfactant that diffuse fast.

The diffusion coefficient at CFSC and CMC of each studied Pluronic can be found in Table 3.1. The explanation of the dependence of diffusion coefficient on concentration can be found in chapter 3.4.3. However, looking at the change in the dynamic contact angle for each of the Pluronic (Figure 3.15) it is impossible to explain the differences between different Pluronic just with the diffusion coefficient.

3.4.5.4.3. Length of Blocks

Earlier works showed that both PEO and PPO have an influence on the CMC of Pluronic.[34]. With the same length of PEO blocks and increasing length of PPO the CMC decreased. The PEO have smaller influence on the CMC. When the PPO length is constant and the PEO blocks increase, the CMC slightly increases. This fits with the surface tension measurements mentioned in section 3.4.1.2. Since the length of the PEO:PPO blocks has an influence on the surface tension curves of the Pluronics, the question is if they also have influence on the dynamic wetting behavior. The information about the length of the PEO and PPO blocks for each Pluronic can be found in table 3.1.

3.4.5.4.3.1. Polypropylene oxide PPO

In this chapter I compare the dynamic wetting behavior of different Pluronics based on the length of the middle PPO blocks. The length of the middle block was given by the produces (Table 3.1). The change of dynamic contact angle for 10%CFSC at 15 mm/s was taken from the data shown in Figure 3.14 In most cases the longer the length of PPO is the smaller is the change in the dynamic contact angle (Figure 3.16.). The shortest PPO block is in P19PG40, which has only 16 PO in the middle. The change in the dynamic contact angle is larger for most of the Pluronics that have a longer PPO block. The weakest change in the dynamic contact angle is for P136PG26 and P55PG88, which have 70 PO blocks. For the other Pluronic, except P84PG17, this trend fits. P84PG17 has 30 PO blocks in the middle, just like P20PG88. However, the change of dynamic contact angle for P84PG17 is stronger than for the other Pluronic. The reason for this might explained by the differences in the amount of PEO in those Pluronic. P20PG88 only has 2 EO blocks on each side, while P84PG17 has 75 EO blocks. The influence of the EO block will be further discussed in the chapter 3.6.4.3.2.

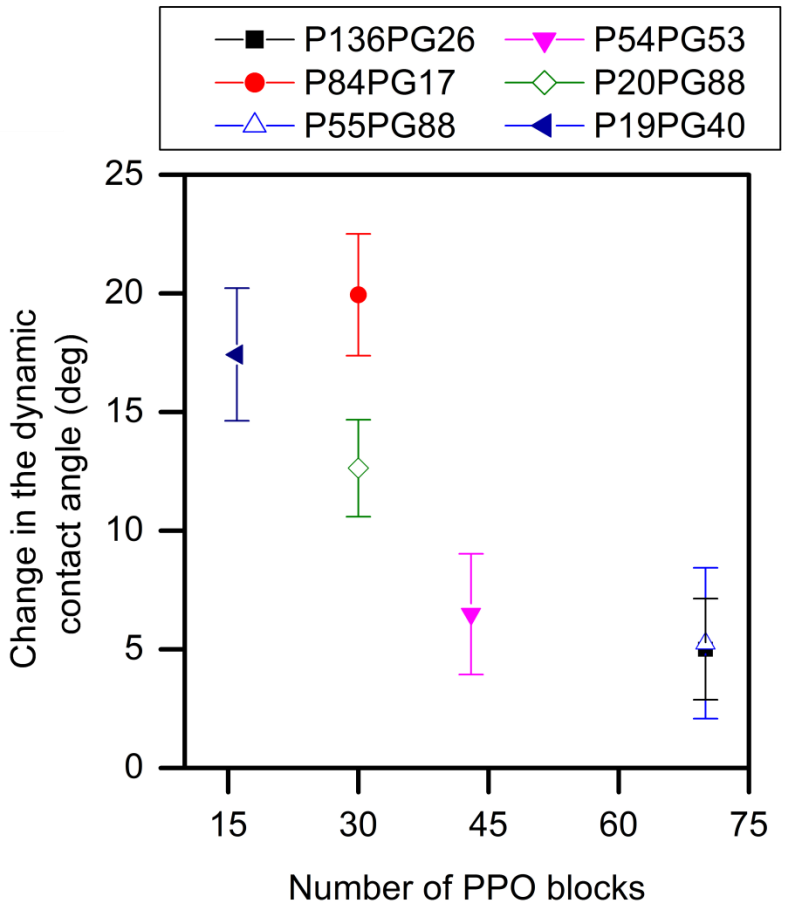

Figure 3.16. The change of the dynamic contact angle at 10 % CFSC and 15 mm/s depending in the length of the middle PPO block. Pluronic are not monodisperse, so there will be differences in the length of the same Pluronic molecules in one batch. In this work, the used PPO block length is the one mentioned by the producer. The data points were taken from the fit visible in Figure 3.14. In most cases the longer PPO blocks the smaller is the change of the dynamic contact angle (for the same %CSFC and velocity). Only the P84PG17 sticks out from this tendency. This might be due to the length of the PEO block (chapter 3.6.4.3.).

As mentioned before in chapter, 3.4.1. PPO blocks have an influence on the surface tension curve of the Pluronic. Furthermore, PPO blocks can displace PEO blocks from the air-water interface. This indicates that hydrophobic PPO blocks will want to adsorb into the interface. The longer the PPO block the stronger will be the driving force of the molecule to the surface. This can explain why the change in the dynamic contact angle for Pluronic with longer PPO block is weaker than for the one of Pluronic with short PPO block. This is visible for the surface tension measurements of PEO and PPO,

described in chapter 3.4.1.2. Adding PEO to water resulted only in a small change in the surface tension, while when PPO was added there was a large reduction in the surface tension. As explained in proposed hypothesis of the flow near the three-phase contact line, chapter 2.1.11, the change in the dynamic contact angle results from gradient in surface tension between the freshly created surface near the three-phase contact line and the bulk. In this case as the bulk is the liquid that is far from the three-phase contact line. This difference is equilibrated by the surfactant in the bulk. The faster this equilibrium is reached the smaller is the change in the dynamic contact angle. Pluronic the PPO blocks faster adsorb into the air-water interface. This means that the difference of the surface tension between fresh surface close to the three-phase contact line and the bulk equilibrates faster.

The changes in the receding contact angles for Pluronic and C12E5 (Figure 3.15) have some similarities. In all cases, the larger is the concentrations of surfactant result in larger change in the dynamic contact angles.

In most Pluronic, P84PG17; P54PG53; P23PG88 and P19PG40, the change in the dynamic contact angle increases with increasing velocity. The way it decreases is stronger at lower concentration than at higher concentration. This happens at all studied velocities. This also happens in the case of smaller surfactants, like C12E5.

However, two Pluronics do not follow this pattern, P136PG26 and P55PG88 (Figure 3.17). For those Pluronics the change in the dynamic contact angle is stronger at higher concentration than at lower ones. This observation is independent from the studied velocities (Figure 3.17). The main difference between them and the other studied Pluronic is the length of the PPO block. Both P136PG26 and P55PG88 have the longest middle block, 70 PPO repeat units. Which is more than for P54PG53, which with 43 PPO blocks have the second largest middle part of the Pluronic. The reason why the curve for change of the dynamic contact angle for Pluronics with a longer PPO block is different is unknown.

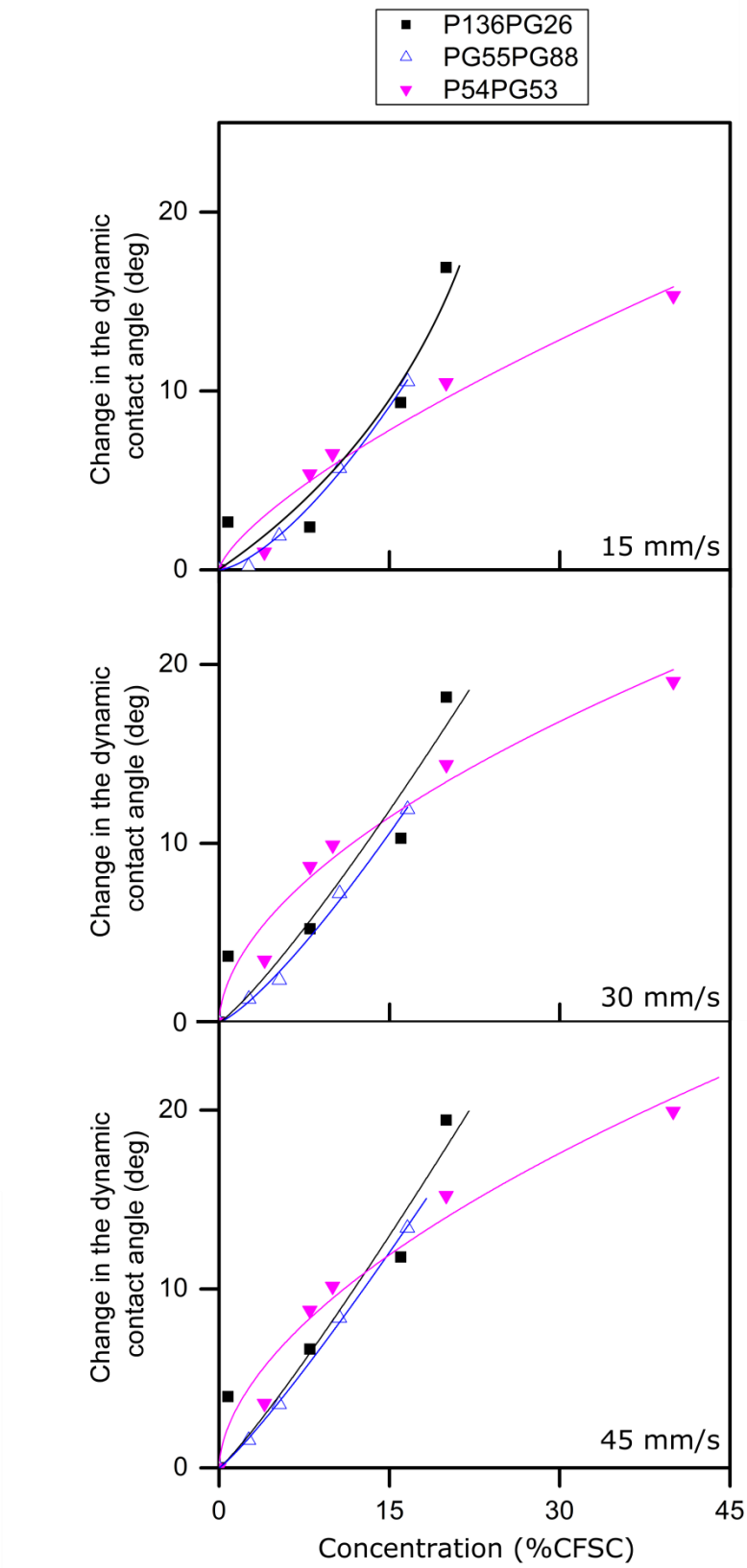

Figure 3.17 Change in the dynamic contact angle for P136PG26, P55PG88 and P20PG88 at different velocities. To guide the eye the data points were fitted. The shape of the curve for P136PG26 and P55PG88 is different than from the P20PG88 and the other studied Pluronics and small molecular weight surfactants visible in Figure 3.15

3.4.5.4.3.2. PEO

The influence of PEO is weaker than the one coming from PPO blocks (Figure 3.18). In this study, there are two pairs of Pluronic that have the same length of middle PPO block but different length of outside PEO blocks. P136PG26 and P55PG88 have both 70 PO repeat units but much different length of PEO, 100 and 5 repeat units on each side respectively. The second pair is P84PG17 and P20PG88, where the middle PPO block has 30 repeat units and the outside PEO 75 and 2 repeat units, respectively.

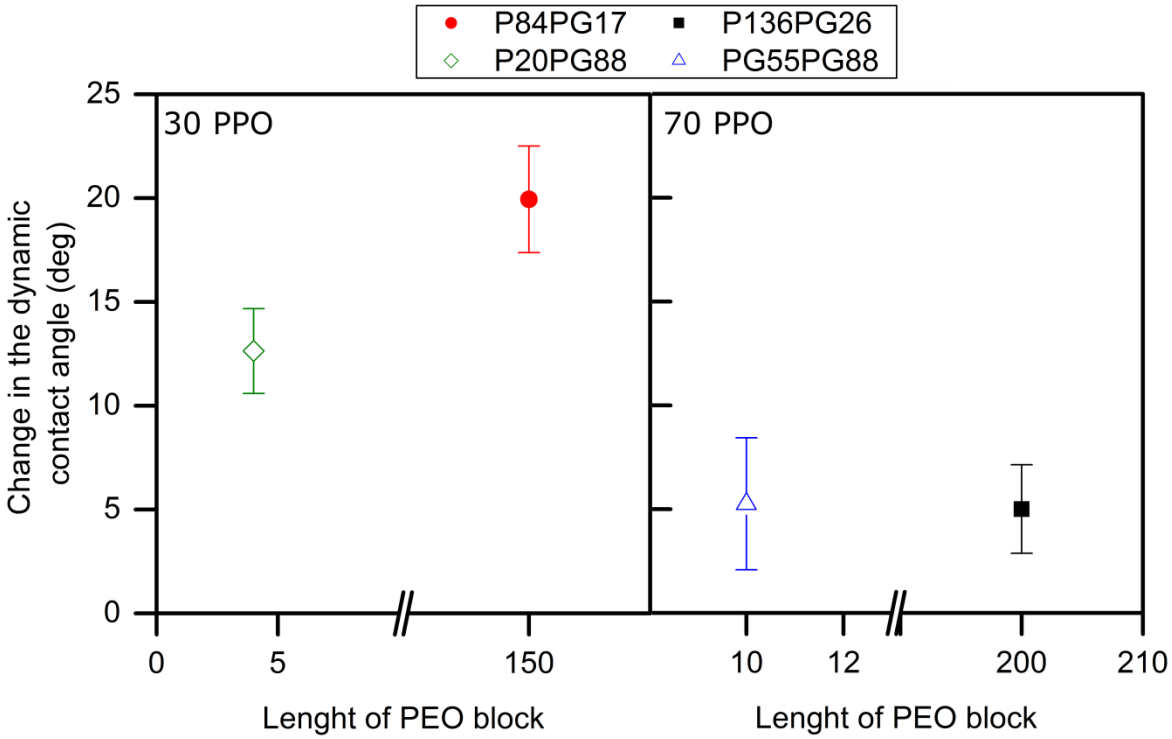

Figure 3.18. The change in the dynamic contact angle for Pluronic with the same length of PPO block but different outside PEO blocks. When the PPO block is long there is not a big difference between the two Pluronic. For the Pluronic with shorter middle block the longer PEO outside blocks results in larger change in the dynamic contact angle.

For Pluronic with a large amount of PPO the change in the dynamic contact angle is rather constant independent from the amount of PEO. This is however, not the case for the second pair of Pluronic but with shorter middle PPO block. There is a clear difference between P20PG88, with 2 PEO blocks on each side, and P84PG17, which

has 75 blocks on each side. In this case, the change of the dynamic contact angle for P84PG17, which has a longer PPO block, was much larger than for P20PG88.

Alexandritis[34] mentioned that the PEO has a slight influence on the CMC. However, the impact of the PEO is weaker than the one from PPO. The longer the block of PEO was the smaller was the CMC. It also seems that length of PEO have an influence on the dynamic wetting behaviour. Also now the influence coming from the PEO is weaker than the one coming from PPO blocks. It also seems to decrease with increasing length of PPO block. Shown data indicates that a combination of both PEO and PPO blocks impact the dynamic wetting behavior of Pluronic. However further works would have to be done to confirm this.

3.5 Conclusions

Adding Pluronic to aqueous solution results in a decrease in the surface tension. A similar effect is observed for low molecular weight surfactants, like CTAB or C12E5. However, for Pluronic some important new features are observed. Mainly the shape of the surface tension curves for Pluronics look different than the ones for small molecular weight surfactants. The curve is composed of three separate segments. One steeper at lower concentration, a less steep one at higher ones and a plateau aboves CMC. This indicates that there is another concentration at which the full surface is fully taken by surfactants that is not the critical micelle concentration (CMC). The last curve is the plateau after the CMC, when the surface tension remains constant regardless of the concentration. The second concentration at which the surface is fully occupied by the surfactants is the concentration of full surface coverage (CFSC).

The existence of two characteristic concentrations was further proven by dilatational surface rheology measurements and study of aggregation using fluorescence correlation spectroscopy. Using the oscillating drop method, it was possible to measure the viscoelastic modulus of Pluronic. A peak in the viscoelastic modulus indicates that the whole surface is fully taken by the surfactant solution[41,85]. Smaller molecular weight surfactants showed only a single peak, while in case of Pluronic two peaks were detected. This means that there are two concentrations at which the surface is fully occupied by surfactants solutions. Additionally, aggregation of Pluronic was studied through fluorescence correlation spectroscopy. This result showed that there are no micelles present at concentrations below the CMC. Those results show further show that Pluronic shows both CFSC and CMC.

For small molecular weight surfactants both of those characteristic concentrations (CFSC and CMC) are equal, while for Pluronic there is a large difference between them. This can then again explain the variety in previously reported critical micelle concentrations for various Pluronic[80-81].

Pluronic decreases the receding dynamic contact angle when added to aqueous solution. This was earlier reported for small molecular weight surfactants[1-4]**.** The main difference between the small molecular weight surfactants and Pluronic is the amount of surfactant needed for the dynamic contact angle to change. In case of some Pluronic, P55PG88, already concentration as low as 0.009 μmol/l, which is 0.08 %CMC, result in a significant decrease in comparison to pure water. For small molecular weight surfactants the amount needed for a significant decrease of dynamic contact angle is larger and varies between 5%CMC-20 %CMC. This large difference made it impossible to compare the dynamic wetting behavior using %CMC as the scaling factor. As mentioned before Pluronics have two characteristic concentrations, CFSC and CMC and there is a large difference between them. When using %CFSC instead of %CMC the change in the dynamic contact angle is more comparable between Pluronic and small molecular weight surfactants (Figure 3.14. This clearly indicates that the concentration of full surface coverage, which is a surface property, rather than the critical micelle concentration, that is a bulk property, is the relevant concentration scale for dynamic dewetting.

The experimental results concerning the dynamic wetting agree with the proposed hypothesis of the flow profile near the 3-phase contact line (Figure 2.21.*)*. The hypothesis states that the of Marangoni stresses close to the 3-phase contact line as well as their equilibration, by both advection and diffusion, are dominating.

While by using the CFSC as scaling factor made the change of the dynamic contact angle of Pluronics closer to each other and to small molecular weight surfactants. There are still some differences between the dewetting of Pluronic. Further aspect of this work was to explain from where those differences come from. Few different properties of the Pluronic were studied, such as molecular weight or the ratio of PPO:PEO blocks. It is clear from my results that the building blocks of Pluronic (hydrophobic PPO and hydrophilic PEO) play a significant role. Specially, the PPO block seems to have a large influence. There is a strong decrease in the change in the dynamic contact angles with increasing length of the middle PPO block. To a smaller degree, the PEO blocks also effects the dynamic dewetting.

The results in this chapter results show that depending on the process, either the critical micelle concentration or the concentration of full surface coverage might be the relevant concentration scale. In case of bulk properties, e.g. aggregation behavior or micelle formation, the critical micelle concentration will be more significant than the concentration of full surface coverage. While for surface properties, such as surface elasticity or dynamic wetting it will be the opposite and concentration of full surface coverage will be more important.

3.6 Outlook

This work investigates the dynamic wetting of high molecular weight surfactants. Even though it did offer some explanation for the behavior of Pluronic there are still open questions regarding this topic.

As shown in chapter 3.4.3 Pluronic can have different forms in the bulk at concentrations below the critical micelle concentrations such as, free surfactants, unimers, and aggregates. All of them could potentially have different influence on the dynamic wetting. Also the influence of the building blocks, polyethylene-oxide (PEO) and polypropylene-oxide (PPO) on the dynamic wetting should be further looked into. While this work showed that there is a large influence coming from the PPO blocks the influence of PEO is not fully understood. Furthermore, it is probably ratio of PPO:PEO blocks that is responsible for the behavior of a specific Pluronic. This means dynamic contact angles of a much larger range of Pluronic, with different combinations, for example with the same length of PPO and increasing length of PEO or with the same number of PEO blocks but increasing length of PPO, would have to be measured.

4. Drop impact at high speeds and low temperatures

This PhD work was part of the Initial Training Network (ITN) CoWet. The main focus of this ITN was wetting of complex liquids. This ITN contained groups from both industry and academia offering a chance for cooperation's with different partners. This work was done in cooperation with Dr. E. Bonaccurso at the Surface Technology department at Airbus Group Innovations in Munich, Germany. The measurements were performed in two sessions. The first one was between 25-29th July in 2016 and the second one was between 13-17th February and 27th February- 03th March in 2017. The goal of both measurements sessions was to observe the impact of supercooled water droplets at high airspeed and low air temperatures (between -15^{o}C and -5^{o}C) in the icing wind tunnel (IWT) iCORE at Airbus Group Innovations. The wind tunnel is presented in chapter 4.2. Since the measurements were performed between -15^{o}C and -5^{o}C the freezing of impacting drops was also studied. During the first measurement session, preliminary results of drop impact on different surfaces were collected. Drop impact was only observed through the bottom of the surface. Between the first and second measurements session the airfoil used for drop impact was further modified to allow observations from more directions, especially frontally and laterally (details are in chapter 4.2). During the second measurement session, the drop impact at high airspeeds (higher than 50 m/s) and temperatures below 0^{o}C was studied. During my stay at the Airbus Group Innovations I had help from V. Vercillo and A. Laroche in using the IWT.

Since measurements are done at low temperatures, the droplets freeze on the surfaces after impacting and a layer of ice is built up on the surface. This ice formation on different surfaces, such as airplanes during flight[1-3] or on wind turbine blades[4,5] causes performance and safety issues. There are different ways the ice formation is being dealt with, such as using anti-freezing liquids or active systems that, e.g., can melt the ice layer. Even though in recent years there have been some studies[1,3,4,6-11] focused on the drop impact at different temperatures, velocities and surfaces, still not much is known on impact, wetting, and splashing dynamics of single supercooled water drops at velocities higher than 50 m/s and temperatures lower than 0 ^{o}C.

4.1. Materials

The aim of this work was to observe the droplet impact of super cooled water droplets on substrates with different hydrophobicity and softness. Due to the used set-up, described in 4.2, all the studied surfaces had to have the same size (15x25x5mm). The information about the properties of the substrates can be found in Table 4.1.

Surface	Advancing static contact angle of ultrapure water [^{o}]	Young Modulus [GPa]	Thermal Conductivity [W/mK]
Glass	$60^o \pm 4^o$.	82	1.1
Hydrophobic glass	$91^o \pm 4^o$	82	1.1
PDMS20	$85^o \mp 4^o$	0.00052[87]	0.15
PDMS50	$93^o \mp 4^o$	0.00052[87]	0.15

Table 4.1. Advancing static contact angle of ultrapure water, Young modulus and thermal conductivity of different studied surfaces.

4.1.1. Glass

The first studied surface was a N-BK7 glass surface. It was ordered from Korth Kristalle GmbH, Germany. It was then used without any further surface modification. It was delivered with a slight hydrophobic coating with a advancing static contact angle of $60^o \pm 4^o$. The advancing static contact angle of ultrapure water (prepared with an Arium® pro VF/UF& DI/UV (Sartorius); electrical resistivity 18.2 MΩ) was measured using goniometer OCA35 (DataPhysic, Germany). Elastic modulus for N-BK7 glass was given by the manufacture and it is 82 GPa.

4.1.2. Hydrophobic glass surface

The second studied surface was hydrophobic glass. Just like for the glass surface the advancing static contact angle was measured using OCA35. In this case, the static contact angle of ultrapure water was $91^o \pm 4^o$. This surface was prepared by hydrophobizing the N-BK7 using two components Episurf from Surfactis Technologies, France. Episurf is composed of a perfluoropolyether phosphonate in hypofluorous acid (HFO) solvent. Before usage the Episurf was mixed with isopropanol in 1:10 ratio. The Episurf was divided into two parts. The first part of Episurf was put on a cleaned glass surface for 10 minutes and then rinsed with deionized water for 30 seconds. This was done to prepare and activate the surface before the hydrophobization. Afterwards the

second part of the Episurf was put on the surface of the glass and left on for 5 minutes. This part contained the perfluoropolyether phosphonate and it bounded with the glass surface. Afterwards, the glass was again rinsed with deionized water for 30 seconds. The glass was then put into the oven, heated to 60 ^{o}C, for a few minutes to dry. Since it is a commercial product I am not able to provide any further details about the composition of Episurf.

4.1.3. Polydimethylsiloxane (PDMS) surfaces

The last two surfaces were polydimethylsiloxane (PDMS) surfaces of different PDMS thickness. The two PDMS surfaces were both prepared using Sylgard®184 from Dow Corning, Germany. Sylgard®184 is a silicone liquid containing two-component, monomer and cross-linker. The monomer was mixed with the cross-linker in 10:1 ratio. Before the PDMS was put onto the surface it was left standing for 5-10 minutes to get rid of air bubbles that got trapped in the PDMS when mixing the components.

In this work two cross-linked PDMS layers, 20 and 50 μm thick, were used. They are further named PDMS20 and PDMS50 respectively. Both were made using spin coating. The glass with the PDMS was spin coated at 1000 rpm for 15 minutes, for a 20μm thick layer, and 3 minutes, for a 50 μm thick layer. Afterwards, the glass was put into an oven at 60^{o} for at least 12 hours for the PDMS to crosslink.

The static contact angle of ultrapure water for 20 μm and 50 μm thick layer was $85^{o}\mp4^{o}$ and $93^{o}\mp4^{o}$ respectively. It was measured using a goniometer, OCA 35. While the static contact angles for the PDMS and hydrophobic glass surfaces are similar the softness is different.

DMS layers will be softer than the other two studied surfaces. One way of defining the softness is looking at the mechanical properties of the PDMS surface. One parameter is the shear modulus, *G*. The higher it is the harder is the substrate. The shear modulus of the PDMS layers with different viscoelasticity was measured before[86,87] The *G* for PDMS with 10:1 ratio of elastomer to cross-linker is around 520kPa[87].

4.2. Measuring method

The measurements were done in the home-built IWT iCORE at Airbus Group Innovations in Munich, Germany. Dr. E. Bonaccurso ,V. Vercillo and A. Laroche supported me in using the IWT. It was possible to control the temperature, down to -20^{o}C and the airspeed to more than 100 m/s. Temperature and airspeed were measured inside the test section using a Pitot tube (Figure 4.1). The IWT is equipped with water nozzles able to produce different sized droplets of water.

The measurements were done at atmospheric conditions at which most of the in-flight icing happens [5]. The droplet impact for each of the studied set-ups was measured at three temperatures (-5, -10 and -15 ^{o}C). Two different airspeeds of 50 and 90 m/s were used, corresponding to 180 and 324 km/h. The velocity of individual impacting droplets differed slightly and depended on their size. It was only possible to determine accurately the velocity of drop impact for large droplets (diameter larger than 80 μm). The velocity of impacting droplets was between 46-52 m/s at 50 m/s airspeed and 82-86m/s at 90 m/s airspeed. However, in this work I will always use the nominal airspeed for comparison.

The main focus of this work was to observe the drop impact from two views, bottom and side of the sample. The tested substrate was positioned inside the test section in a sample holder with the shape of an airfoil for minimally disturbing the airflow (Figure 4.1 B). Furthermore, it had to be done in a way, which makes it possible to observe the drop impact from the two directions. The sides of the test section are made of transparent Plexiglas. Two high speed-cameras (Camera 1 and Camera 2 in Figure 4.1) were placed on the sides of the test-section. Camera 2 was positioned so to observe the drop impact from the side (red dash arrow in Figure 4.1 B). Observing the frontal drop impact from behind the impacted transparent surface (purple dash arrow in Figure 4.1 B) was done using a prism. In this case, Camera 1 was positioned on the opposite side of the test section to Camera 2. The prism acted as a mirror and made it possible to look on the bottom of the substrate. The reason we used a prism instead of a mirror was that the prism is more robust and easier to place and remove from the substrate holder. Lastly, the prism was isolated from the environment inside the wind tunnel and the water did not condensed on it. Water condensation was an important factor to take into consideration, since as soon as water condensed on either part of the setup (optics, substrate, prism or wall of the test section) it was impossible to continue the measurements. Ice formation on prism or studied substrate. This ice formation would also make it impossible to continue measurements.

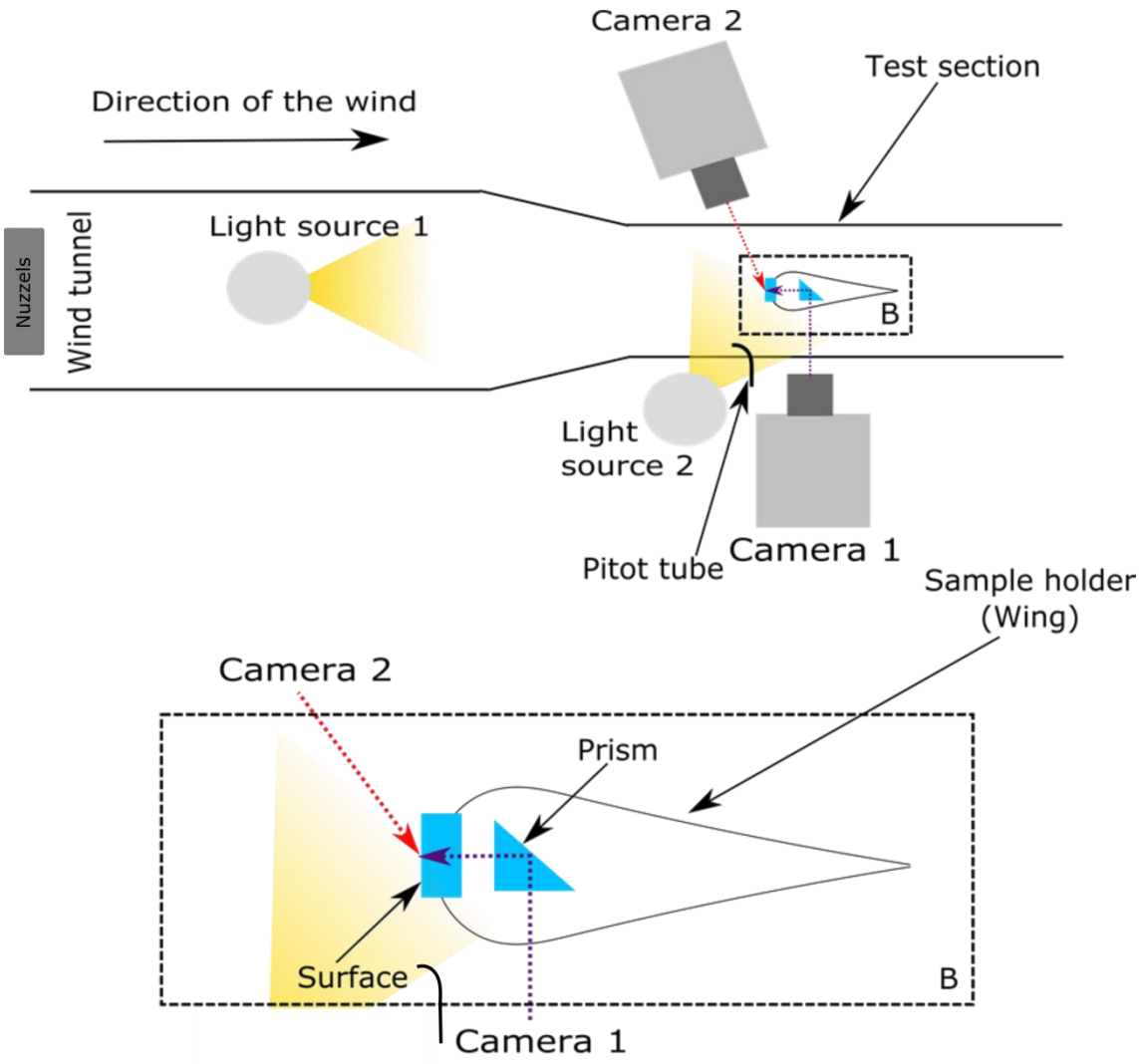

Figure 4.1. Figure 4.1. Sketch of the used experimental set-up. The airfoil was put into the test section of the IWT. Airspeed and temperature in the test section were measured using a Pitot tube. Inside the test section there was an airfoil-shaped surface holder. The drop impact was observed from two directions, frontal and lateral. Camera 1 observed through the bottom of the surface (purple dashed arrow) and Camera 2 observed the drop impact from the side of the surface (red dashed arrow).

As sample holder a 3D printed airfoil provided by Airbus Group Innovations was used (Figure 4.2). The surface holder had an aerodynamic shape to minimize turbulence during the measurments. From this point on the sample holder will be named airfoil.

The airfoil was modified to contain a prism, through which it was possible to observe the drop impact from the bottom of the surface (purple dashed arrow in Figure 4.1 B). The prism was put into a removable prism holder for easily removing the prism when

needed. In front of the airfoil a surface holder was fitted. Also surfaces could be easily removed from the airfoil for exchanging among the four used types.

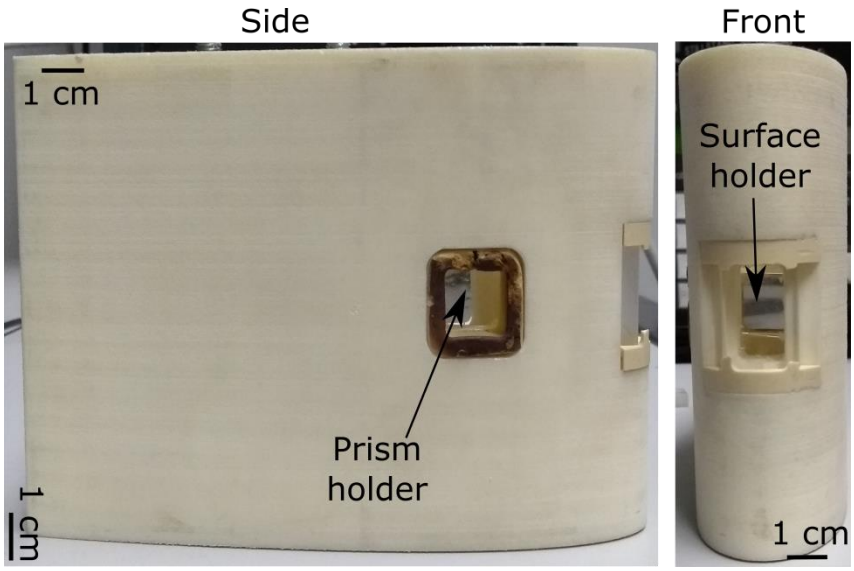

Figure 4.2. Picture of the modified sample holder (airfoil). It is possible to observe from the bottom of the tested surface through the prism (purple dashed arrow in Figure 4.1 B) or look from the side (red dashed arrow in Figure 4.1 B). Prism and surface holder can be removed from the test airfoil.

To observe the drop impact from two sides using high-speed camera, two separate light sources were needed (Figure 4.1) (Volpi IntraLED3 and IntraLED5). The light source for camera 2 was positioned on the opposite side of the test section, next to Camera 1. The light source for Camera 1 had to be inserted in the wind tunnel and was coaxial with the flow. Since measurements were done at airspeeds between 50 and 90 m/s and temperature of -15, -10, and -5 ^{o}C it was necessary to design a holder that could withstand those conditions. Additionally, it was important to design it in such a way to minimize the condensation on the visual observation path.

The light source holder (Figure 4.3) was designed by me, sketches for it can be found in the appendix at the end of this chapter (4.7).

The light source was put inside the wind tunnel. Unlike the airfoil, the light source holder was not put inside the test section of the wind tunnel. Instead it was positioned further in the wind tunnel, between nozzles and test section. The distance between the airfoil and the light source holder was around 1 m. The light source holder was made put vertically to the airfoil direction inside the wind tunnel (Figure 4.3). Inside the light source holder there was mirror, oriented at a 45^{o} angle, to reflect the light source into the direction of the airfoil. It was positioned in a way, that the maximum light intensity

was hitting the prism inside the airfoil and going into the Camera 1.An additional, window between the light source and the mirror separated the warmer (upper) and colder (lower) part of the light source holder to prevent condensation on the mirror, which could prevent from further measurements.

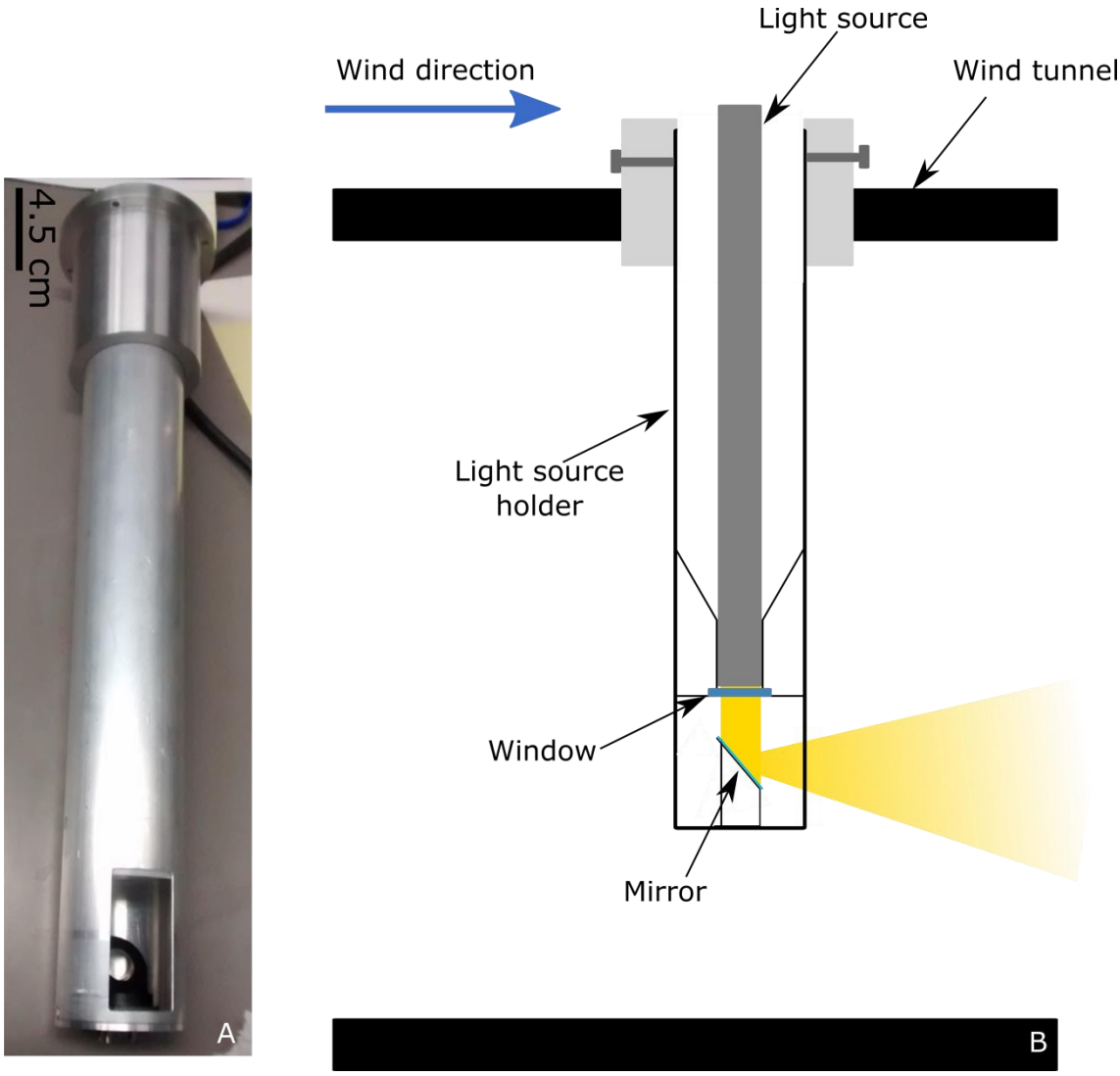

Figure 4.3 Picture of light source holder (A) and how it was situated inside the wind tunnel (B). The light source holder was built in the mechanical workshop in the Max Planck Institute for Polymer Research. It was put inside the wind tunnel vertically to the wind direction. Unlike airfoil, it was not inserted inside the test section of the wind tunnel. Instead it was inserted between nozzles that generate the droplets and the test section (Figure 4.1).

Two Photron Fastcam SA-1 cameras were used for high-speed imaging. Connected to them was a navitar tube and 2x objectives (Mitutoyo, Japan). The videos were made with frame rates of either 125 kHz or 180 kHz. The field view was 2x3 or 2x2 mm,

respectively. The reason for using such high frame rates was the speed of the drop impact, which can be observed only at these high frame rates. Both cameras were focused on the same spot on the surface (Figure 4.2.1.) and synchronised. This made it possible to observe the same droplet hitting the surface from the different views (Figure 4.4.). The bottom view allowed to observe the spreading of the contact radius and the freezing of the drop during impact. The side view allowed to observe splashing of the drop during impact. Splashing of droplets is described in chapter 4.4.1. From both views it is possible to observe how the droplet spreads and retracts, though the bottom view data was more accurate and was used for analysis.

From the bottom (Camera 1 in Figure 4.1) the whole view is "sharp" because the impact plane coincides with the focal plane of the objective. From the side (Camera 2 in Figure 4.1) only a line is sharp, because only a part of the drop is in the volume of focus. It was not possible to place Camera 2 perpendicular to the axis of the airflow , instead it was placed at an angle to the axis..

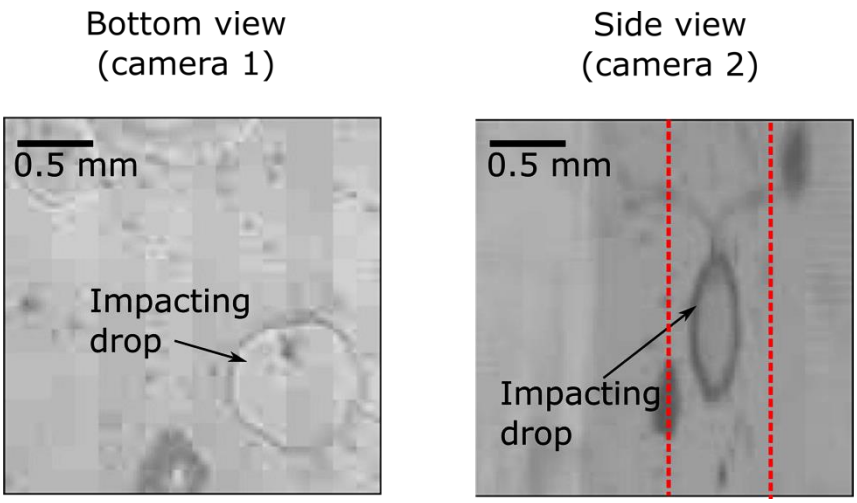

Figure 4.4. Impact of the same droplet on glass surface at a velocity of 50 m/s at -5^{o}C. Both views can give different information about the drop impact. From the bottom, the freezing process of the impacting droplet can be observed. From the side, it is possible to look how the drop impacts, such as if it splashes or not. From both sides, it is possible to look at the spreading and retracting of impacting droplets. From the side view only part of the video was sharp. The dashed red lines show the area of the surface for which camera 2 could be focused on. Outside these lines the features in the images were blurred.

4.3. Size of the droplets

The nozzles produce a cloud of droplets with a size distribution depending on the gas pressure applied to the nozzles, to the water mass flow rate, and to a minor extent to the airspeed. Usually, the droplets cloud is characterized by its median volume diameter (MVD), which gives no information on the size of individual drops, though. From the recorded high-speed videos, I estimated the volume by measuring the diameter of the droplet just before it impacted the substrate. All analysed droplets fit into two categories:

- small droplets, a the diameter between 40 - 80μm.
- large droplets, a the diameter between 100 - 450μm.

The droplets were divided into those two groups according to their splashing behaviour (Figure 4.5). Small droplets did not splash upon hitting the surface, while large droplets did. Splashing means that upon impact, smaller droplets are generated at the quickly expanding rim of the drop. Then they are ejected at high speed from the rim. Wheter. the droplet splashes or not depends on different parameters such as drop velocity, volume, properties of the liquid and properties of the surface[88-90].When a drop hits a solid or liquid surface small droplets break off the original drop. Splashing occurs when the kinetic energy of the impinging drop overcomes the surface tension force that keeps the drop as a whole

In this work only the large droplets splashed. Upon impact, smaller droplets separated from the main droplet while it spread (Figure 4.5 2 and 3). The separation of the smaller droplets during splash at both set airspeeds is faster than the exposure time of the camera and the splash shown in Figure 4.5 (2 and 4) is only hard to see. For this reason, the small droplets separating from the main drop are pointed out by arrows in Figure 4.5. After splashing and spreading ended (Figure 4.5 4), the drop reached its maximum wetting diameter. What happened afterwards is explained in detail in chapter 4.4.1.2.

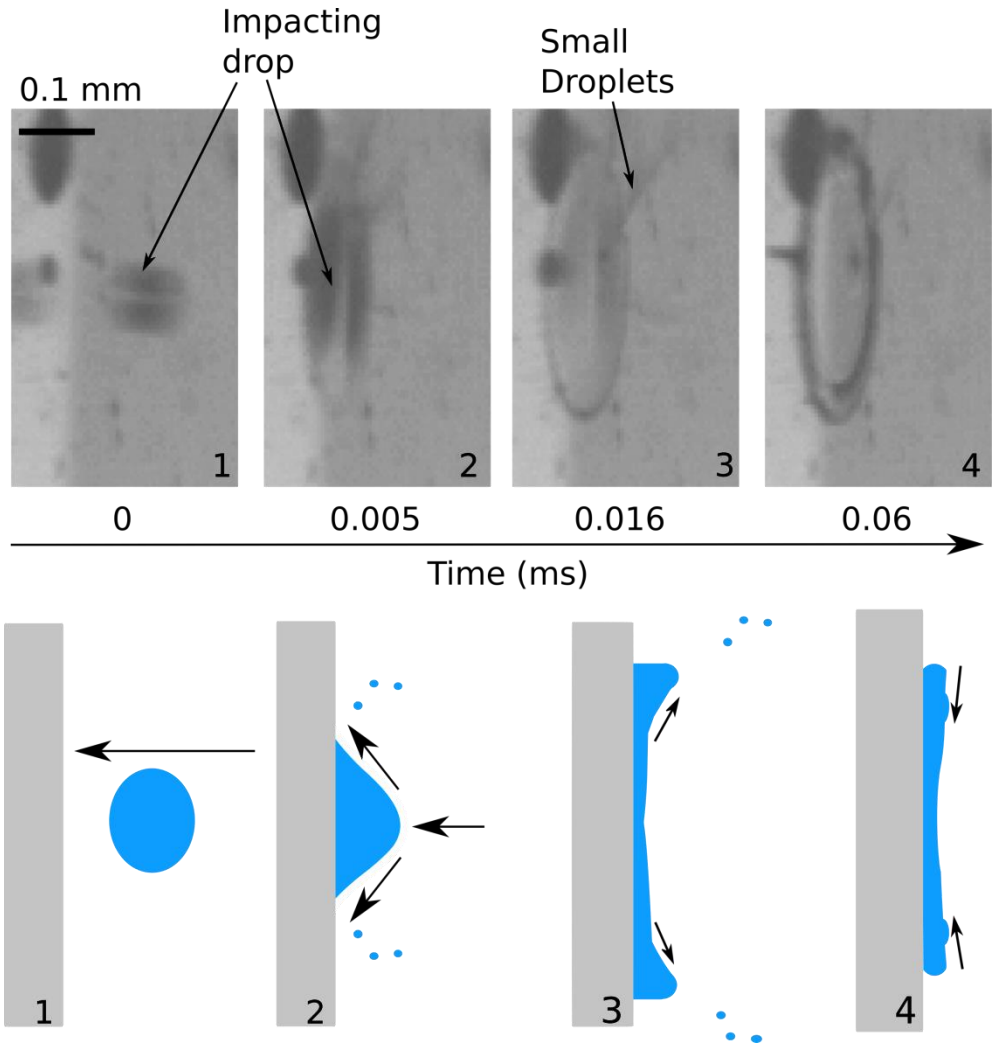

Figure 4.5. Side view of impacting drop on hydrophobic surface at 50m/s and -5°C. When the drop impacts with the surface it starts spreading (2 and 3). During spreading it splashes and small droplets separate from the main drop (2 and 3) The drop continues this until it reaches the maximum diameter (4).

The distance between the nozzles and the surface is approx. 1 m. The droplets generated by the nozzles have temperature above 0°C and take some time to equilibrate their temperature with that of the air inside the IWT. It could well be that some of the largest droplets are not supercooled to the surrounding airflow temperature when they impact on the substrate.

As mentioned in chapter 2.2.2 when droplets have diameter larger than 50 μm, they are called supercooled large droplets (SLD)[72]. As mentioned above it is not sure that the tested droplets are supercooled to the same temperature of the air. But just considering the diameter of the tested droplets, all large droplets and most small droplets would be considered as supercooled large droplet.

Impact of small droplets was only studied on glass and on hydrophobized glass. Impact of large droplets was studied on all four surfaces, glass, hydrophobized glass, PDMS20 and PDMS50.

As mentioned in chapter 2.2.3 one of the parameter to describe the drop impact is the Weber number. The dimensionless Weber (We) number describes the ratio between the deforming inertial forces and the stabilizing surface tension forces. The Weber number can also indicate if the droplet tends to splash upon impact because of releasing the kinetic energy at impact. The higher the Weber number the higher and more dominant is the kinetic energy. Further explanation about splashing can be found in chapter 4.4.1.

The diameter of impacting droplets varied between 40-80 μm for small and 100-400 μm for large droplets. Therefore, also We was different for each droplet. Table 4.2 gives the average We for small and large droplets. Also, the impacting velocity of the droplets varied depending on their size. Due to the limited resolution of the high-speed video images, it was not possible to measure the impacting velocity for small droplets, because they moved too fast to correctly estimate their velocity. The velocity of impact of large droplets varied with the size of the droplets between 46-52 m/s at 50 m/s airspeed and 82-86 m/s at 90 m/s airspeed. For calculations, I used the average droplet velocity. At 50 m/s airspeed it was 48 m/s and at 90 m/s airspeed it was 85 m/s. However, for comparison of We with small droplets I used the airspeed instead of the droplet velocity.

Airspeed (m/s)	Average Weber number- small droplets	Uncertainty	Average Weber number- large droplets	Uncertainty
50	2200	200	6300	1400
90	7000	400	24000	4000

Table 4.2. Average Weber number (We) for small and large studied droplets. We is independent from the surface the droplet is impacting on and temperature. Weber number is dependent on the size and the velocity of the droplet. The size of the droplets varied between 40-80μm for small droplets and 100-400μm for large ones. The average Weber number was compared to the airspeed even though for large droplets the drop velocity was used for calculations. The uncertainty is the standard deviation.

4.4. Experimental results and discussion

4.4.1. Drop Impact

There are some similarities in the drop impact independent o the of temperature, airspeed or the studied surfaces. All droplets smaller than 40μm just landed on the surface and did not spread or retract. Droplets with diameter larger than 40μm impacted in a similar way. After the droplet touched the surface, it started until the maximum diameter was reached (Figure 4.6 and 4.9). Afterwards the droplet started to retract. The way the impacts ends depends on temperature, and the surface. During the impact, large droplets did splash (Figure 4.5). The small droplets did not splash.

The start of the impact was considered as the first moment the droplet touched the surface. Deciding when the impact ended (the droplet no longer was moving) was more difficult and depended on the temperature and how fast the droplet froze. When the drop was liquid after it spread into to the maximal diameter it started to retract and continued to retract until it reached its minimal diameter. The drop also remains liquid after the retraction. The end of the impact is when the droplet stops further retracting. Under a few conditions it happened that the drop freezes during retraction. The point at which the droplet freezes during retraction is considered the end of the impact. The timespan between the moment the droplets touched the surface and when the impact ended is called the time of movement.

From the difference between the surface area of the droplet at the maximum diameterand its minimal diameter I estimated how much the droplet retracted. In case of small droplets, the analyzed droplets had diameters between 40-80 μm, while for large droplets the size varied between 100 μm and 450 μm. To normalize the change in surface area of a droplet between the beginning and end of the impact to be independent of the actual size of a droplet I use the relative change in percent. Large percentage of retractions means that the droplet is much smaller at the end than at the beginning of the drop impact. Small percentage of retraction indicates that the drop only slightly retracted during impact. When a drop separates into a group of smaller droplets after the impact, the sum of the surface areas of all droplets was taken into an account. This especially happened for PDMS surfaces, and it is explained in detail in chapter 4.4.1.2.

4.4.1.1. Small Droplets

4.4.1.1.1. Experimental results

The small droplets can be divided into two categories depending on the size. Droplets, that have less than 40 μm diameter, are too small to spread after the impact. Instead they

just land on the surface. In the case of larger droplets (diameter between 40 and 80 μm) the droplets spread and retract during impact (Figure 4.6).

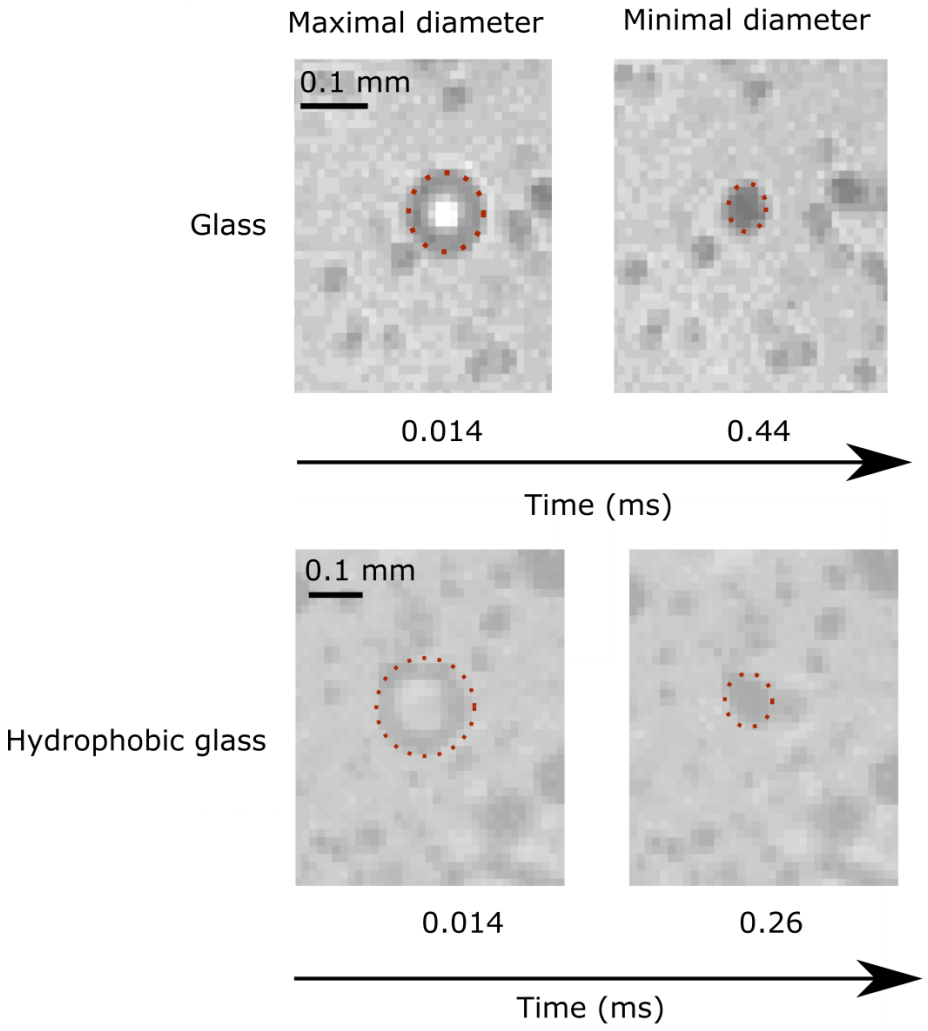

Figure 4.6. Impact of small droplets on a glass and hydrophobic glass at 50 m/s at -5°C. Upon impact the droplets spread and then retract. In both cases at the end of the impact, the droplets remain in one piece. For better view the outline of the droplet at the start and the end of impact was highlighted with red dotted line.

Drop impacts on glass (Figure 4.6.) and hydrophobic glass ((Figure 4.6.) are rather similar. At the beginning of impact and at the end the droplet remains round. For each droplet, it was possible to measure the percentage of retraction area and the time of movement. For each temperature, airspeed and surface of at least 4 separate droplets were analyzed. In comparison between the surfaces the average values are used and the uncertainty is the standard deviation. Even though the impact of the small droplets on

both surfaces, hydrophobic glass and glass, is similar there are differences in the percentage of retraction area (Figure 4.7) and the time of movement (Figure 4.8).

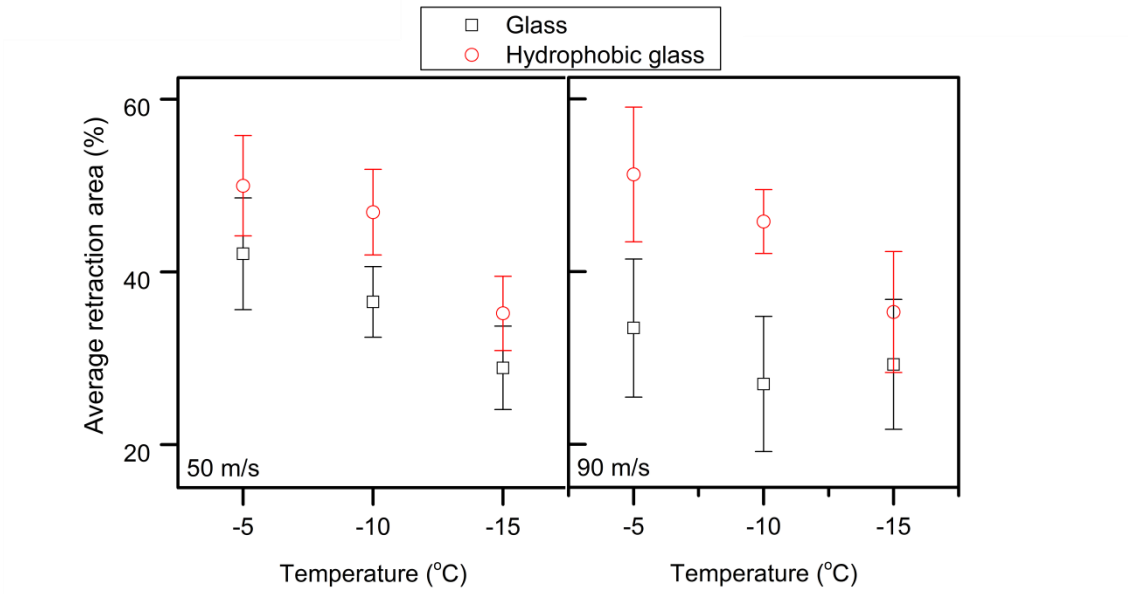

Figure 4.7. Average retracting area in percentage of small droplets at 50 and 90 m/s at different temperatures. At 50 m/s the difference in the average retraction between the two surfaces is smaller than at 90 m/s. With decreasing temperature, the retracting decreases, which can be connected to droplets freezing during retracting.

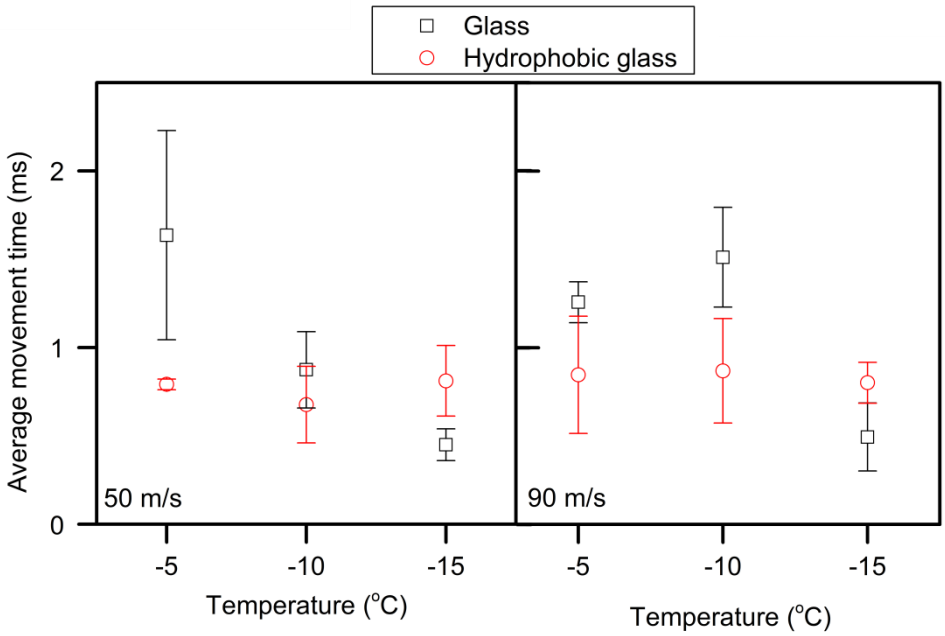

Figure 4.8. The average time of movement for small droplets on glass and hydrophobic glass at different temperatures at 50 m/s and 90 m/s airspeed. The time of movement of impacting droplets are similar on both surfaces.

4.4.1.1.2. Discussion

The average retraction area for small droplets is dependents on:

- temperature
- velocity of impacting droplets
- surface

In all cases, the temperature has an impact on retracting area of the impacting droplets (Figure 4.7). When drop impacts on the surface it first spreads until it reaches the maximal diameter. Afterwards, it starts to retract. When the drop freezes during retracting the percentage of retraction area is smaller compared to case when the drop remains liquid through the whole retraction process. This explains why the percentage of retraction area decreases with decreasing temperature. The velocity of the wind also seems to have an influence on the percentage of retraction area (Figure 4.7). At 50 m/s airspeed the percentage of retraction area is similar for both surfaces. At airspeed of 90 m/s the difference between the two surfaces is more prominent. On the hydrophobic surface the average retraction area is larger than on the glass surface. The difference between those two surfaces can be explained by the difference in the hydrophobicity. As mentioned in chapter 4.1, the advancing static contact angle of ultrapure water on glass surface is $60^{o}\mp4^{o}$, which means that used glass is already slightly hydrophobic. The hydrophobic glass surface is slightly more hydrophobic and the advancing static contact of ultrapure water is $91^{o}\mp4^{o}$. Moreover, both of the surfaces are not homogenous, which means that on both of them there will be pinning spots at the surface. Because of this pinning the drop will stop retreating and the droplet will have a larger diameter at the end of the retraction process. Thus, the percentage of the retraction will be smaller for glass than for hydrophobic glass.

The movement time of small drops depends on:

- velocity of impacting droplets
- size of the drop
- surface

The movement time did not change as much as the average retraction area depending on the airspeed. In case of hydrophobic glass, there is not a large difference in the movement time at 50 m/s and 90 m/s airspeed. For glass, the influence of airspeed is more pronounced, especially at $-5^{o}C$ and $-10^{o}C$. At $-5^{o}C$ the movement time decreases, while at $-10^{o}C$ it increases. As mentioned above, the average movement time was measured from at least 4 separate drops impacting the surface. The diameter of the

impacting drops did differ and for small drops it was between 40-80μm. At –10°C and airspeed of 50 m/s the drops were smaller (average diameter of 58μm) than at 90 m/s airspeed at the same temperature (average diameter of 66μm). The bigger the drop the slower it retracts. This difference in diameter can explain why the average movement time at 90m/s airspeed was longer than at 50m/s. Lastly, the surface has an influence on the movement time. The movement time of impacting droplets at the hydrophobic glass is shorter than at glass. This is visible at -5°C and -10°C. It might be connected with the hydrophobicity of the surface. Glass is more hydrophilic than hydrophobized glass. As mentioned above the surfaces are not homogenous and there pinning spots to which the retracting droplet can pin to at the surface. This would result in the droplet retracts slower. There are more pinning spots at the glass surface than at the hydrophobized glass. At -15°C the movement time of droplets on hydrophobic glass is slower than on glass. The reason for it is that at this temperature drops freeze during retraction. More explanation on the freezing of small drops can be found in chapter 4.4.2.1.

4.4.1.2. Large droplets

4.4.1.2.1. Experimental results

The impact of large droplets on glass and hydrophobic glass is similar (Figure 4.9.). In both cases, the droplet at first spreads after hitting the surface. Then it retracts. In the end of the impact the droplet remains in one piece. The shape of the drop at the end of the impact is not always round (Figure 4.9 Glass). The reason for it is that during retraction part of the drop can pin to one of the pinning side present on the surface. This part of the droplet does not retract any further, while the rest of the drop continues to do so. As a result, the drop has an irregular shape. On the hydrophobic surface (Figure 4.9 hydrophobic glass) the droplets have a round shape after they stop retracting. Large droplets tend to splash during impact (Figure 4.6.).

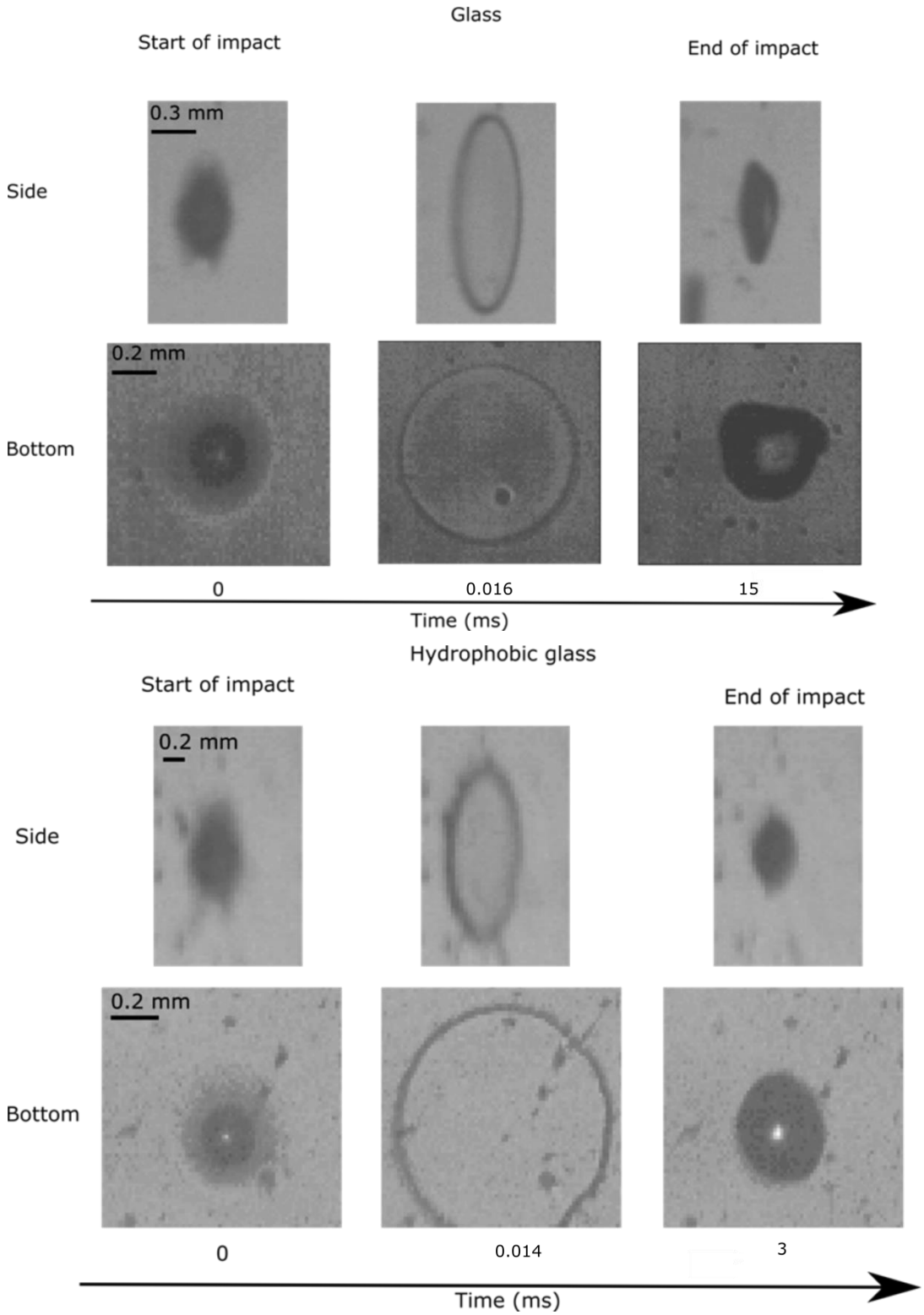

Figure 4.9. Droplet impact of large droplets at glass and hydrophobic glass at 50 m/s and -5^{o}C from bottom and side view. The bottom view made it possible to observe changes in the shape of droplet during impact.

From the bottom view, it is possible also to observe the surface. The pinning sides for the droplets can either be microscopic elevations on the surface or other impurities. The impurities can either be dust particles are small droplets that have already frozen on the surface. The frozen small droplets can either be part of a larger drop that splashed or be part of a group of droplets with a diameter lower than 40μm. The dust particles that stay on the surface are more hydrophobic then the small frozen droplets. Sometimes, when a drop impacts on spot that contains such an impurity, it breaks during retracting (Figure 4.10). The holes will then appear in the place where the impurities were present. This can be observed for glass and hydrophobic glass at different airspeeds and temperatures.

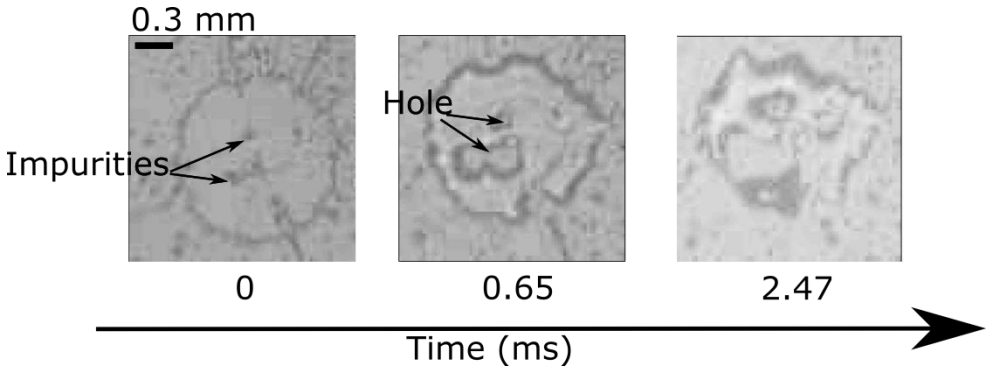

Figure 4.10. Drop impact of a droplet on a hydrophobic glass at 90 m/s at -15^{o}C. On the surface, there were small impurities are present, such as dust particles. The holes during of the impacting drop will appear then at the spot with impurities.

The drop impact on a PDMS surfaces differs from the one on the other substrates. Even though there were no mentioned earlier impurities on the surface, the drop tends to break inside during retracting. This often happens on both PDMS surfaces, PDMS20 and PDMS50 at different airspeeds and temperatures. For the PDMS surfaces, only large droplets were studied. This breakage inside the droplet is visible for large droplets of various diameters. This behavior happens also regardless of the airspeed. The breaking of the drop during impact happens more often at higher temperatures than at the lowers one. The breaking of the droplet happens during the retraction.

The droplet breaks differently depending on the thickness of the PDMS layer. In case of the PDMS20 surface during impact of the drop several small holes appear in the middle of it. Afterwards the drop continues to retract. Unlike in the case of glass or hydrophobic surface the drop is not in one piece after it stops retracting. Instead it separates into a group of smaller droplets with irregular shape (Figure 4.11 A).

For the PDMS50 surface the impact of the droplets is slightly different. In this case, while the drop is retracting a hole in the middle appears (Figure 4.11. B). As a result, the impacting drop has a donut shape for some time. This hole increases while the droplet continues to decrease. At some point one of the sides of the retracting droplet starts thinning more than the other. It continues to thin out until it breaks. As mentioned before the temperature has an influence on the drop impact at PDMS surfaces. At higher temperature, the drop remains liquid long enough to first spread and then fully retract after the impact. At lower temperature, it freezes while retracting. The breakage inside the droplet happens during the retraction. This means that at -5^{o}C the droplet will retract until it ends up in one piece. While at -10^{o}C and -15^{o}C it does also brake inside but freezes before it has a chance to retract to one piece.

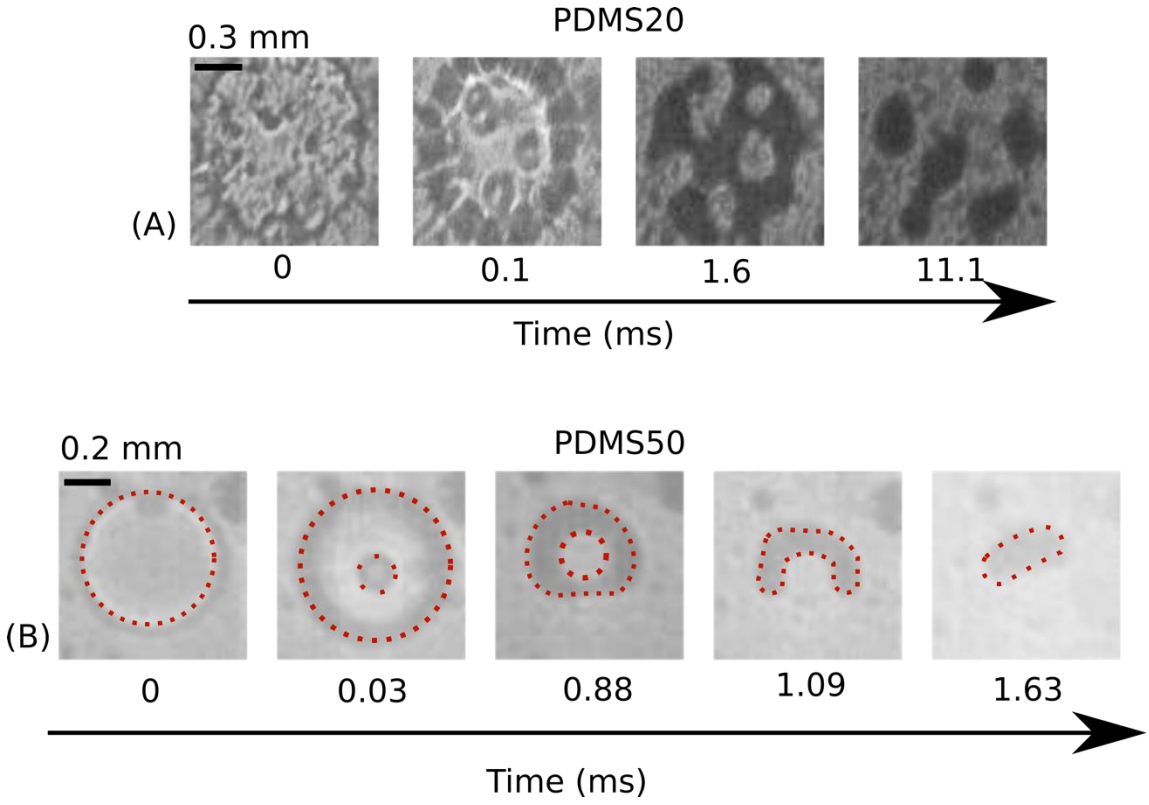

Figure 4.11. Drop impact on PDMS20 (A) and PDMS50 (B) at 50 m/s at -5^{o}C. During impact on both surfaces the droplet brakes inside. However, the way it breaks is different. For a better view in case of PDMS50 the outline of the droplet during impact is highlighted with red dash line.

The average retracting area and the average movement time was calculated by analyzing at least 5 separate drops at each temperature, airspeed and surface. In

comparison between the surfaces the average values are used and the uncertainty is the standard deviation. Since in this chapter, only large droplets are compared, only droplets with diameter larger than 100μm were analyzed. Furthermore, only undisturbed droplets were used. This means that during impact the droplet was from the beginning till the end of the impact not hit by another droplet impacting with the surface. When the drop was not in one piece after impact the surface area taken into consideration was the sum of the small droplets resulting from the impact. This happened when the droplet impacted with the surface with impurities (Figure 4.10) or when impacting with PDMS20 (Figure 4.11 A).

There is a large difference between the average movement time of PDMS50 and other surfaces. Compare to others surfaces, the drop moves much faster on PDMS50. This is independent from the temperature and airspeed.

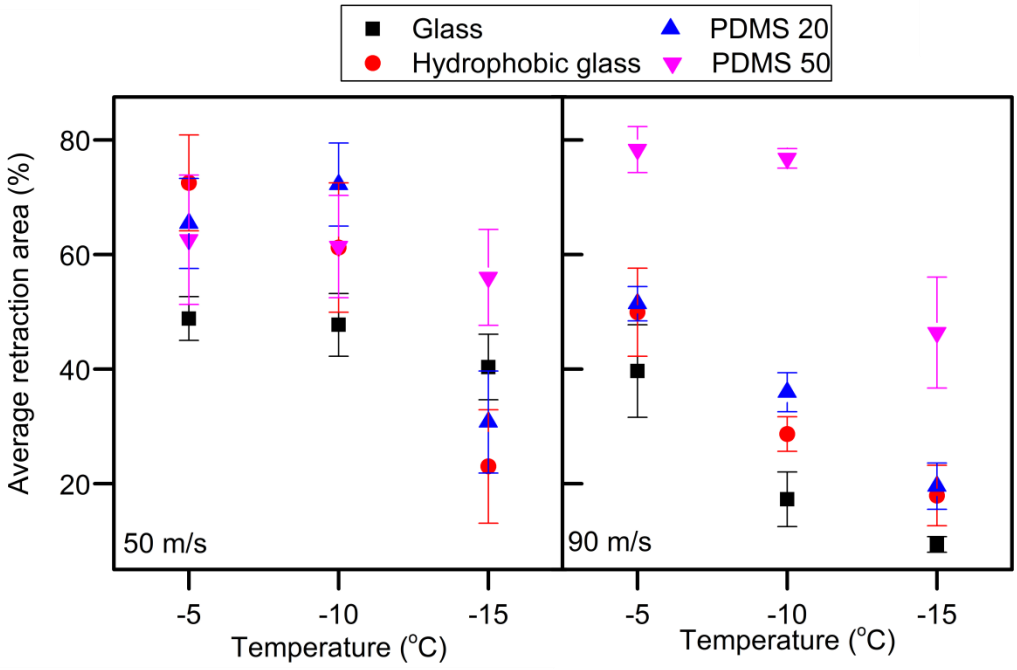

Figure 4.12. Average retraction of impacting droplets on different surfaces at 50 and 90 m/s at different temperatures. At 50 m/s the average retraction for different surfaces are similar to each other. At 90 m/s there is a clear difference between PDMS50 and the other surfaces. This can be explained by the way the droplets impact on the surfaces (Figure 4.9. and 4.11.).

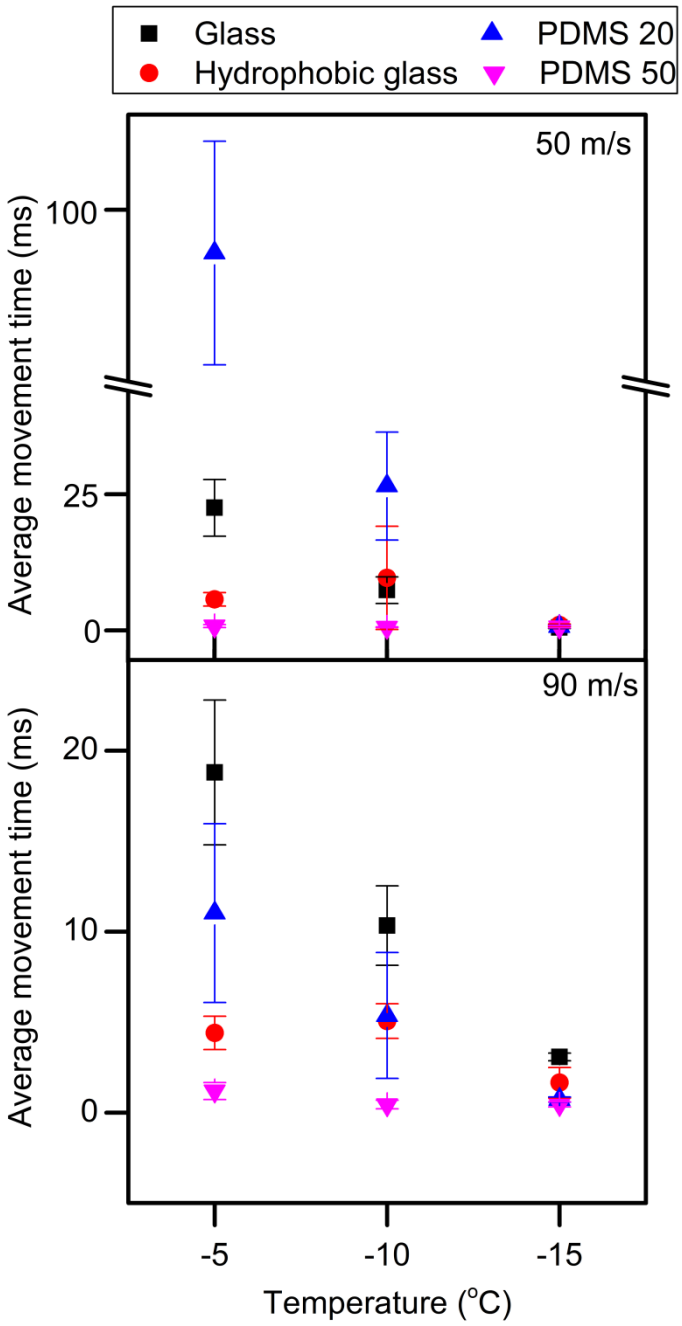

Figure 4.13. Average time of movement for large impacting droplets on different surfaces at 50 m/s and 90 m/s at different temperatures. There is strong temperature dependence visible, especially for glass and PDMS20. With decreasing temperature, the time of movement of the impacting drop decrease as well. Even though the drop impact for PDMS50 is faster than for the other surfaces the droplet does not necessarily freeze during the retraction, at -5 ^{o}C the remained liquid during the retraction.

4.4.1.2.2. Discussion

The reason for droplets to impact differently at glass, hydrophobic glass (Figure 4.9) and PDMS surfaces (PDMS 4.11) is the difference between the softness of the surfaces. Both studied PDMS layers are softer than either glass or hydrophobic glass (Table 4.1). Wetting and drop impact at soft surfaces have been studied before[86,87,92-101]. The works concerning the drop impact[86,97-101] have shown that the softness of the surface does influence the drop impact, for example the splash (Figure 4.5) is less likely to happen when the surface if softer[101]. Those measurements were done at lower velocities with larger sized droplets, and are hard to compare with my results. In my experiments, I could not distinguish if droplets splash more on the studied hard surfaces than on the soft surfaces.

Earlier works have showed that when drop is deposited on a soft surface it slightly deforms close to the three-phase contact line[96,99,100,102,103]. The soft surface forms a wetting ridge below the three-phase contact line. This does not happen on hard surfaces. This deformation could also explain why the drop impact on the two studied PDMS surfaces differ from the one on glass and hydrophobic glass. Earlier works[86,87,97] also pointed out that the formation of the wetting ridge during impact of soft surfaces, results in entrapment of air bubble underneath the drop. This can explain why they break while retracting.

The average retracting area for large droplets (Figure 4.12) depends on:

- surface
- temperature
- velocity of the impacting droplets.

The average amount of retraction area for large droplets at 50 m/s (Figure 4.12) shows, that there are some minor differences between different surfaces. Those differences then increase with decreasing temperature. However, the data points are rather close to one another. They follow the same trend, with decreasing temperature the droplet retracts less. This is because the impacting droplets tend then to freeze faster while retracting.

The retraction area of impacting droplets on the glass, hydrophobic glass and PDMS20 surfaces at 90 m/s is comparable to each other. However, there is a large difference between those three surfaces and the PDMS50 surface. This can be connected to the way the drop retracts on different surfaces. In case of the glass and hydrophobic glass

surface the drop retracts after impact and ends up in one piece in the end (Figure 4.9). In case of the PDMS20 (Figure 4.11 A) the drops brake into a group of smaller droplets after impact. Each of those smaller droplets on its own has different small surface area. The sum of these areas was compared to the surface area of the impacting droplet. In the end the surface area for PDMS20 was more comparable with the one of glass and hydrophobic glass surface.

The second parameter, which seems to have an impact on the retracting of the droplets, is the temperature. At both velocities, with decreasing temperature the droplets retract less. This can be explained by the droplets freezing while retracting at temperatures lower than -5 ^{o}C.

Lastly, the velocity of the impacting droplets seems to play a role in the retracting of the droplets. In case of impact on glass, hydrophobic glass and PDMS20 surfaces, with increasing velocity the droplets retract less. The opposite can be said for PDMS50, where with increasing velocity the droplet retracts more. The reason why PDMS50 and PDMS20 strongly differ from each is the way the droplet is impacting with the surface. On PDMS20 the droplet brakes into a group of small droplets during retraction (Figure 4.11 A). On the other hand, the drop on PDMS50 is in one piece after the impact (Figure 4.11 B). This can explain why there is a large difference between PDMS20 and PDMS50. However, the exact reason why the droplets impact differently on PDMS20 and PDMS50 is still unknown.

The average retraction area for small and large droplet on glass and hydrophobic glass is similar to each other (Figure 4.7 and 4.12). It seems that the size of the droplet does not have an influence on the amount the drop retracts.

The time of movement for impacting large droplets (Figure 4.13.) depends on:

- surface
- temperature
- velocity of the impacting droplets

The time of movement of impacting droplets at different surfaces differs largely from each other. However, this difference gets smaller with decreasing temperature. Independent from the velocity the droplets retract faster at hydrophobic glass and PDMS50 surface than at glass and PDMS20 surface. In case of glass surface the short movement, time might be the result of lower hydrophobicity in comparison to other studied surfaces. This explanation, however, does not fit to PDMS20. Since the

hydrophobicity of it was similar to the one of hydrophobic glass and PDMS50. The softness of the surface can be the reason for such a short time of movement. As mentioned above the way the soft surface behaves close to the three-phase contact line differs than of the one on hard surfaces. At soft surfaces, there is a wetting ridge close to the three-phase contact line[96,102,103]. This can also influence the speed at which the droplet retracts.

Also, the mentioned earlier impurities on the surface, such as frozen droplets on the surface or dust particles, might also influence the time of movement. It might be that the droplet can pin to the impurities and thus slow down the retraction. In case of softer PDMS layers it can also be that the dust particles will stick to the surface, which will change the smoothness of the surface. The surface can then become rougher and have more pinning side. The presence of contamination can explain why the impact on the PDMS20 is so much longer than for other surfaces.

There is also a strong dependence between the temperature and movement time. With decreasing temperature, the time shortens. It is especially visible for glass and PDMS20 surfaces. For PDMS20 the average time of movement for impacting droplets at 50 m/s at -5^{o}C is 92 ∓ 14.8 ms. With decreasing temperature, it decreases to 26 ∓ 5.4 ms at -10 ^{o}C and 0.7 ∓ 0.1 ms at -15 ^{o}C. For glass the difference in the same conditions is smaller, from 22 ∓ 2.7 ms at –5^{o}C to 0.5 ∓ 0.08 ms at -15 ^{o}C. For hydrophobic glass and PDMS50 the movement time also decreases with decreasing temperature. However, the change is smaller than in the case of glass and PDMS20 surface. The decreasing movement time with decreasing movement time can be explained by the faster freezing of the droplets. With decreasing temperature, the drop freezes faster, thus making the movement time shorter. This is true for all studied surfaces. The icing process for large droplets will be further discussed in chapter 4.4.2.2.

Additionally, the velocity of the impacting droplets plays a role. The movement time is shorter for all tested surfaces at 90 m/s than it was on 50 m/s. In case of the PDMS50 and hydrophobic glass the differences between those two velocities are small. For hydrophobic glass the time of movement at -5^{o}C is 5.7 ∓ 0.3 ms at 50 m/s and 4.4 ∓ 0.6 ms at 90 m/s. The difference between the two velocities becomes even smaller with decreasing temperature. In case of glass and PDMS20 the difference between the two velocities is much larger. In case of PDMS20 the time of movement at 50 m/s and 90 m/s decreases from 92 ∓ 14.8 ms to 11 ∓ 4.3 ms.

4.4.2. Icing

In the recorded videos, it was possible to distinguish if a drop was liquid or frozen. It is visible on the pictures in Figure 4.14 and Figure 4.16 that a liquid drop looks different than a frozen droplet. Therefore, it was possible to estimate how long it will take on each surface for ice to appear. The time it takes for the first ice to appear was measured in similar way to the time of movement of impacting droplets. In this case, the start was the frame at which first droplet hit the surface and the end was the first frame at which the ice was visible.

4.4.2.1. Small droplets

4.4.2.1.1. Experimental results

Just as mentioned before small droplets spread and retracts during impact on a glass or hydrophobic glass surface. Independent from the temperature and velocity the droplets are always liquid when they hit the surface. For small droplets only two surfaces where studied, hydrophobic glass and glass.

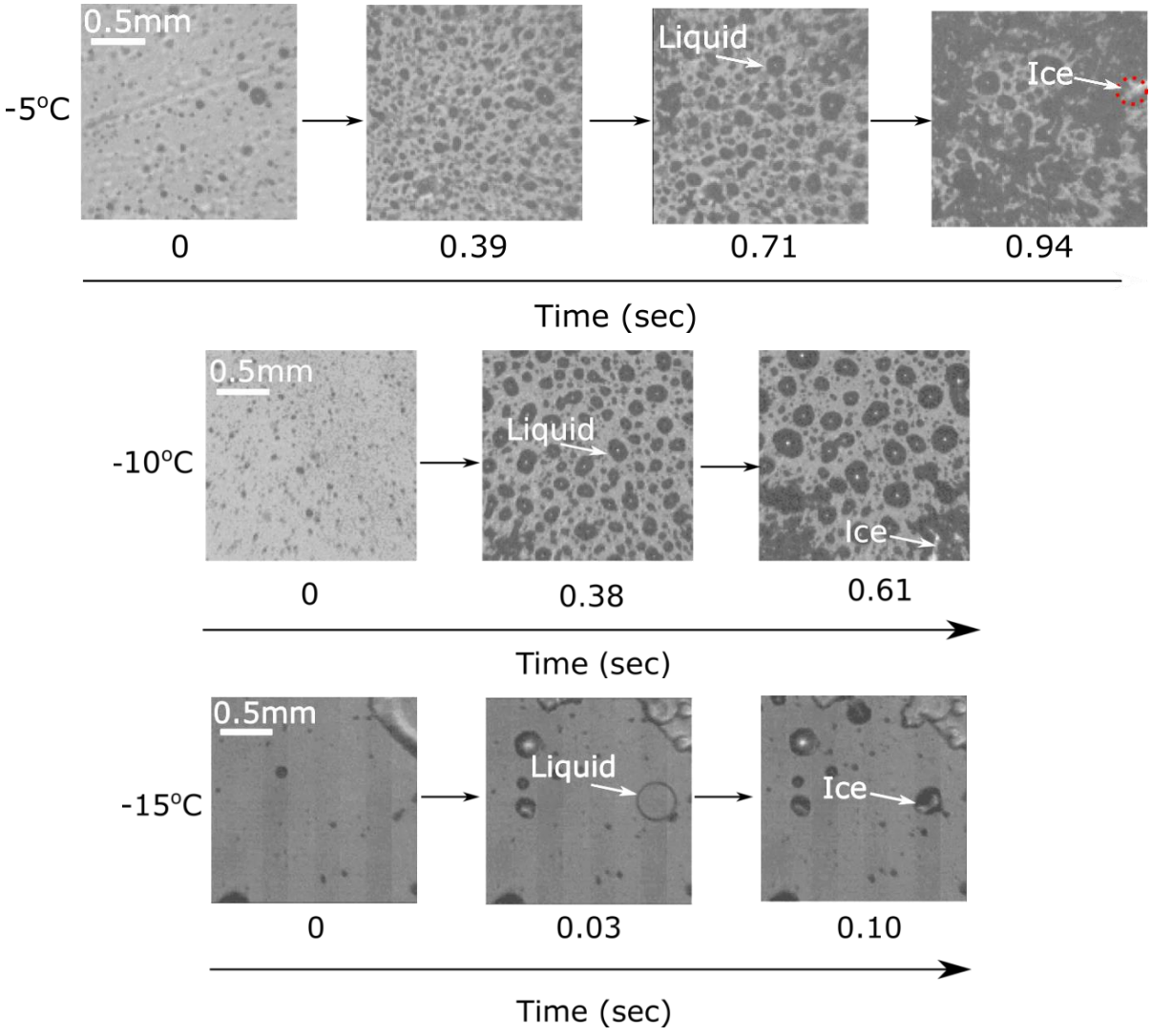

Figure 4.14. Drop impact of small droplets on hydrophobic surface at 50 m/s at different temperature. There are two different ways of icing visible at different temperatures. In this case at -5^{o}C and -10^{o}C the droplets accumulate together before the first icing appears. At the lowest temperature, -15^{o}C, the icing is much faster. As the droplets freeze during retracting.

At higher temperatures, i.e., for -5^{o}C at 50 m/s and 90 m/s and for -10^{o}C at 50 m/s, the droplets remain liquid during the spreading and retracting. Moreover, the droplet remains liquid longer than 0.5 sec. Afterwards, more and more droplets continue to impact on the same surface. This leads to merging of the small droplets into larger ones. Freezing of droplets is observed during this continuous rain of droplets on the surface (Figure 4.14).

At -10^{o}C at 90 m/s and -15^{o}C for both velocities the impacting droplets are liquid when they first hit the surface (Figure 4.14.). Due to the small size of those droplets, diameter smaller than 80 μm, it is impossible to exactly pinpoint the location where the icing starts inside of the droplet

For small droplets for each velocity, temperature and surface two videos were made. At higher temperatures, for -5^{o}C at 50 m/s and 90 m/s and for -10^{o}C at 50 m/s, the droplets remain liquid for more than 0.5 seconds. The first icing was from the moment the first drop touched the surface until somewhere in the view ice was visible (Figure 4.14). From two videos the average was calculated. At lower temperatures, at -10^{o}C at 90 m/s and -15^{o}C for both velocities, the droplet froze during retracting. In this case, the first ice formation was also measured from when the first droplet touched the surface and until the first ice was seen. In this case, the first ice formation and time of movement is equal. In this case, the average was also calculated as the average from the two measurements. The uncertainty for the first ice formation was 500 frames, which is 5 ms. The 500 frames where chosen as within this range I was certain that there was ice on the videos.

In one case, -5^{o}C at 50 m/s at glass, the first ice formation took longer than 1.93 sec, the max time of a video, see chapter 4.2. This made it impossible to measure the exact time of first ice formation. It is certain that there was a layer of ice after measurements ended. After recording the video, the test section was opened to see how the surface looks and if needed to defreeze it. At -5^{o}C at 50 m/s when the test section was opened after the measurement, there was clearly ice on the surface.

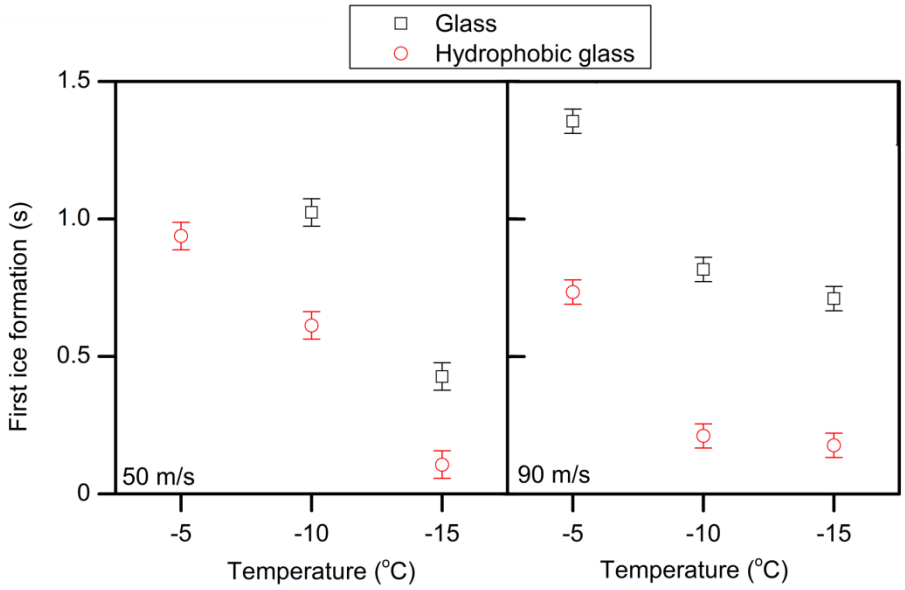

Figure 4.15 The time it took for first ice to appear on the surface at glass and hydrophobic glass at different temperatures and velocities. With decreasing temperature and increasing velocity, the time for ice to appear is shorter. Additionally, this time also depends on the surface. In this case, the icing is faster on hydrophobic glass.

4.4.2.1.2. Discussion

The first ice formation depends on type of surface, temperature and the velocity of impacting droplets. As mentioned before (Figure 4.15) with decreasing temperature the time needed for icing decreases. This time also decreases with increasing velocity. Lastly, the type of surface has an influence. For small droplets, the icing appears faster on a hydrophobic glass than on glass. The airspeed seems to have an influence on the first ice formation on both glass and hydrophobic glass (Figure 4.15). At 50 m/s the with decreasing temperature the freezing happens faster. At 90 m/s for temperatures below -5^{o}C the temperature does not to have influence on the first ice formation for the hydrophobic glass. The reason for it might be the convective flow inside the droplet during impact. With increasing airspeed, this convective flow will be stronger and as a result the drop will freeze faster.

4.4.2.2. Large droplets

4.4.2.2.1. Experimental results

The icing for large droplets is similar to the one of small droplets (Figure 4.16). Also in this case, the droplets that hit the surface are always liquid, independent from temperature, velocity and tested surface. Afterwards they spread, retract and freeze.

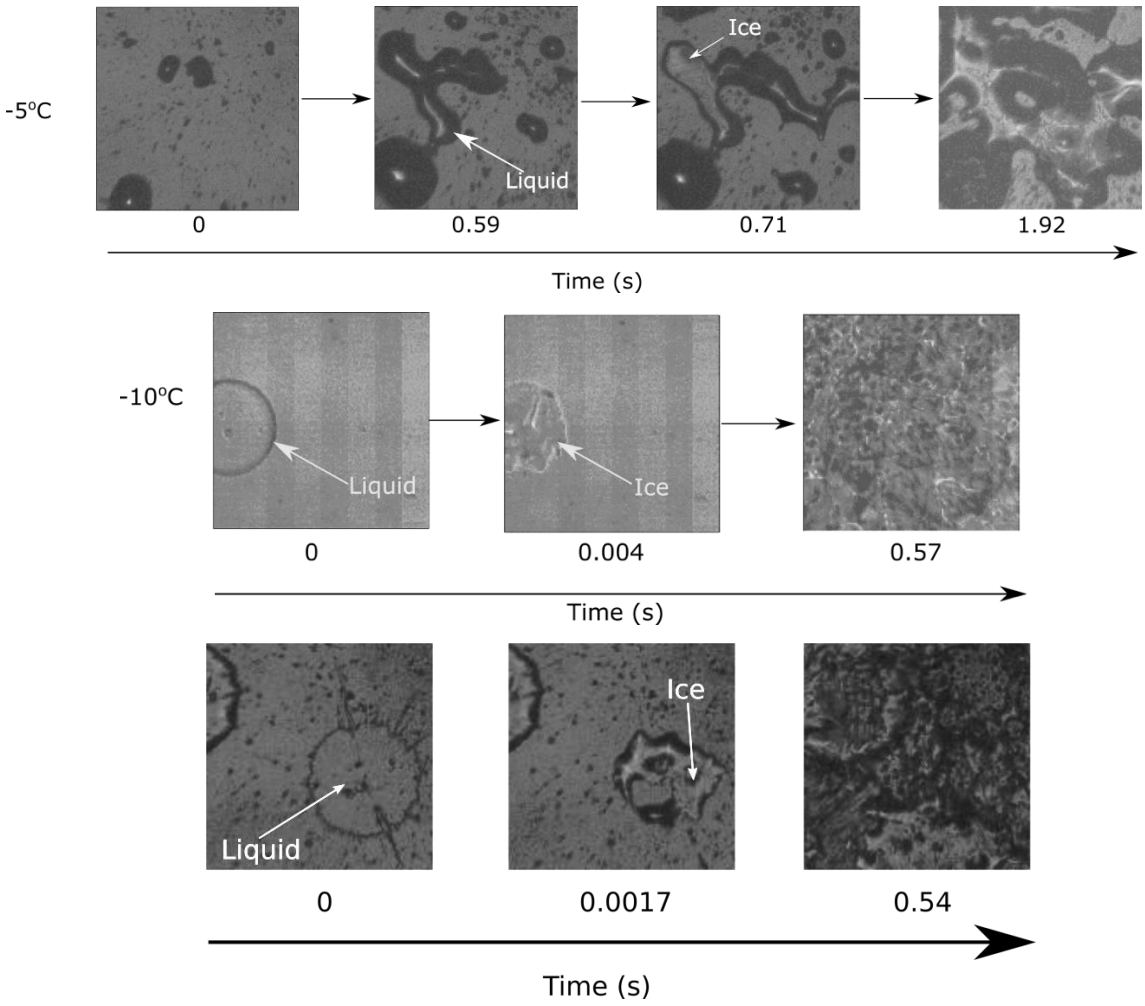

Figure 4.16. Process of icing at glass at 90 m/s at different temperatures. Two different ways ice appears can be distinguished. In the first one, the droplets remain liquid for a longer period of time. In the meantime further droplets hit the surface. The droplets merge together. This continues till the first ice appears. With decreasing temperature, the icing happens faster, since the droplets freeze while they are retracting.

What happens next depends on the temperature, velocity and the surface. For all surfaces at -5°C at 50 m/s and 90 m/s, the droplets remain liquid for the spreading and retraction after impact and remains liquid for longer time afterwards, even longer than 0.4 s. With time, more and more droplets impact on the studied surface, causing the droplets to accumulate. Freezing of droplets is observed during this continuous rain of droplets on the surface (Figure 4.16). Also in case of all studied droplets at -15°C at 90

m/s the impacting droplets freeze during retraction (Figure 4.16.). In this case, the first ice formation and time of movement is equal. For the others, the first ice formation and time of movement are two separate times. At the other temperatures and velocities, -10°C at 50 m/s and 90 m/s and -15°C at 50 m/s, the way icing happens will depend on the studied surface.

In case of PDMS50 the droplets remain liquid for longer than 0.3 sec at -10 °C for velocities of 50 m/s and 90 m/s, and at -15 °C for velocities of 50 m/s. During this time, more droplets impact on the surface, leading to a merging of the droplets and only after some time the ice appears on the surface. For the PDMS20 surface the situation looks different. At -10 °C and -15 °C at 50 m/s and -10°C at 90 m/s the impacting droplets tend to freeze while retracting.

Some of the droplets are freezing already while retracting (Figure 4.16). This made it possible to observe the freezing process of large droplets impacting on glass (Figure 4.17.) and hydrophobic glass surface (Figure 4.18)). In both cases only droplets were chosen, which were not disturbed during the freeing process by other impacting droplets. Some steps of icing are common for both surfaces. The droplets are always liquid when they hit the surface (Figure 4.17 (1) and Figure 4.18 (1)). During this impact, the droplets tend to splash (Figure 4,5.), which due to the small size of the droplets that separate from the main drop it is not so easily seen on the pictures (Figure 4.17 (2) and Figure 4.18 (2)). Afterwards, the droplet retracts (Figure 4.17. (3) and Figure 4.18. (3)). The retraction of droplets at different surfaces was discussed in detail in chapter 4.4.1.2.

The next steps depend on the studied surface. In case of glass, the ice will first appear on the rim on one side of the droplet (Figure 4.17. (4)). Then the ice starts to spread through the droplet (Figure 4.17. (5)). This continues until the whole droplet is completely frozen. In case of hydrophobic glass, the ice first appears rather in the middle of the drop (Figure 4.18. (4)). From there the ice then spreads. This happens at temperature and velocities at which the droplet freezes during retraction. For glass, it is at -10°C and -15°C at both studied velocities. For hydrophobic glass, it happens at -10°C at 90 m/s and -15°C at both studied velocities.

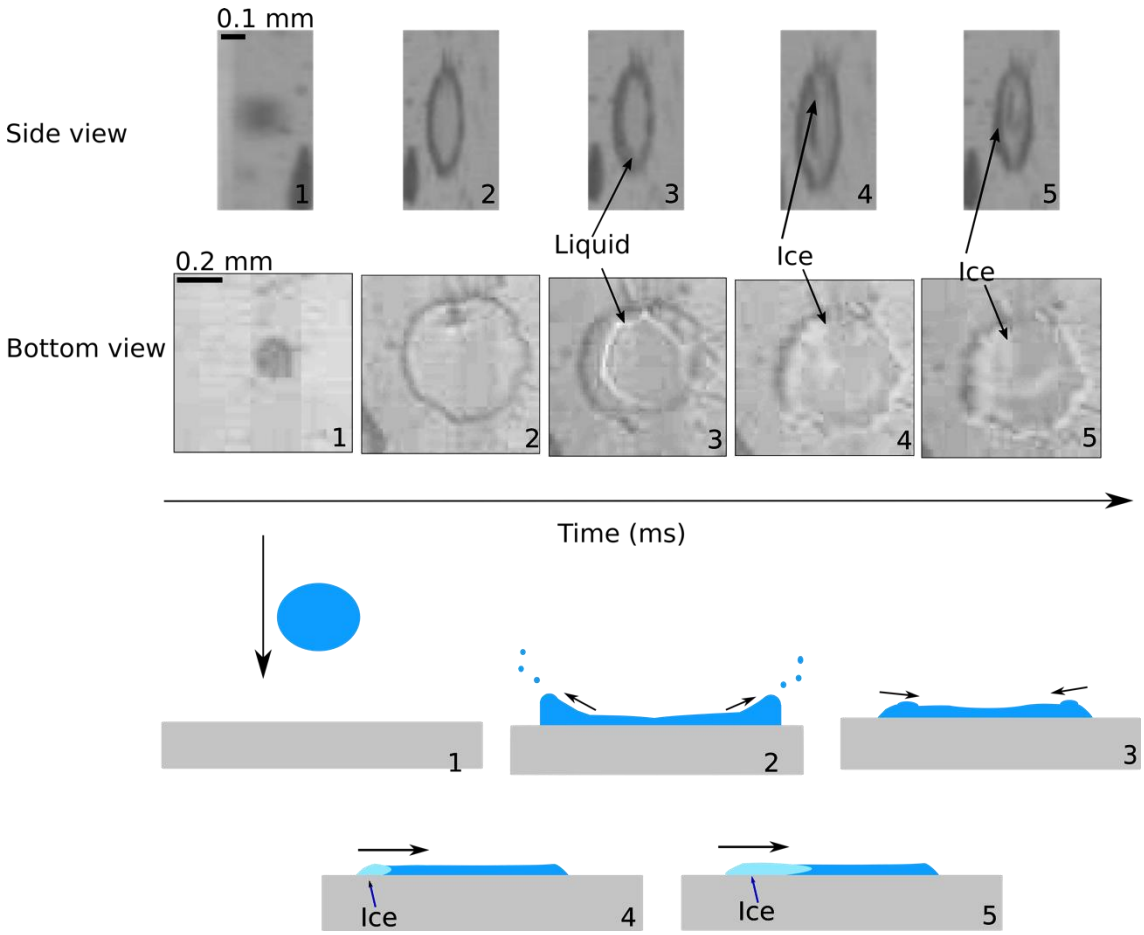

Figure 4.17. Freezing of large droplets impacting on a glass surface at -10°C and 50 m/s. The drop is liquid at the moment it hits the surface and even makes a splash (2). It starts to retract (3). At some point one side of the drop freezes (4). From there the ice spreads through the drop (5).

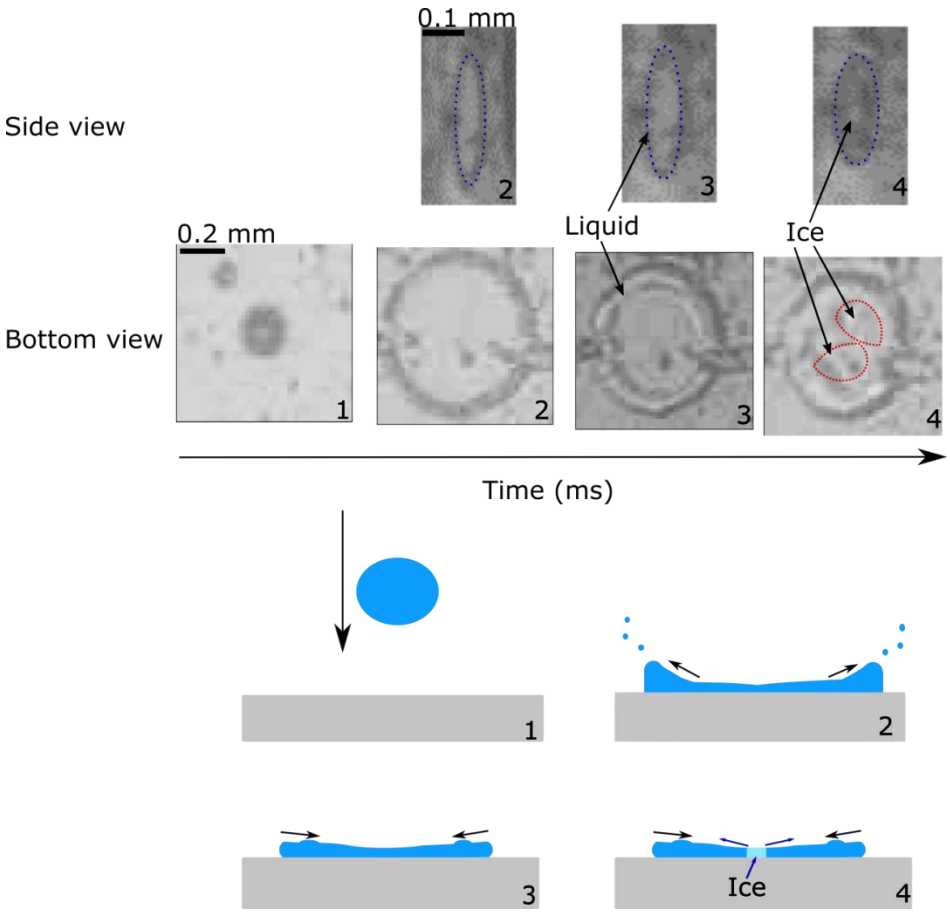

Figure 4.18. Freezing of droplet impacting on hydrophobic glass surface at -15°C at 50 m/s. At first the liquid droplet hit the surface and splashes (2). Afterwards the droplet retracts (3). At some point in time some spots inside the droplet freeze (4). From there the ice spreads through the droplet. For better view the outline of the droplet in the side view has been highlighted with blue dotted line.

For glass and hydrophobic surface for each velocity and temperature two videos were made. For PDMS surfaces only one video per temperature and velocity was made. This was due to limited measurement time in the wind tunnel in Airbus Innovation Group in Munich. The first ice formation time is the time between the first droplet touching the surface until ice appeared on the surface (Figure 4.16). For the hydrophobic glass and glass the first ice formation is the average from the two measurements. There was small difference in the first ice formation between the two videos taken with the same velocity and temperature. The difference varied between 50-150 frames, which is 0.5 - 1.5 ms. In some cases, it happened that first ice formation happened during the retraction. In this situation, the first ice formation and movement time are equal. The uncertainty for the

first ice formation was 500 frames, which is 5 ms. The 500 frames where chosen as within this range I was certain that there was ice on the videos.

For both velocities at -5°C the time it took for ice formation to happen was so long it was not possible to estimate it from the recorded videos. Between the measurements, the test section of the wind tunnel was opened to see how the surface looked after the drop impact. In the case of PDMS50 at -5°C at both velocities the studied surface did have a layer of ice. This makes it certain that there was ice formation on the surface. The maximum length of the videos was 1.93 sec. It is only possible to say the first ice appeared after 1.93 sec but it is impossible to say exactly when.

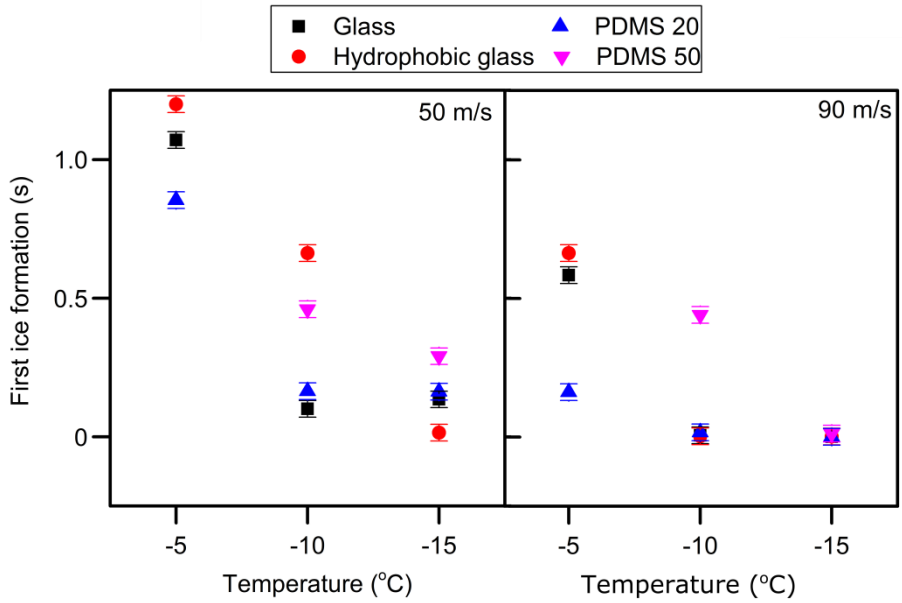

Figure 4.19. The time it took for the first ice to appear for larger droplets. This time depends on the temperature, velocity and type of surface. With decreasing temperature and increasing velocity this time shortens.

4.4.2.2.2. Discussion

This first ice formation (Figure 4.19) time depends on factors such as:

- surface
- temperature
- velocity of impacting droplets

One of the reason why the first ice formation differs for the two PDMS surfaces (Figure 4.19) can be that the way the droplets retract after impact (Figure 4.11). It was shown that the freezing time depends on the studied surface[104,105]. On hydrophobic surfaces the droplets froze slower than on hydrophilic ones. It can be connected to the ratio of the

surface area to volume of the droplet. The larger area would make the cooling process more efficient, thus the freezing of the droplet would be faster. The average retraction area (Figure 4.12) for PDMS50 is larger than for PDMS20. This means that the ratio of surface area to the volume of the droplet on PDMS20 is larger than at PDMS50. Another reason might be the difference in the thermal resistance. The heat that is generated during the freezing of the droplet is faster conducted through the thinner PDMS layer (PDMS20) than through the thicker one (PDMS50). For that reason, droplet freeze faster on PDMS20 than PDMS50. Larger surface area can also explain the difference in the first ice formation between the small and large droplets. The large droplets have larger ratio of surface area to volume after the impact compared to the small droplets. Resulting in a more effective the cooling for the larger droplets and the first ice formation is shorter than for small droplets. On all studied surface at both velocities this time shortens with decreasing temperature. There are large differences in the time it takes for first ice to occur between the studied surfaces. For all of them the first ice formation decreases with decreasing temperature. Lastly, this time also decreases with increasing velocity of the impacting droplets. For example, at -5^{o}C on a glass surface the time for ice to appear decreased from 1.07 ∓ 0.005 s at 50 m/s to 0.58 ∓ 0.005 s at 90 m/s. This can be due to the convective flow inside the drop increasing with increasing velocity. The stronger this flow is the faster the droplet freeze. At almost all temperatures and velocities the ice formation is the slowest for the PDMS50 surface.

4.5. Conclusions

The goal of this work was to study impact, spreading and freezing of supercooled water droplets. In this work, a special set-up was developed to allow observing drop impact from two views. This made it possible to observe both the spreading and freezing from the bottom and splash from the side.

This work showed that the impact of droplets at high speeds and low temperatures depends on various factors, such as temperature, velocity, size of droplets or property of the surface the droplet is impacting on. For example, the small droplets with diameter below 80 μm impact differently than the large droplets with diameter larger than 100 μm. The size also influences the splashing of droplets during impact.

When the droplet hit the surface it is always liquid. After the impact, drops retracted and froze at some point in time. The exact time needed for first ice formation varied depending on the size of the droplet, velocity, temperature and the surface. The first ice

formation was faster for larger droplets (diameter larger than 100 μm) than for smaller droplets (diameter between 40-80 μm). Additionally, the first ice formation was influenced by the velocity of the impacting droplets, with increasing airspeed, the first ice formation was faster. There is even a stronger temperature influence on freezing. With decreasing temperature, the freezing time was shorter, meaning that at temperatures of -10^{o}C and -15^{o}C the droplets already started to freeze during retraction. Lastly, the type of surface (glass, hydrophobic glass, PDMS20 and PDMS50) influenced the drop impact. By changing the surface, the way the drop impacted changed. While on glass and hydrophobic glass the droplets impacted in a similar way, the process looked different on PDMS. On PDMS the impacting droplets tended to brake inside during retracting after impact and at the end of the impact the droplet was no longer in one piece.

4.6. Outlook

This work was a first step into empirically studying the impact of super cooled droplets at different surfaces with the aim of establishing a solid database of impact phenomena and relating the impact outcomes to atmospheric conditions and surface properties.It showed that the drop impact differs depending on the type of studied surface, temperature and velocity of the impacting drops. However, more analysis work should be done on all the data to gain a more profound understanding of the physical process that are influenced by each parameter. This would also pinpoints which of the parameters has the strongest influence. The airspeed influences the drop impact. With increasing velocity, the movement time of the drop on the surface is shorter and the first ice formation is faster. So far only two airspeeds, 50 m/s and 90 m/s, where studied.

4.7. Appendix

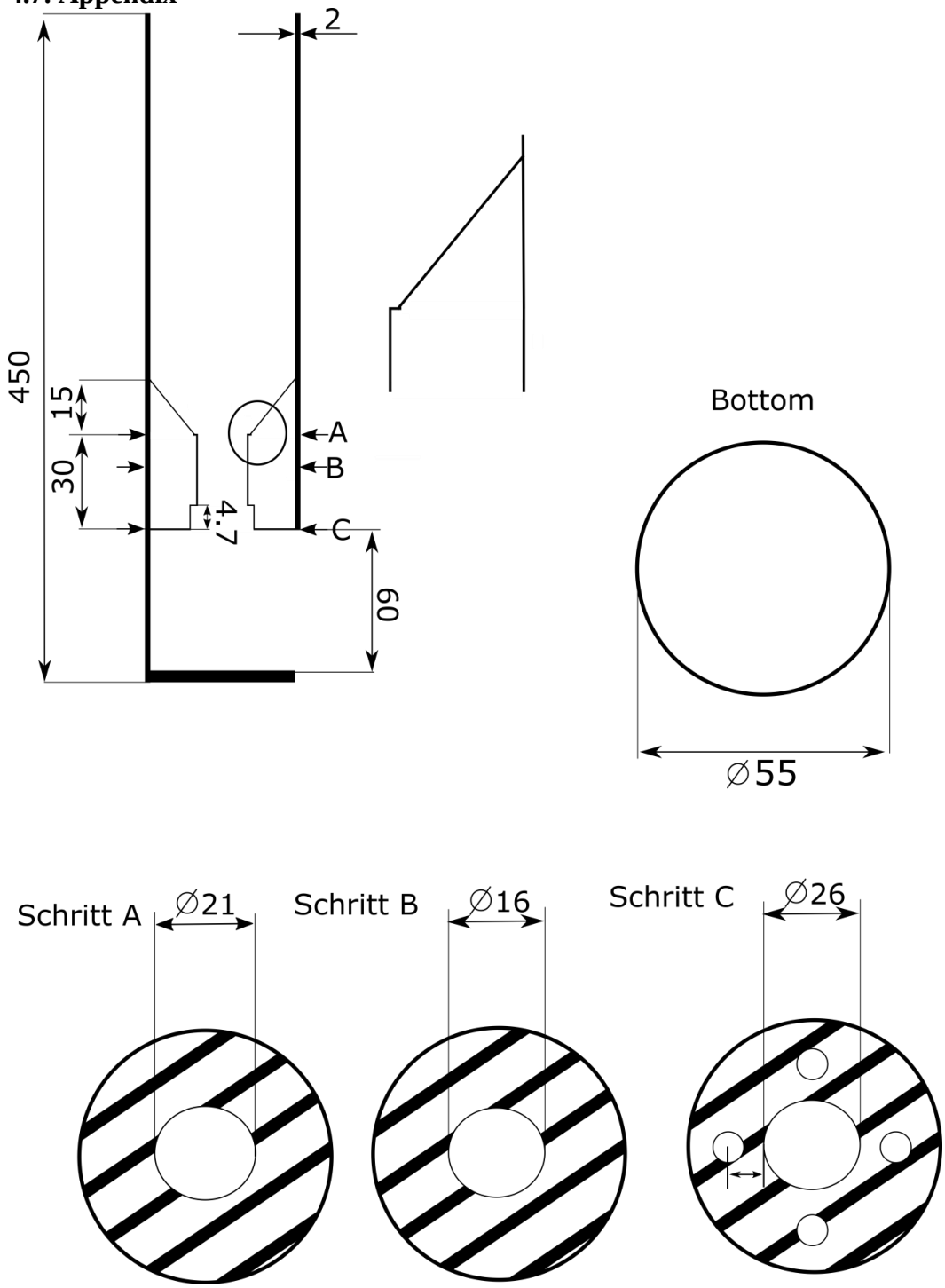

Figure 4.20. Sketch of the holder for the light source. The light holder was design that the light source can be fitted inside it and be hold in space in specific part. On the bottom of the holder for light source a smaller holder with mirror was put. This made it possible for the light to be directed outside the light source holder. Between the part the light source is hold and mirror there is a place for window to be held. This window will separate the two parts of the light source holder.

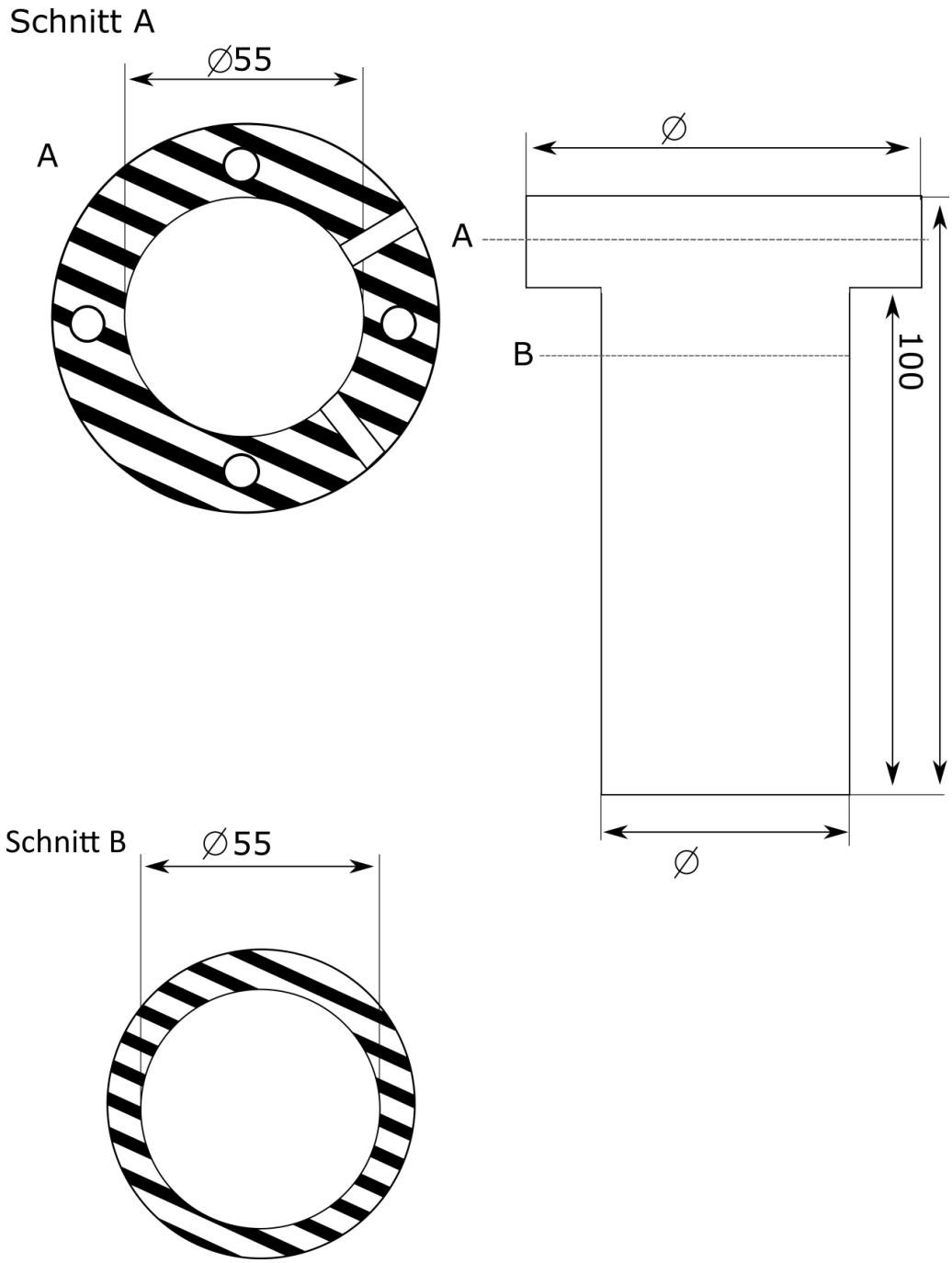

Figure 4.21. Sketch of the connection part to put the holder for the light source inside the wind tunnel.

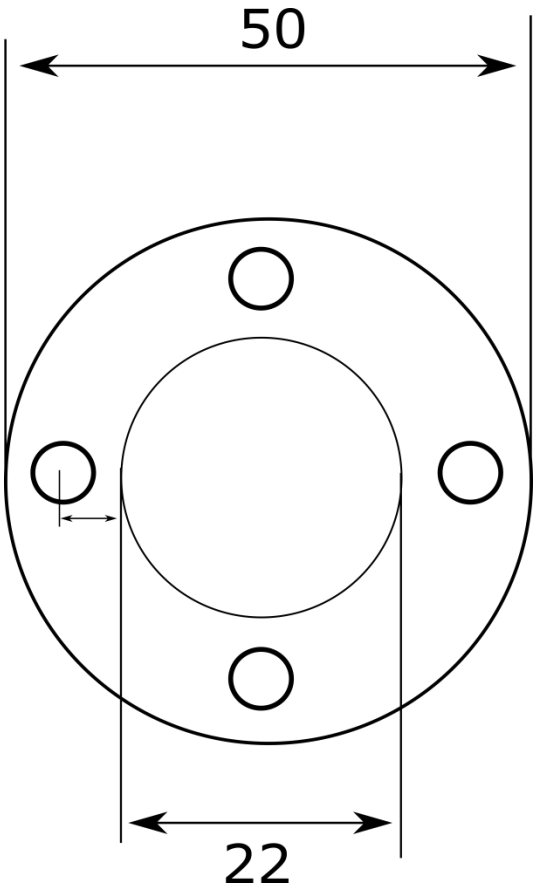

Figure 4.22 Holder for the window inside the holder for the light source. It was designed inside the holder to prevent condensation and icing of the light source during the measurements.

5.Bibliography

1. Fell, D. Dynamic wetting of complex liquids. *University of Mainz* (2013).
2. Fell, D. *et al.* Influence of Surfactant Concentration and Background Salt on Forced Dynamic Wetting and Dewetting. *Langmuir* **27,** 2112–2117 (2011).
3. Fell, D., Pawanrat, N., Bonaccurso, E., Butt, H.-J. & Auernhammer, G. K. Influence of surfactant transport suppression on dynamic contact angle hysteresis. *Colloid Polym Sci* **291,** 361–366 (2013).
4. Henrich, F. *et al.* Influence of surfactants in forced dynamic dewetting. *Soft Matter* **12,** 7782–7791 (2016).
5. Jung, S. *et al.* Are Superhydrophobic Surfaces Best for Icephobicity? *Langmuir* **27,** 3059–3066 (2011).
6. Lv, J., Song, Y., Jiang, L. & Wang, J. Bio-Inspired Strategies for Anti-Icing. *ACS Nano* **8,** 3152–3169 (2014).
7. Fakorede, O. *et al.* Ice protection systems for wind turbines in cold climate: characteristics, comparisons and analysis. *Renewable and Sustainable Energy Reviews* **65,** 662–675 (2016).
8. Zhang, C. & Liu, H. Effect of drop size on the impact thermodynamics for supercooled large droplet in aircraft icing. *Physics of Fluids* **28,** 062107 (2016).
9. Wang, Y., Xue, J., Wang, Q., Chen, Q. & Ding, J. Verification of Icephobic/Anti-icing Properties of a Superhydrophobic Surface. *ACS Appl. Mater. Interfaces* **5,** 3370–3381 (2013).
10. Cober, S. G., Isaac, G. A., Cober, S. G. & Isaac, G. A. Characterization of Aircraft Icing Environments with Supercooled Large Drops for Application to Commercial Aircraft Certification. *http://dx.doi.org/10.1175/JAMC-D-11-022.1* **51,** 265–284 (2012).
11. Cober, S. G., Strapp, J. W., Isaac, G. A. & Strapp, J. W. Characterizations of Aircraft Icing Environments that Include Supercooled Large Drops. *http://dx.doi.org/10.1175/1520-0450(2001)040<1984:COAIET>2.0.CO;2* **40,** 1984–2002 (2001).
12. Fu, S.-P. *et al.* Dynamic Study of Liquid Drop Impact on Supercooled Cerium Dioxide: Anti-Icing Behavior. *Langmuir* **32,** 6148–6162 (2016).
13. Abdollahi, V., Habashi, W. G., Baruzzi, G. S. & Fossati, M. Quasi-molecular modeling of a single supercooled large droplet impact. *Applied Mathematical Modelling* **40,** 4560–4571 (2016).
14. Young, T. An essay on the cohesion of fluids. *Philosophical Transactions of the Royal Society of …* (1805). doi:10.2307/107159
15. Bonn, D., Eggers, J., Indekeu, J., Meunier, J. & Rolley, E. Wetting and spreading. *Rev. Mod. Phys.* **81,** 739–805 (2009).
16. SNOEIJER, J. H. & ANDREOTTI, B. Moving Contact Lines: Scales, Regimes, and Dynamical Transitions. *http://dx.doi.org/10.1146/annurev-fluid-011212-140734* **45,** 269–292 (2013).
17. Ivanova, N. A. & Starov, V. M. Wetting of low free energy surfaces by aqueous surfactant solutions. *Current Opinion in Colloid & Interface Science* **16,** 285–291 (2011).
18. Marmur, A. Solid-Surface Characterization by Wetting. *Annual Review of Materials Research* **39,** 473–489 (2009).
19. Herminghaus, S., Brinkmann, M. & Seemann, R. Wetting and Dewetting of Complex Surface Geometries.

http://dx.doi.org/10.1146/annurev.matsci.38.060407.130335 **38,** 101–121 (2008).
20. Starov, V. M., Velarde, M. G. & Radke, C. J. *Wetting and Spreading Dynamics*. (CRC Press, 2007).
21. Miller, R. & Liggieri, L. *Bubble and Drop Interfaces*. (CRC Press, 2011). doi:10.1163/ej.9789004174955.i-558
22. Eggers, J. Existence of receding and advancing contact lines. *Physics of Fluids* **17,** 082106 (2005).
23. Chen, L., Yu, J. & Wang, H. Convex Nanobending at a Moving Contact Line: The Missing Mesoscopic Link in Dynamic Wetting. *ACS Nano* **8,** 11493–11498 (2014).
24. Theodorakis, P. E., Müller, E. A., Craster, R. V. & Matar, O. K. Insights into surfactant-assisted superspreading. *Current Opinion in Colloid & Interface Science* **19,** 283–289 (2014).
25. Koopal, L. K. Wetting of Solid Surfaces: Fundamentals and Charge effects. *Advances in Colloid and Interface Science* **179-182,** 29–42 (2012).
26. Venzmer, J. Superspreading — 20years of physicochemical research. *Current Opinion in Colloid & Interface Science* **16,** 335–343 (2011).
27. Potapczuk, M. G. Aircraft Icing Research at NASA Glenn Research Center. *Journal of Aerospace Engineering* **26,** 260–276 (2013).
28. Parent, O. & Ilinca, A. Anti-icing and de-icing techniques for wind turbines: Critical review. *Cold Regions Science and Technology* **65,** 88–96 (2011).
29. Jung, S., Tiwari, M. K., Doan, N. V. & Poulikakos, D. Mechanism of supercooled droplet freezing on surfaces. *Nature Communications* **3,** 615 (2012).
30. Mortensen, K. PEO-related block copolymer surfactants. *Colloids and Surfaces A: Physicochemical and Engineering Aspects* **183-185,** 277–292 (2001).
31. Llamas, S., Mendoza, A. J., Guzmán, E., Ortega, F. & Rubio, R. G. Salt effects on the air/solution interfacial properties of PEO-containing copolymers: Equilibrium, adsorption kinetics and surface rheological behavior. *Journal of Colloid and Interface Science* **400,** 49–58 (2013).
32. Li, S., Guo, J., Patel, R. A., Dadlani, A. L. & Leblanc, R. M. Interaction between Graphene Oxide and Pluronic F127 at the Air–Water Interface. *Langmuir* **29,** 5742–5748 (2013).
33. Sarkar, B., Ravi, V. & Alexandridis, P. Micellization of amphiphilic block copolymers in binary and ternary solvent mixtures. *Journal of Colloid and Interface Science* **390,** 137–146 (2013).
34. Alexandridis, P., Holzwarth, J. F. & Hatton, T. A. Micellization of Poly(ethylene oxide)-Poly(propylene oxide)-Poly(ethylene oxide) Triblock Copolymers in Aqueous Solutions: Thermodynamics of Copolymer Association. *Macromolecules* **27,** 2414–2425 (1994).
35. Alexandridis, P. & Alan Hatton, T. Poly(ethylene oxide)・poly(propylene oxide)・poly(ethylene oxide) block copolymer surfactants in aqueous solutions and at interfaces: thermodynamics, structure, dynamics, and modeling. *Colloids and Surfaces A: Physicochemical and Engineering Aspects* **96,** 1–46 (1995).
36. Akash, M. S. H. & Rehman, K. Recent progress in biomedical applications of Pluronic (PF127): Pharmaceutical perspectives. *J Control Release* **209,** 120–138 (2015).
37. Kurumada, K.-I. & Robinson, B. H. in *Trends in Colloid and Interface Science XVI* 12–15 (Springer Berlin Heidelberg, 2004). doi:10.1007/978-3-540-36462-7_4

38. Wanka, G., Hoffmann, H. & Ulbricht, W. Phase Diagrams and Aggregation Behavior of Poly(oxyethylene)-Poly(oxypropylene)-Poly(oxyethylene) Triblock Copolymers in Aqueous Solutions. *Macromolecules* **27,** 4145–4159 (1994).
39. Li, X., Yu, Y., Ji, Q. & Qiu, L. Targeted delivery of anticancer drugs by aptamer AS1411 mediated Pluronic F127/cyclodextrin-linked polymer composite micelles. *Nanomedicine: Nanotechnology, Biology and Medicine* **11,** 175–184 (2015).
40. Taha, E. I., Badran, M. M., El-Anazi, M. H., Bayomi, M. A. & El-Bagory, I. M. Role of Pluronic F127 micelles in enhancing ocular delivery of ciprofloxacin. *Journal of Molecular Liquids* **199,** 251–256 (2014).
41. Liggieri, L. & Miller, R. Relaxation of surfactants adsorption layers at liquid interfaces. *Current Opinion in Colloid & Interface Science* **15,** 256–263 (2010).
42. Arayik Hambardzumyan, Véronique Aguié-Béghin, Mohamed Daoud, A.Roger Douillard. β-Casein and Symmetrical Triblock Copolymer (PEO−PPO−PEO and PPO−PEO−PPO) Surface Properties at the Air−Water Interface. *Langmuir* **20,** 756–763 (2004).
43. Desai, P. R., Jain, N. J., Sharma, R. K. & Bahadur, P. Effect of additives on the micellization of PEO/PPO/PEO block copolymer F127 in aqueous solution. *Colloids and Surfaces A: Physicochemical and Engineering Aspects* **178,** 57–69 (2001).
44. Pérez-Mosqueda, L. M., Maldonado-Valderrama, J., Ramírez, P., Cabrerizo-Vílchez, M. A. & Muñoz, J. Interfacial characterization of Pluronic PE9400 at biocompatible (air–water and limonene–water) interfaces. *Colloids and Surfaces B: Biointerfaces* **111,** 171–178 (2013).
45. Frank, C., Strey, R., Schmidt, C. & Stubenrauch, C. Coexisting lamellar phases in water–oil–surfactant systems induced by the addition of an amphiphilic block copolymer. *Journal of Colloid and Interface Science* **312,** 76–86 (2007).
46. Fainerman, V. B. *et al.* Surface tension isotherms, adsorption dynamics and dilational visco-elasticity of sodium dodecyl sulphate solutions. *Colloids and Surfaces A: Physicochemical and Engineering Aspects* **354,** 8–15 (2010).
47. Noskov, B. A. Dilational surface rheology of polymer and polymer/surfactant solutions. *Current Opinion in Colloid & Interface Science* **15,** 229–236 (2010).
48. Brown, W., Schillen, K., Almgren, M., Hvidt, S. & Bahadur, P. Micelle and gel formation in a poly(ethylene oxide)/poly(propylene oxide)/poly(ethylene oxide) triblock copolymer in water solution: dynamic and static light scattering and oscillatory shear measurements. *The Journal of Physical Chemistry* **95,** 1850–1858 (1991).
49. Zhou, Z. & Chu, B. Light-scattering study on the association behavior of triblock polymers of ethylene oxide and propylene oxide in aqueous solution. *Journal of Colloid and Interface Science* **126,** 171–180 (1988).
50. Lyklema, J. *Fundamentals of Interface and Colloid Science. Vol. IV : Particulate Colloids*. (Elsevier, 2005).
51. Liggieri, L., Ferrari, M., Mondelli, D. & Ravera, F. Surface rheology as a tool for the investigation of processes internal to surfactant adsorption layers. *Faraday Discuss.* **129,** 125–140 (2005).
52. Ravera, F., Loglio, G. & Kovalchuk, V. I. Interfacial dilational rheology by oscillating bubble/drop methods. *Current Opinion in Colloid & Interface Science* **15,** 217–228 (2010).
53. Butt, H. J., Graf, K. & Kappl, M. *Physics and Chemistry of Interfaces*. (2006).
54. Blake, T. D. The physics of moving wetting lines. *Journal of Colloid and*

Interface Science **299,** 1–13 (2006).
55. Cappelli, S., Xie, Q., Harting, J., de Jong, A. M. & Prins, M. W. J. Dynamic wetting: status and prospective of single particle based experiments and simulations. *New Biotechnology* **32,** 420–432 (2015).
56. Blake, T. D. & Shikhmurzaev, Y. D. Dynamic Wetting by Liquids of Different Viscosity. *Journal of Colloid and Interface Science* **253,** 196–202 (2002).
57. Billingham, J. On a model for the motion of a contact line on a smooth solid surface. *European Journal of Applied Mathematics* **17,** 347–382 (2006).
58. Voinov, O. V. Hydrodynamics of wetting. *Fluid Dynamics* **11,** 714–721 (1977).
59. Blake, T. D. & Haynes, J. M. Kinetics of displacement. *Journal of Colloid and Interface Science* **30,** 421–423 (1969).
60. Huh, C. & Scriven, L. E. Hydrodynamic model of steady movement of a solid/liquid/fluid contact line. *Journal of Colloid and Interface Science* **35,** 85–101 (1971).
61. Cox, R. G. The dynamics of the spreading of liquids on a solid surface. Part 1. Viscous flow. *Journal of Fluid Mechanics* **168,** 169–194 (2006).
62. Cox, R. G. The dynamics of the spreading of liquids on a solid surface. Part 2. Surfactants. *Journal of Fluid Mechanics* **168,** 195–220 (2006).
63. Tanner, J. E. Use of the Stimulated Echo in NMR Diffusion Studies. *The Journal of Chemical Physics* **52,** 2523–2526 (1970).
64. Ablett, R. XXV. An investigation of the angle of contact between paraffin wax and water. *Philosophical Magazine Series 6* **46,** 244–256 (1923).
65. Truszkowska, D. *et al.* Forced dewetting dynamics of high molecular weight surfactant solutions. *Colloids and Surfaces A: Physicochemical and Engineering Aspects* 30–37 (2016). doi:10.1016/j.colsurfa.2016.07.073
66. Magde, D., Elson, E. L. & Webb, W. W. Fluorescence correlation spectroscopy. II. An experimental realization. *Biopolymers* **13,** 29–61 (1974).
67. Elson, E. L. & Magde, D. Fluorescence correlation spectroscopy. I. Conceptual basis and theory. *Biopolymers* **13,** 1–27 (1974).
68. Raupach, M. R., Thom, A. S. & Edwards, I. A wind-tunnel study of turbulent flow close to regularly arrayed rough surfaces. *Boundary-Layer Meteorology* **18,** 373–397 (1980).
69. Chamorro, L. P. & Porté-Agel, F. A Wind-Tunnel Investigation of Wind-Turbine Wakes: Boundary-Layer Turbulence Effects. *Boundary-Layer Meteorology* **132,** 129–149 (2009).
70. Atkins, P. & de Paula J. *Atkins physical chemistry*. (Oxford University Press, 2010).
71. Rosenfeld, D. & Woodley, W. L. Deep convective clouds with sustained supercooled liquid water down to -37.5|[thinsp]||[deg]|C. *Nature* **405,** 440–442 (2000).
72. Criscione, A., Kintea, D., Roisman, I., Jakirlic, S. & Tropea, C. A new approach for water crystallization in the kinetics-limited growth region. (2013).
73. in *Encyclopedia of Microfluidics and Nanofluidics* (ed. Li, D.) 2185–2185 (Springer US, 2008). doi:10.1007/978-0-387-48998-8_1689
74. Hillenkamp, F., Karas, M. & Beavis, R. C. Matrix-assisted laser desorption/ionization mass spectrometry of biopolymers. *Analytical chemistry* (1991).
75. Lewis, J. K., Wei, J. & Siuzdak, G. *Matrix-Assisted Laser Desorption/Ionization Mass Spectrometry in Peptide and Protein Analysis*. **60,** (John Wiley & Sons, Ltd, 2000).
76. Rigler, R. & Elson, E. S. Fluorescence Correlation Spectroscopy. (2012).

77. Jerschow, A. & Müller, N. 3D Diffusion-Ordered TOCSY for Slowly Diffusing Molecules. *Journal of Magnetic Resonance, Series A* **123,** 222–225 (1996).
78. Holz, M. & Weingartner, H. Calibration in accurate spin-echo self-diffusion measurements using 1H and less-common nuclei. *Journal of Magnetic Resonance (1969)* **92,** 115–125 (1991).
79. Wu, D. H., Chen, A. D. & Johnson, C. S. An Improved Diffusion-Ordered Spectroscopy Experiment Incorporating Bipolar-Gradient Pulses. *Journal of Magnetic Resonance, Series A* **115,** 260–264 (1995).
80. Batrakova, E. *et al.* Fundamental relationships between the composition of pluronic block copolymers and their hypersensitization effect in MDR cancer cells. *Pharm. Res.* **16,** 1373–1379 (1999).
81. Mikhail Yu Kozlov, Nikolai S Melik-Nubarov, Elena V Batrakova, A.Alexander V Kabanov. Relationship between Pluronic Block Copolymer Structure, Critical Micellization Concentration and Partitioning Coefficients of Low Molecular Mass Solutes. *Macromolecules* **33,** 3305–3313 (2000).
82. Horn, D., Klingler, J., Schorf, W. & Graf, K. in *Structure, Dynamics and Properties of Disperse Colloidal Systems* **111,** 27–33 (Steinkopff, 1998).
83. Bonné, T. B., Papadakis, C. M., Lüdtke, K. & Jordan, R. Role of the tracer in characterizing the aggregation behavior of aqueous block copolymer solutions using fluorescence correlation spectroscopy. *Colloid Polym Sci* **285,** 491–497 (2007).
84. Koynov, K. & Butt, H.-J. Fluorescence correlation spectroscopy in colloid and interface science. *Current Opinion in Colloid & Interface Science* **17,** 377–387 (2012).
85. Stubenrauch, C., Fainerman, V. B., Aksenenko, E. V. & Miller, R. Adsorption behavior and dilational rheology of the cationic alkyl trimethylammonium bromides at the water/air interface. *J Phys Chem B* **109,** 1505–1509 (2005).
86. Chen, L., Bonaccurso, E., Deng, P. & Zhang, H. Droplet impact on soft viscoelastic surfaces. *Phys. Rev. E* **94,** 063117 (2016).
87. Chen, L., Auernhammer, G. N. K. & Bonaccurso, E. Short time wetting dynamics on soft surfaces. *Soft Matter* **7,** 9084–9089 (2011).
88. Yarin, A. L. DROP IMPACT DYNAMICS: Splashing, Spreading, Receding, Bouncing…. *Annual Review of Fluid Mechanics* **38,** 159–192 (2006).
89. Liu, J., Vu, H., Yoon, S. S., Jepsen, R. A. & Aguilar, G. SPLASHING PHENOMENA DURING LIQUID DROPLET IMPACT. *AAS* **20,** 297–310 (2010).
90. Deegan, R. D., Brunet, P. & Eggers, J. Complexities of splashing. *Nonlinearity* **21,** C1–C11 (2007).
91. Antonini, C., Amirfazli, A. & Marengo, M. Drop impact and wettability: From hydrophilic to superhydrophobic surfaces. *Physics of Fluids* **24,** 102104 (2012).
92. Gielok, M., Lopes, M., Bonaccurso, E. & Gambaryan-Roisman, T. Droplet on an elastic substrate: Finite Element Method coupled with lubrication approximation. *Colloids and Surfaces A: Physicochemical and Engineering Aspects* **521,** 13–21 (2017).
93. Lubbers, L. A. *et al.* Drops on soft solids: free energy and double transition of contact angles. *Journal of Fluid Mechanics* **747,** 614 (2014).
94. Karpitschka, S., Das, S. & Andreotti, B. Dynamic contact angle of a soft solid. *Preprint at http://arXiv …* (2014).
95. Weijs, J. H., ANDREOTTI, B. & SNOEIJER, J. H. Elasto-capillarity at the nanoscale: on the coupling between elasticity and surface energy in soft solids. *Soft Matter* **9,** 8494–8503 (2013).

96. Marchand, A., Das, S., SNOEIJER, J. H. & ANDREOTTI, B. Contact Angles on a Soft Solid: From Young's Law to Neumann's Law. *Phys. Rev. Lett.* **109,** 236101 (2012).
97. Chen, L., Wu, J., Li, Z. & Yao, S. Evolution of entrapped air under bouncing droplets on viscoelastic surfaces. *Colloids and Surfaces A: Physicochemical and Engineering Aspects* **384,** 726–732 (2011).
98. Alizadeh, A. *et al.* Influence of substrate elasticity on droplet impact dynamics. *Langmuir* **29,** 4520–4524 (2013).
99. Mangili, S., Antonini, C., Marengo, M. & Amirfazli, A. Understanding the drop impact phenomenon on soft PDMS substrates. *Soft Matter* **8,** 10045–10054 (2012).
100. Rioboo, R. *et al.* Drop Impact on Soft Surfaces: Beyond the Static Contact Angles. *Langmuir* **26,** 4873–4879 (2010).
101. Howland, C. J. *et al.* It's Harder to Splash on Soft Solids. *Phys. Rev. Lett.* **117,** 184502 (2016).
102. Park, S. J. *et al.* Shedding new light on the mystery of wetting on soft solids. (2013).
103. Jerison, E. R., Xu, Y., Wilen, L. A. & Dufresne, E. R. Deformation of an elastic substrate by a three-phase contact line. *Phys. Rev. Lett.* **106,** 186103 (2011).
104. Chaudhuri, R. G. & Paria, S. Dynamic contact angles on PTFE surface by aqueous surfactant solution in the absence and presence of electrolytes. *Journal of Colloid and Interface Science* **337,** 555–562 (2009).
105. Hao, P., Lv, C. & Zhang, X. Freezing of sessile water droplets on surfaces with various roughness and wettability. *Applied Physics Letters* **104,** 161609 (2014).

List of abbreviations

2,5-DHB	2,5-dihydroxy benzoic acid
A	Interfacial area
ΔA	Change in the interfacial area
A_m	Area pro molecule
a	Activity
a^0	Standart activity
Bo	Bonn number
b	Radius curvature
c	Concentration
c_i^α	Concentration of i component in phase α
c_i^β	Concentration of i component in phase β
c_d	Curvature of the drop apex
Ca	Capillary number
CFSC	Concentration of full surface coverage
CMC	Critical micelle concentration
CTAB	Cetyl trimethyl ammonium bromide
D	Diffusion coefficient
d	Diameter
d_i	Distance of flight for travelling ions
E	Dilatational viscoelasticity
E_r	Real part of dilatational viscoelasticity
E_i	Imaginary part of dilatational viscoelasticity
E_k	Kinetic energy
EO	ethylene oxide
$F_{\gamma\theta}$	Force resulting from Wilhelmy technique measurements
F_w	Driving force for the movement of the three-phase contact angle in molecular kinetic theory
FCS	Fluorescence correlation spectroscopy
fps	Frames per second
G	Shear modulus
G_s	Gradient strenght

g	Gravitational acceleration
I	Intensity of the signal
$I(G)$	Intensity of the signal with gradient
$I(0)$	Intensity of the signal without gradient
IWT	Icing wind tunnel
k_B	Boltzmann constant
L	Macroscopic length scale
L_m	Microscopic length scale
l	Length of the Wilhelmy plate
M_w	Molecular weight
m	Mass of travelling ions
MS	Molecular spectroscopy
(m/z)	Mass to charge ratio
MALDI	Matrix-assisted laser desorption/ionization
MVD	Median volume diameter
N_A	Avogardo number
N_i	Number of molecules of component i
ODG	Oscilating drop generator
ΔP	Difference in interfacial pressure over the interface
%PPO	Amount of PPO in comparison of overall molecular mass of Pluronic in %
PAT	Profile analysis tensiometry
PDMS	Polydimethylsiloxane
PDMS20	20 μm thick PDMS layer
PDMS50	50 μm thick PDMS layer
PEO	Polyethylene oxide
PO	propylene oxide
PPO	Polypropylene oxide
PVC	polyvinyl chloride
PEG	Polyethylene glycol
R_{app}	Hydrodynamic radius
R	Gas constant
R_1	Meridional curvature
R_2	Azimuthal curvature

r_i	Radius of the inner du Noüy ring
r_a	Radius of the outer du Noüy ring
S	Arc length along the drop profile
s	length of the drop in PAT
S-1DeS	Sodium 1-decansulfonate
SLD	Super cooled large droplets
SWD	Super cooled water droplets
T	Temperature
T_F	Flight time
t	Time
THF	Tetrahydrofuran
TOF	Time of flight
U	Velocity
V_α	Volume of phase α
V_β	Volume of phase β
v	Velocity of travelling ions
We	Webber number
X	Coordinate in the coordinate system in PAT
x	horizontal length in PAT
z	vertical length in PAT
α	Activity coefficient
Γ_i	Interfacial excess
γ	Surface tension
γ_{LV}	Interfacial tension between liquid-vapor
γ_{SL}	Interfacial tension between liquid-solid
γ_{SV}	Interfacial tension between solid-vapor
δ	Duration of pulse field gradient
ζ	friction parameter
η	Viscosity
θ	Contact angle
θ_{eq}	Equilibrium contact angle
θ_{adv}	Advancing contact angle
θ_{rec}	Receding contact angle
θ_{app}	Apparent contact angle

θ_m	Microscopic contact angle
κ^o	Equilibrium frequency
λ	Characteristic distance of displacement
μ	Chemical potential
μ^o	Standard chemical potential
ρ	Density
$\Delta\rho$	Density difference
σ	Interface
τ	Delay time
Υ	Gyromagnetic ratio of nucleus
φ	Contact angle of the drop profile in PAT

Curriculum vitae

Publications

2017
Linke. D, Henrich. F, Butt H.-J & Auernhammer G.K. Dependence of dynamic dewetting of Pluronic solutions on molecular weight. (in preparation)

2016
Henrich, F., Fell, D., Truszkowska, D., Weirich, M., Anyfantakis, M., Nguyen, T. H., & Butt, H. J. (2016). Influence of surfactants in forced dynamic dewetting. *Soft Matter*, *12*(37), 7782-7791.

Truszkowska, D., Henrich, F., Schultze, J., Koynov, K., Räder, H. J., Butt, H. J., & Auernhammer, G. K. (2016). Forced dewetting dynamics of high molecular weight surfactant solutions. *Colloids and Surfaces A: Physicochemical and Engineering Aspects*.

International conference contributions

2017

05/2017 Summer School in Jerusalem, Israel. "Dynamic wetting of complex liquids" - talk

02/2017 Winter School in Thessaloniki & Metsovo

2016

11/2016 Summer School "CoWet", Madrid, Spain. "Wetting of high molecular weight surfactants" talk

09/2016 – Practical School in Lublin, Poland

06/2016 Surfactant in solutions, Jinan, China - Talk

2015

10/2015 Droplets 2015, Twente, The Netherlands. "(De)Wetting of high molecular weight surfactant solutions"- Poster

09/2015 Summer School "CoWet", Madrid, Spain

07/2015 6th international workshop on bubble and drop interfaces 2015, Potsdam, Germany –talk

05/2015 15th Conference of the Intenrational Association of Colloid and Interface Scientists (Iacis 2015)- poster

01/2015 Winter School "CoWet" Loughborough, England - talk

Acknowledgments